RIGOROUS TESTING OF THE RAPID RADIATIVE TRANSFER MODEL ACROSS THE INFRARED SPECTRUM

A Thesis

by

WILLIAM LARK HENNING

Submitted to the Office of Graduate and Professional Studies of
Texas A&M University
in partial fulfillment of the requirements for the degree of

MASTERS OF SCIENCE

Chair of Committee,	Ping Yang
Committee Members,	Mark Lemmon
	Brendan Roark
Head of Department,	Ping Yang

May 2016

Major Subject: Atmospheric Sciences

ABSTRACT

Global circulation models (GCMs) and climate simulations often use radiative fluxes and heating rates from radiative transfer models. However, the calculations that are used are those where scattering of a cloudy atmosphere is neglected. In this study, computed fluxes and heating rates are compared when absorption is the only process, and when scattering is included. Computations for the absorption only process were performed using the Rapid Radiative Transfer Model (RRTM), and the Discrete Ordinates Radiative Transfer Model (DISORT) is used when scattering is included.

Over 8,000 model runs were conducted across various cloud layers, cloud water paths, cloud particle sizes, cloud particle shapes, and atmospheric profiles to deduce the effects of scattering in the infrared (IR) portion of the electromagnetic spectrum due to clouds. On average, the difference in upward flux at the top of the atmosphere (TOA) was roughly 4-12 W/m^2 and difference in downward flux at the surface (SFC) was roughly 1-4 W/m^2. These differences were found mainly in the middle portion of the IR spectrum, although some instances were found to be close to the far IR portion of the spectrum as well. As mentioned in other similar studies, these numbers are significant when compared to average longwave radiation budget values. Neglecting them could lead to inaccurate calculations in GCMs and climate simulations.

Similar tests were also computed when carbon dioxide was doubled in the atmosphere. Results show that the differences in fluxes compared to an atmosphere with current carbon dioxide values was less than 0.5 W/m^2.

ACKNOWLEDGEMENTS

I would like to thank the United States Air Force for allowing me the opportunity to come to Texas A&M to further my education in atmospheric sciences and to pursue research in radiative transfer. I would also like to thank my committee chair, Dr. Ping Yang, and my committee members Dr. Mark Lemmon and Dr. Brendan Roark for their assistance in this project as well as providing a great learning environment.

I would like to thank my fellow graduate students who helped me through not only the classroom portion of graduate school but made life in College Station, TX a great one.

Finally, many thanks to my family for their encouragement and my husband for his patience, understanding, and love.

TABLE OF CONTENTS

LIST OF FIGURES

LIST OF TABLES

1. INTRODUCTION

Electromagnetic radiation is the cornerstone of our Earth's energy budget. The budget can be broken down into two main components: incoming and outgoing radiation. The global average of incoming radiation from the Sun is estimated to be 341 W/m^2 (Trenberth, Fasullo, and Kiehl 2009). However, due to processes in the atmosphere like absorption and scattering, only 161 W/m^2 make it to the surface. In physics, we know that anything that has a temperature above absolute zero will emit energy per some unit of area. This is known as the Stefan-Boltzmann law (shown in equation 1).

$$M = \epsilon\sigma T^4 \quad (1)$$

Where M is the energy in W/m^2, ε is emissivity (unit-less), σ is the Stephan-Boltzman constant and T is temperature in Kelvin. Because of the solar radiation we receive that heats our surface, the Earth must also emit energy. Radiation leaving the surface of the Earth is an estimated 396 W/m^2. Similarly to our incoming radiation, absorption and scattering in the atmosphere causes the infrared radiation leaving the Earth to be reduced. By the time it leaves our atmosphere, outgoing longwave radiation is an estimated 239 W/m^2. Trenberth, Fasullo, and Kiehl's work included a highly detailed diagram of the Earth's radiation budget. Knowing the temperature of the Sun and the Earth, we can use Wien's displacement law to get the maximum wavelength of our incoming solar and outgoing terrestrial radiation. Equation 2 describes Wien's displacement law.

$$\lambda_{\max} = \frac{2898\ \mu m\ K}{T} \quad (2)$$

Where T is temperature in Kelvin. Using this equation, we find that the peak incoming solar radiation is roughly 0.5 μm and our peak outgoing longwave radiation is roughly 10 μm. By exploring blackbody curves from Planck's Law we know that radiation

reaching our planet extends from the ultraviolet to the near infrared, and radiation leaving our planet extends from the near infrared to radio waves. Planck's law is described in equation 3.

$$B(\lambda, T) = \frac{2hc^2}{\lambda^5} * \frac{1}{\frac{hc}{e^{\lambda kT}-1}} \quad (3)$$

Where h is Planck's constant, c is the speed of light, T is temperature in Kelvin, k is the Boltzman constant, and λ is the wavelength.

While the incoming radiation is a key component to our energy balance, the focus of this paper is on the outgoing radiation at the top of the atmosphere, the back radiation at the surface, and the processes that can alter these fluxes. Although the Earth does emit some radiation in the micro and radio portions of the electromagnetic (EM) spectrum, the majority is emitted in IR. IR radiation is defined as 0.70 – 1000 μm (14,285 – 10 cm-1) in the EM spectrum (Petty 2006). IR can further be broken down into three main categories: near, thermal, and far. Petty defines near IR as 0.7 to 4 μm; thermal IR as 4 – 50 μm; and far IR as 50 to 1000 μm. Because the peak wavelength of our planet is roughly 10 μm, thermal IR is the bulk of what our planet emits.

As IR radiation leaves the surface and travels upward, it begins to undergo absorption processes by our atmosphere. The atmosphere mostly comprises of nitrogen (75%) and oxygen (23%), but also has secondary smaller amounts of argon, carbon dioxide, methane, ozone, nitrous oxide and water vapor (Wallace and Hobbs 2006). Absorption of IR by these chemical compounds can ultimately block IR from transmitting further up the atmosphere. Because of their spectral properties, these chemicals affect different sections of the IR spectrum. Portions of the spectrum that are unhindered by these chemicals are known as atmospheric windows; as they allow IR to transmit to the top of the atmosphere almost completely. The largest IR window is located from roughly

8-14 µm with secondary windows near both 4 and 18 µm. For wavelengths shorter than 4 µm and those beyond 20, µm absorption of IR by water vapor and other chemical species is near 100%. A very small amount of near IR is also subjected to a minute amount of Rayleigh scattering in the atmosphere. A detailed view of the transmission of IR and the absorption bands in our atmosphere can be seen in Figure 1.

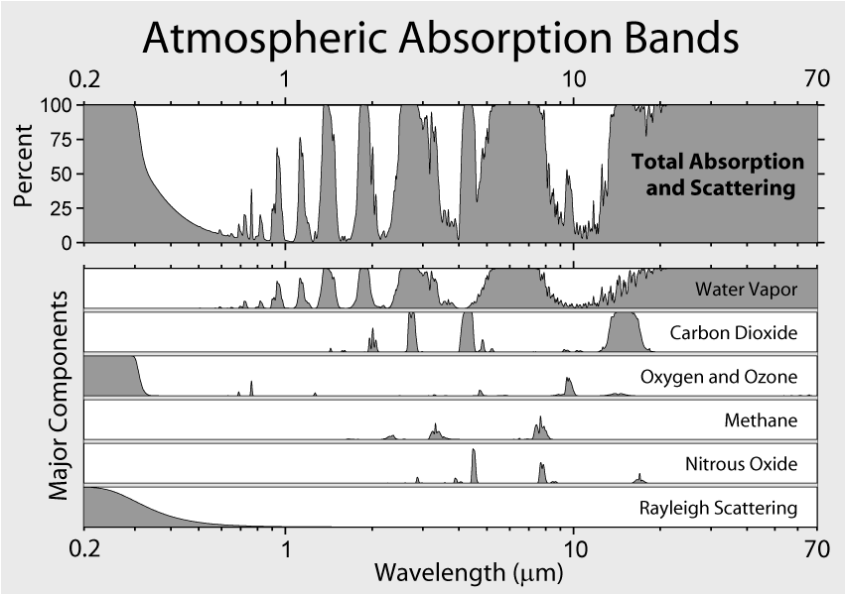

Figure 1: Atmospheric Absorption Bands. Common chemical species in the Atmosphere. Image created by Robert A. Rohde / Global Warming Art.

Gas absorption by the atmosphere alone is not the only factor that can block or change the direction of IR radiation. The other key component that affects IR radiation in the atmosphere and acts as a secondary factor in our planet's energy budget is cloud cover. Clouds affect both solar and IR radiation in many different ways. They act as a reflector and absorber of incoming solar radiation. They also act as an absorber and emitter of IR. One of the most comprehensive cloud climatological studies to date, the

International Satellite Cloud Climatology Project (ISCCP), explains that depending on the latitude, cloud cover can make up 45-80% of the total sky cover, with relative maxima in the tropics and upper mid-latitudes (Drake 1993). In this study, it was identified that (depending on latitude), low clouds such as cumulus and low stratus made up 10-40% of the total clouds, middle clouds like altocumulus and nimbostratus made up 10-20% of total cloud cover, and high cirrus and cirrostratus made up the remaining 30% of cloud cover. Regardless of being over land or over water, Liou (1986) also states that cirrus clouds make up roughly 20-30% of the total global sky cover.

Clouds make the transfer of atmospheric radiation quite different from gases, as they vary in shape, size, depth, optical depth, and are composed of many particles much larger than those of molecules. Different types of clouds will affect both solar and IR radiation differently. Low clouds are composed of spherical particles of water, and are almost completely absorbing in the far IR spectrum (Yang et al. 2003). Mid-level clouds are typically composed of spherical water particles, but may have some ice particles in them. High clouds are completely made of ice with varying particle structure, and affect all wavelengths even when optical depth is low. Cirrus clouds can be composed of hexagons, bullet rosettes, columns, plates, and other types of crystalline objects (Yang et al. 2005). Being able to parameterize the radiative properties of clouds (especially cirrus clouds) has been the subject of studies by Fu (Fu and Liou 1993) and Hong (Hong et al. 2009). It has been deduced that the main factors of clouds that affect transfer of radiation at a given wavelength is the cloud water path (or cloud water content) and the cloud particle radius (Hu and Stamnes 1993). Thus, extensive studies have been made to find accurate values of these two parameters.

Cloud water path (CWP) is defined as the total amount of liquid (or ice) between two points in the atmosphere and is measured in g/m^2. CWP is related to liquid water content (or ice water content) by the following relationship:

$$CWP = LWC * D \quad (4)$$

Where LWC (or IWC) is measured in g/m^3 and D is the depth of the cloud measured in meters. CWP has been found to be anywhere from 10 to 300 g/m^2 depending on the location in the world (O'Dell, Wentz, and Bennartz 2008). Horváth and Davies (2007) found an average cloud water path of roughly 100 g/m^2 for warm (low) clouds, but struggled to determine cold (high) clouds or clouds where precipitation was taking place. As part of the ISCCP, Drake (1993) notes that cloud water path varies by latitude from roughly 10-200 g/m^2. Based on seasonal fluctuations, cloud water path for the Antarctic and Arctic regions vary anywhere from 33 g/m^2 to 100 g/m^2, respectively (Briegleb and Bromwich 1998).

Briegleb and Bromwich (1998) also explained seasonal variability affects cloud particle sizes, particularly in the Polar Regions. Cloud particle sizes range from 10 μm in liquid and 20-30 μm in ice during June, July, August (JJA) to 10-30 μm of ice only in the northern hemisphere winter. Using the Moderate Resolution Imaging Spectroradiometer (MISR), effective cloud radius values were found to be anywhere from 5 to 25 μm in liquid clouds and 16 to 32 μm in ice clouds (King et al. 2013).

As noted above, these highly variant properties of clouds can have noticeable effects on the transfer of radiation. The more optically thick a cloud is, the more absorption of IR will take place, while optically thinner clouds may allow for more scattering of IR to occur. Different cloud particle shapes will affect the directions IR can be scattered to as

well. It is also possible, too, that multiple cloud layers may play a role in IR transmission through the atmosphere.

The transfer of radiation, specifically by scattering, in our atmosphere is not a modern idea. Its inception begins in 1905 with Schuster and his “foggy atmosphere” experiments. Schuster proposed that although absorption may be a primary process, scattering still exists if a medium has suspended particulates in it (Schuster 1905). Schwarzschild began using Schuster’s ideas by applying them into continuous fields of radiation. By 1916, the Eddington Approximation was developed. In the 1940s and 50s, Subrahmanyan Chandrasekhar began to apply radiative transfer to a so-called “plane parallel” atmosphere (Liou 2002) which was key to the development of the discrete ordinates method of radiative transfer. Through modern time, however, our potential for more knowledge of radiative transfer has increased. In 1989 the Atmospheric Radiation Measurement (ARM) program was developed, aiding to improve radiative transfer theories and knowledge with physical measurements of incoming and outgoing radiation from around the globe (Stokes 1994). The ARM program was a major milestone in gathering true values of radiative flux. The Southern Great Plains site in Lamont, Oklahoma continues to operate to this day.

With the advent of technology, computer models were also established to help predict the flow of radiation in the atmosphere. These models, aptly dubbed radiative transfer models, calculate the transmission (flux) of radiation and the heating rate at a given wavelength and given altitude. Fluxes are measured in W/m^2 and heating rates are measured in K/day. Some radiative transfer models take into account the key elements in our atmosphere that alter the flow of radiation as mentioned above: gas molecules and clouds. These different models can range in complexity. Undoubtedly the most rigorous

type is Line-By-Line Radiative Transfer Model (LBLRTM) (Wendisch and Yang 2012). LBLRTM calculates the transmissivity in the atmosphere by first calculating the absorption coefficient for every single spectral line across a set of wavenumbers. In high spectral resolution, there may be upwards of 50,000 lines just in water vapor alone (Zdunkowski, Trautmann, and Bott 2007). Absorption coefficients are also calculated at every level in the atmosphere due to its dependence on pressure and temperature. These computations require an enormous amount of time and computer resources, and are therefore seldom used. LBLRTM can make upwards of 10^6 calculations (Mlawer 1997), depending on the spread of wavelengths, atmospheric constituents, and the depth of the atmosphere. Thus, faster models called "band models" have been developed. These models use a statistical model approach in order to postulate a probability distribution function of line intensities/strengths. Because band models use statistics and not observed line spectra, they often have difficulty performing to the accuracy of line by line models especially with cloudy atmospheres.

Another statistical method to solve the radiative transfer problem in our atmosphere is the k-distribution. In any given spectrum, absorption coefficients are a highly repetitive occurring constant. Rather than integrating them in the order they appear, rearranging those absorption coefficients in order of strength (Lacis and Oinas 1991) can result in not only the same answer, but reduce calculation time. This grouping is also known as a frequency distribution. Taking the frequency distribution one step further and arranging them as a cumulative frequency distribution puts the absorption coefficients now in a so-called "g-space" ranging from zero to one. Taking the inverse of this cumulative frequency distribution is known as the k-distribution. During this process,

no spectral information is lost, thus the resulting answer is equal to that of the line by line method, without the immense amount of calculations (Mlawer 1997).

Dividing the g-space into subintervals can provide even fewer calculations by assigning a similar absorption coefficient for segments of the g-space. This, however, does induce some minor error when compared to the line-by-line method because fewer absorption coefficients are now being utilized instead of all of them in the spectral space.

The k-distribution method is for a single, homogeneous layer in the atmosphere. If we apply this method for a path that travels through multiple layers in the atmosphere, we get the correlated k-distribution (CKD) method. CKD applies to vertically inhomogeneous atmospheres by assuming a correlation between the absorption coefficient distributions and pressure/temperature for a given altitude (Fu and Liou 1992). This means that the k-distributions at one pressure/temperature can be the correlated with a different height since the distributions are rendered from a frequency domain. This method also allows for scattering processes by clouds and aerosols to be considered that random statistical models cannot handle well (Wendisch and Yang 2012).

One of the most well-known and developed radiative transfer models, the Rapid Radiative Transfer Model (RRTM), was developed by the Atmospheric and Environmental Research (AER) group in Massachusetts and ultimately ended up playing a role in the ARM program (Iacono 2000). RRTM calculates upward, downward, net fluxes, and heating rates across 16 bands in the IR spectrum. RRTM is validated against LBLRTM (Mlawer 1997) to a very high degree of accuracy, while only needing to compute on the order of hundreds of calculations, versus millions. RRTM utilizes the CKD method described above and also divides the g-space into 16 subdivisions. This method is the key to RRTM's extremely fast calculations. RRTM also uses a delta-M (Wiscombe 1977)

method of truncation, to help reduce scattering phase functions that are highly asymptotic (Coakley and Yang 2014).

The flux values and heating rates that radiative transfer models like RRTM calculate can be used in general circulation models (GCMs) and climate models (Hu and Stamnes 1993; Ebert and Curry 1992; Fu, Yang, and Sun 1998). GCMs and climate models take radiative flux values and heating rates and apply them to a defined grid space across the entire globe. While some use a coarser resolution, the amount of calculations needed to be performed worldwide is still extensive. Therefore, it is imperative that the speed of the radiative transfer models be quite fast. Unlike line-by-line models, the design of RRTM is ideal for these rigorous simulations and has even been applied to highly developed models like the European Centre for Medium-Range Weather Forecasts (ECMWF) (Morcrette 2001).

General circulation and climate simulations, however, use flux values and heating rates of IR radiation that either consider clear sky conditions (neglecting any existence of clouds) or are only affected by absorption of various mediums in the atmosphere (aerosols, clouds, and molecules). They have neglected scattering (Briegleb and Bromwich 1998) by these obstacles. Although this method produces similar accurate results for clear sky conditions, cloudy skies begin to diverge from the solutions provided by GCMs (Li 2002). Even Trenberth's global energy flow calculations did not mention scattering of IR in the outgoing longwave range. It is possible, as Schuster even suggested, that by including scattering of IR radiation by clouds into these simulations, the flux values and heating rates calculated throughout the atmosphere may be different enough that they are unable to be ignored (Stephens, Gabriel and Partain 2001). Stephens notes that outgoing longwave radiation errors of 8 W/m^2 (globally) and 20 W/m^2

(locally) can impact the lower latitudes of the Earth more than Polar Regions (where more cirrus clouds are less likely to be present). Even as recent as 2015, Qiang Fu suggests that neglecting scattering can potentially lead to errors in outgoing longwave radiation (Fu 2015). Therefore, it is imperative that further investigation into this topic be addressed.

The main objective of this research is to examine the validity of neglecting the scattering of IR radiation by clouds. Following similar studies done by Fu et al. (1997), Chou et al. (1999), and Joseph and Min (2003), an in-depth look at scattering of upwelling and downwelling infrared radiation in cloudy atmospheres will be examined as well as net flux and heating rates near the cloud layers. In all three studies, they concluded that neglecting scattered IR radiation could negatively affect general circulation models and climate models.

Through careful comparison of outputs from the validated and timely RRTM under numerous cloud parameters and characteristics, the goal is to provide more information about how the absorption and scattering of IR radiation by clouds may impact our global energy budget. Because RRTM is also broken into 16 bands within IR, another objective includes investigating which wavelength(s) are most affected by scattering. This additional analysis was not performed by any other of the previous studies.

2. PREVIOUS STUDIES

Three major studies were conducted in the past three decades that compared radiative transfer models with scattering of infrared radiation by clouds included and neglected. When applying radiative transfer models into GCMs and climate models, all studies note that the treatment of scattering of infrared radiation is usually ignored, as the absorption process is much more important (and more widely studied). Here we will discuss the three main studies, their different methodologies, and their results.

2.1 Fu et al. (1997)

The authors noted that while solar radiation and absorption of gas molecules and atmospheric particulates are studied widely, little attention is placed on the scattering of infrared radiation. Their study included comparing a multiple scattering discrete-ordinates delta-128 stream radiative transfer model to that of absorption only (AA), a modified scattering delta-2 stream (D2S), a modified scattering delta-4 stream (D4S) and a modified scattering delta-2 and delta-4 stream combination (D2/4S). All four methods were tested against an atmosphere that had 5 different cloud layer combinations:

- Only low clouds
- Only mid-layer clouds
- Only high clouds
- All three layers combined
- No clouds (clear sky)

Downward fluxes were calculated first, by setting the top of the atmosphere equal to zero and then working backward to calculate upward fluxes. The D2S approximation is the simplest form of multiple scattering effects. The D4S approximation uses the same

methods as the D2S, but now with four streams instead of two. The D2/4S approximation solves the plank function first with the D2S method, then calculates the fluxes with the D4S. All methods divide the atmosphere into a number of homogeneous layers and use a CKD approach. There are 11 optical depths that are used, ranging from 0.1 to 50. The atmospheric profiles used are mid-latitude summer (MLS) and sub-arctic winter (SAW). The range of the infrared spectrum applied is from 4.54 μm (2200 cm^{-1}) to 10,000 μm (roughly 1 cm^{-1}). Chemical species included in the absorption bands were H_2O, CO_2, O_3, CH_4, and N_2O. The mixing ratio of CO_2 was 330 ppm. LWC was 0.22 g/m^3 and 0.28 g/m^3 with an effective radius of 5.89 μm and 6.2 μm for low and mid-layer clouds respectively. High clouds had an IWC of 0.0048 g/m^3 and an effective radius of 41.5 μm. Vertical resolution was 0.25km and surface emissivity was 1.0. With this resolution the LWCs (IWCs) in terms of CWP is 55, 70, and 1.2 g/m^2 for low, mid, and high clouds respectively.

Under clear sky conditions, all the scattering approximations (D2, D4, D2/4S) computed fluxes both upward and downward with less than 1 W/m^2 difference in the AA approximation. This means that without any clouds in the atmosphere, the flux values when IR scattering was included were roughly the same as when it was neglected. Thus, they determined that scattering of gas molecules can be considered zero or negligible.

But when clouds were included, the AA flux values began to diverge from the values in the delta-128 stream case. When only low clouds were considered, the difference in flux values between the AA case and the delta-128 was 5.2 W/m^2 at the top of the atmosphere (TOA) and -0.6 W/m^2 at the surface (SFC). When mid-layer clouds were only considered, difference in flux values between AA and delta-128 were 6.4 and -1.3 W/m^2 for TOA and SFC, respectively and when high clouds were only considered, the difference was 6.0 and .5 W/m^2 for TOA and SFC respectively. When all three cloud

layers were considered, the values were 8.2 and -0.6 W/m^2 for TOA and SFC respectively. All of the other scattering methods (D2, D4, and D2/4S) values for all combinations of cloud cover ranged between -1.9 to +0.2 W/m^2 for the TOA and -0.1 to +1.5 W/m^2 for the SFC.

As a final test, they compared the 128-stream flux values to the non-modified original two-stream approximation and discrete-ordinates methods. These results produced differences in flux values ranging between -3.9 to +33.3 W/m^2 at the TOA and -0.8 to +63 W/m^2 at the SFC.

They concluded the original two-stream approximations need to be modified in order to be considered for all atmospheres (cloudy and clear) and that scattering needs to be included when computing infrared radiation fluxes in cloudy atmospheres. They also note that the biggest divergence in values comes from optically thin cirrus clouds.

This study had two important pieces of information missing: the depth of the atmosphere (and how many layers were being used), and the shape of the particles used, which are critical details. They also did not specify the actual heights (in meters or in millibars) of the clouds they used.

2.2 Chou et al. (1999)

The authors note that scattering in longwave (IR) radiation is often not included in GCMs and climate models because the absorption process dominates and scattering calculations take excessive computer resources and time. The main objective of their study was to develop a multiple scattering parameterization that can handle scattering of IR while not adding computational time. This was then compared to an absorption only scheme developed by Chou et al. (1993) and Chou and Suarez (1994). Their scattering method includes the discrete-ordinates method developed by Stamnes et al. (1998). The

comparisons were done using a k-distribution (not a CKD like in the previously mentioned study). Their atmosphere stopped at 20mb and they did not include the gases N_2O, CH_4, O_3, or any CFCs. Clouds are set at three layers:

- Low clouds between 800-875 mb
- Mid-layer clouds between 500-575 mb
- High clouds between 200-275 mb

Cloud particle effective radius for the low, mid, and high clouds is 8, 8, and 50 µm respectively. The high clouds were significantly different than from Fu et al. (1997). Optical thickness ranges from 0.5 to 20. The atmosphere was broken into 75 layers, each layer being roughly 25 mb thick. Atmospheric profiles were done using mid-latitude summer (MLS) and sub-arctic winter (SAW). Liquid clouds were parameterized with Mie Theory as spherical particles, and ice clouds were parameterized as hexagons from the Fu et al. (1998) parameterization scheme. The part of the IR spectrum that they analyzed extended from 4 to 100 µm (100 to 2500 cm^{-1}).

Results of the Chou et al. study show that when scattering is neglected, TOA flux differences range between roughly 4 and 8 W/m^2 for high clouds, 4 and 7 W/m^2 for mid-layer clouds, and between 2 and 3 W/m^2 for low clouds. SFC flux differences did not diverge as much, having a spread of roughly -1 to -1.5 W/m^2 for high clouds, -2 to +3 W/m^2 for mid-layer clouds, and -2.5 to -3.5 W/m^2 for low clouds. They did not perform any tests when all three cloud layers were included together.

Additional comparisons were done with high cloud radii being increased to 95 µm (even higher than in Fu et al. (1997)) and mid/low clouds increased to 16 µm. Results dropped the difference in flux values at the TOA by roughly 4 W/m^2 for high clouds, and

by 2-4 W/m^2 for mid and low clouds respectively. SFC flux values decreased by roughly 1-1.5 W/m^2 for all three cloud layers. The biggest flux differences in all three cloud layers occurred when optical thickness was approximately 2.

Heating rates were compared in this study as well, with the same conditions applied when computing flux values. Compared to when scattering is not included in the calculations, heating rates at the cloud layers would peak near -1 °C/day (cloud top) and +1 C/day (cloud bottom) for high and mid-layer clouds, and -.5 °C/day (cloud top) to +.5 C/day (cloud bottom) for low clouds. When optical depth of the clouds was increased from 5 to 25, heating rates differences dropped from 8% to 3%.

They concluded that the effect of scattering was too high to be left out of GCMs, especially in high, optically thin cirrus clouds. These clouds had the biggest change in flux values on the TOA and low clouds had the biggest change in flux values at the SFC. If an additional scaling of optical depth was performed (that allowed backscattering in the emission layer), their differences in flux at the TOA and SFC was reduced to roughly 4 and 2 W/m^2 respectively. Magnitudes were reduced slightly when particle sizes were doubled in both the high and low/mid-layer clouds. Difference in flux values for the SAW profile were on the order of 1 W/m^2 lower than MLS.

Unlike the Fu et al. (1997) study, no actual computed values were presented in the article, only graphs. Thus, all values of the flux and heating rate differences presented here were interpolated by me. Their study also did not include an atmosphere when all three cloud layers were in existence simultaneously. As noted from the Fu et al. (1997) study, the highest differences in flux values were in the case when multiple cloud layers were stacked together. It is possible that similar results would occur in this case as well. The vertical resolution was also measured in millibars, not kilometers, therefore the

resolution changed instead of remaining constant. By consequence, higher clouds will be physically thicker than lower clouds, which is generally incorrect.

2.3 Joseph and Min (2003)

Four years after the Chou et al. (1997) study, Joseph and Min (2003) did a similar study of comparing flux values at the SFC and TOA when scattering of IR is neglected. They note that IR radiative transfer in cloudy conditions has not been a priority due to the dominance of absorption of water vapor being such a primary process in the atmosphere and computing time would increase when applied in a climate model. Joseph and Min (2003) also cite the Fu et al. study performed in 1997. The objective of this study is to not only examine the negligible effect of scattering on IR flux values, but also to attempt to quantify these results with real data from the Great Plains site in the ARM program.

The authors use a radiative transfer model developed by Fu and Liou (1992). This includes cirrus clouds being parameterized as hexagons, and a delta-4 stream (D4S) approximation used to compute the IR portion of the spectrum, which is divided into 12 bands. Atmospheric conditions are taken directly from soundings performed at the ARM site, instead of generalized MLS or SAW profiles as done before. This was a major difference than previous studies, as it used real-time meteorological conditions instead of theoretical ones. Conditions were acquired on 28 October 1997 between 14 and 16 Zulu (Z) time and between 18 and 20Z. This particular date was chosen because only thin cirrus clouds were present. Clouds were input based on a combination of lidar heights, reflectivity from the radar, and temperature/moisture profiles from the soundings. Cloud particle size was estimated to be 30 μm in radius. They also performed the same comparison with particle size radii of 20 and 50 μm. Optical depth was between 0.1 and 10.

Results from the study were similar in nature to the previous two, noting that when scattering of IR by clouds was neglected, outgoing radiative flux was about 6-7 W/m^2 higher and downward incoming flux at the surface was lower by about 2 W/m^2. These maximums occurred when optical depth was between 2 and 4. Using a smaller radius of 20 μm, the differences went up by about 1 W/m^2 and using a higher radius of 50 μm, the differences went down by about 2 W/m^2.

Similarly to the Chou et al. (1999) study, the greatest increase in flux differences occurred when optical depth rose from 0.5 to 2, and slowly decreased past optical depths of about 4, before showing an asymptote around 5 W/m^2 (TOA) and 1 W/m^2 (SFC).

Heating rates were also compared in this study, with the same atmospheric conditions used above. When IR scattering by clouds was neglected, the base of the cloud difference was approximately -0.2 K/day and the top of the cloud was +0.2 K/day. These differences varied very little when optical depth was changed or when particle size was changed.

Joseph and Min (2003) go further to note that radiative transfer models always assume plane-parallel cloud layers, but in reality clouds are non-homogenous and vary greatly in depth and width. Instead of using fixed optical properties, they used half-hourly time averaged cloud properties and atmospheric conditions. Difference in TOA flux values from these nonhomogeneous conditions when scattering was neglected varied widely between -20 to +35 W/m^2. SFC flux values varied between -10 and +5 W/m^2. Heating rate differences maxed at -0.5 and roughly 1.3 K/day for the bottom and top of the cloud respectively.

The authors conclude that the neglect of scattering in calculations produced an approximate 3% difference in observed irradiance at the ARM site and claimed this was

“relatively important”. Changes in optical depths and cloud particle sizes from those observed on 28 October 1997 would result in a few W/m^2 change as well. The biggest source of differences, however, came from applying non-homogenous atmospheric conditions, increasing flux value differences as much as 14% of observed irradiance. This is significant because most radiative transfer models use atmospheric conditions that are constant, which is not the case in day to day (or even hour to hour) observations.

This study did not have any clouds located in the low or middle layer(s) of the atmosphere, which could have produced different results for both TOA and SFC. The authors never mentioned at what range of wavelengths (or wavenumbers) the radiative transfer calculations were made, but it is assumed to be between 4 and 100 μm (100 – 2500 cm^{-1}) as similar studies have often truncated the very far and near-IR portions of the spectrum. They also neglected to mention which chemical species were included in the atmosphere. Similar to the Chou et al. (1999) study, no tables of actual calculated results were presented; so all flux values and difference in flux values presented here are estimated by me from their graphs.

3. METHODOLOGY

In order to deduce the importance of scattering of IR radiation using RRTM for this study, numerous tests across various atmospheric profiles and cloud characteristics must be conducted. RRTM will run with the same atmospheric conditions using both an absorption only method, and a scattering method. Absorption only method was done using RRTM's algorithm, and scattering was done using the discrete-ordinates method (DISORT) developed by Stamnes et al. (1988). This is similar to the three studies mentioned above. The number of quadrature angles used in the absorption only method is 2 and the number of streams used in the DISORT method is 16. The following parameters were set:

- Atmosphere Profile: Mid-latitude summer (MLS), Subarctic Summer (SAS), Mid-latitude Winter (MLW), Tropical (TRP), a profile from the International Radiative Transfer working group (Garand et al. 2001), and the Garand profile but with a doubled carbon dioxide concentration. Figure 2 shows the atmospheric temperature profiles. All five profiles were updated with modern (400 ppm) carbon dioxide amounts as of June 2015.

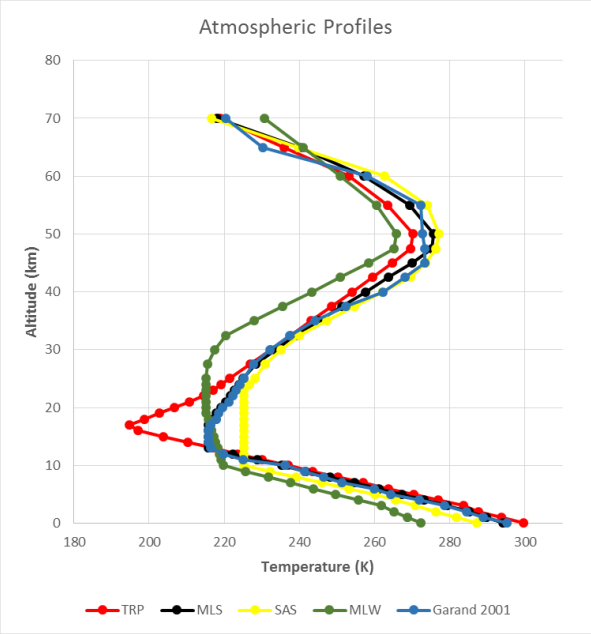

Figure 2: Atmospheric profiles. This includes Tropical, MLS, SAS, MLW, and Garand 2001

- Cloud Particle Size (radius) in μm: Limitations on particle radius in RRTM for spherical particles is 5 – 131 μm and 5 – 140 μm in hexagons. Particle sizes chosen were 10, 20, 30, 40, 50, 60, 70, 80, 90, and 100 as these span a range of typical observed values around the globe. These values were chosen to show a wide array of possible effective cloud radii and were used in both low and high clouds.
- Cloud Particle Shape: spheres for low, liquid water clouds (Key and Schweiger 1997) and hexagons for high, ice clouds (Fu, Yang, and Sun 1998).
- Cloud Water Path (CWP) in g/m^2: In order to asses different optical thicknesses of clouds, CWP was chosen from extremely miniscule to incredibly thick. These values are 1, 5, 10, 45, 85, 125, 225 and 375 to span a wide variety of observed values as noted from section one. They are used simultaneously in both low and high

clouds. These values correspond to liquid (or ice) water content (LWC/IWC) of 0.004, 0.02, 0.04, 0.18, 0.34, 0.5, 0.9, and 1.5 g/m^3 respectively.

- Cloud Layers: three different combinations of clouds will exist:
    - Only at 750mb
    - Only at 250mb
    - Both 250 and 750mb.

In order to assure proper controls, only one parameter was changed in each RRTM run, while the rest remained constant. This amounted to 8,640 total model runs to calculate heating rate (K/day), upward flux (W/m^2), downward flux (W/m^2), and net flux (W/m^2) throughout the atmosphere. Calculations were then compared in the following methods:

Method 1: Absorption Only in RRTM VS. Absorption + Scattering in DISORT

Method 2: Absorption Only in RRTM VS. Absorption Only in DISORT

Method 3: Absorption Only in DISORT VS. Absorption + Scattering in DISORT

The atmosphere that was examined was 66.1 km in height, broken into 82 separate plane-parallel homogeneous layers with the surface (SFC) starting at layer 0 and the top of the atmosphere (TOA) ending layer 82. This height spanned the entire troposphere and the majority of the stratosphere. Each layer from the surface to 15 km (roughly the tropopause) was 0.25 km thick. Each layer above 15 km was 2.5 km thick, with the last layer being 1.1 km thick. For consistency issues, layer numbers were used to identify key features as the height of these layers were different based on the relationship of pressure and temperature in the atmospheric profile. Clouds were inserted at layer 10 and layer 42. The tropopause, roughly the beginning the stratosphere, was at layer 60.

The chemistry of the atmosphere included gas molecules of H_2O, CO_2, N_2O, O_3, O_2, N_2, CH_4, CO and four halocarbons/chlorofluorocarbons: CCL_4, CFC_{11}, CFC_{12}, and CFC_{22}. The emissivity of the surface was set to 1.0 across the entire spectrum.

These tests were conducted across the IR spectrum from 3.08 to 1000 μm in wavelength (3250-10 cm^{-1} in wavenumber). This part of the IR spectrum was broken down into 16 different bands. Appendix H shows the breakdown of the 16 bands and the chemistry included in each one. Although much of the consideration will be paid to the difference in upward flux values at the TOA and downward flux values at the SFC, all layers were analyzed. All 16 bands were analyzed as well to see which ones were most susceptible to scattering processes.

The parameterizations for the cloud particle shapes have produced two slightly different single scattering albedos (SSA) and asymmetry factors (AF). Figure 3 shows the SSA for spheres.

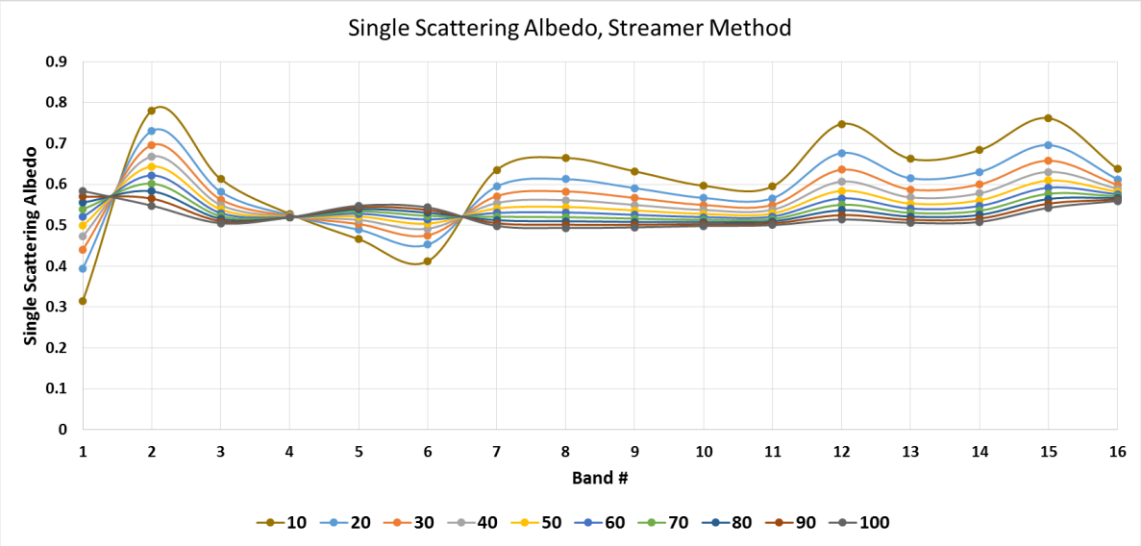

Figure 3: Single Scattering Albedo for Spheres

Figure 4 shows the SSA for hexagons.

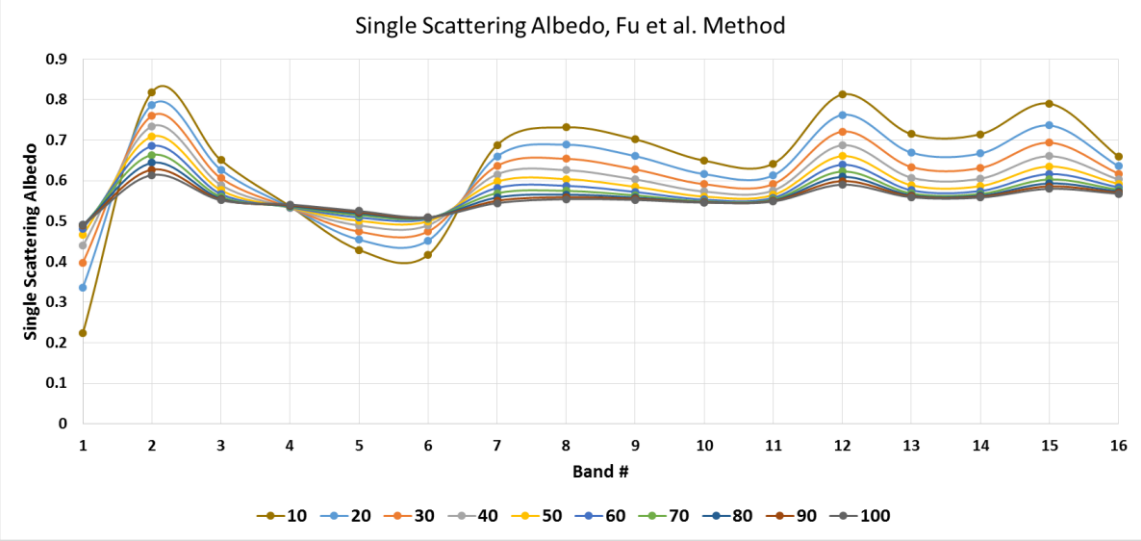

Figure 4: Single Scattering Albedo for Hexagons

These values are shown for all 10 particle sizes mentioned above. SSA is a ratio of the scattering coefficient to the total extinction coefficient. Values closer to zero indicate that more absorption takes place, whereas values closer to one indicate that more scattering takes place. AF is a measurement of the angular distribution of the radiation scattered by the particle. Values closer to -1 indicate more backwards scattering, whereas values closer to +1 indicate more forward scattering.

For both the spherical particles and hexagonal particles, it is important to note that the SSA for bands 1, 5, and 6 decrease when particle size decreases. For bands 2, 3, and 7-16, SSA increases when particle size decreases. Band 4 has roughly the same SSA for every single particle size (roughly 0.53). Hexagonal particles show a larger spread in values based on particle size and are also generally higher in value than spherical particles.

The AF is roughly the same for both particle shapes, with a pattern of increasing forward scattering as particle size increases. The two major differences between the two lies in the lower bands (far infrared) where spherical particles have lower values, especially in smaller particle sizes, and in the higher bands (near infrared) where hexagon particles have lower values, especially in smaller particles. It should be noted that values for all particle shapes and sizes are positive, leaving the amount of backscattering to an extreme minimum. Figure 5 shows the AF for spheres.

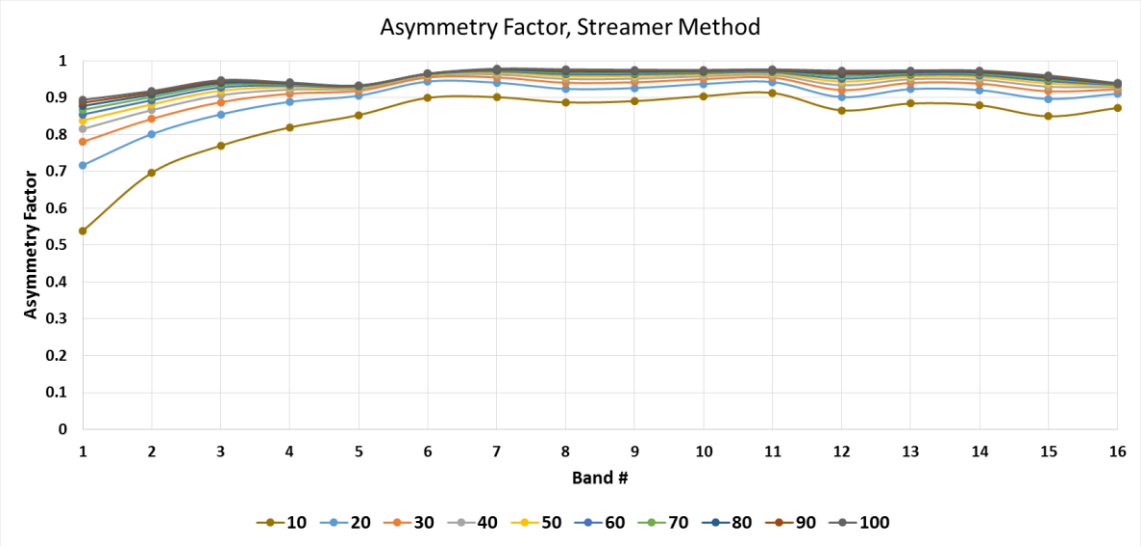

Figure 5: Asymmetry Factor for Spheres

Figure 6 shows the AF for hexagons.

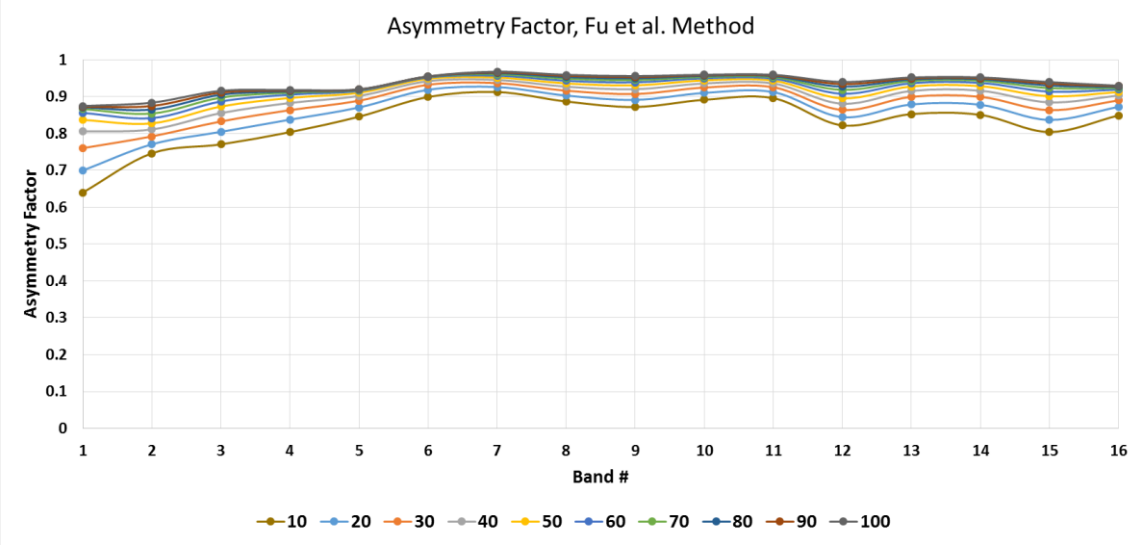

Figure 6: Asymmetry Factor for Hexagons

RRTM's absorption only method calculates fluxes by integrating the radiance function over a hemisphere. The radiance is given by Equation 5:

$$R' = R_o + A(B_{eff} - R_o) \quad (5)$$

Where R' is the outgoing radiance, R_o is the incoming radiance for the subinterval, A is the absorptance, and B_{eff} is the effective Planck function. The effective Planck function is defined as equation 6:

$$B_{eff} = \frac{B_{lay} + .2\tau B_{bnd}}{1 + .2\tau} \quad (6)$$

Where B_{lay} is the Planck function at the mean layer temperature, B_{bnd} is the Planck function at the temperature of the layer's exiting boundary, and τ is the optical depth.

The version of RRTM that is being utilized is v3.3, dated May 2010 and was downloaded from AER's website: http://rtweb.aer.com/.

4. DATA AND ANALYSIS

Output from RRTM's calculations was produced in column format and showed the upward flux, downward flux, net flux, and heating rates for all layers of the atmosphere. This output was designed to be imported easily by programs like Microsoft Excel.

Figure 7 shows an example of upward flux for the entire 82-layer atmosphere across the entire spectrum domain when absorption by the cloud(s) and gas(es) were the only considerations. These fluxes only changed slightly across the various atmospheric profiles and the two different cloud particle shapes. The values changed much more drastically among the different particle sizes and the different cloud water paths. Heating rates spiked just below the cloud surfaces and decreased significantly in the stratospheric layers of the atmosphere due to the increased amount of ozone.

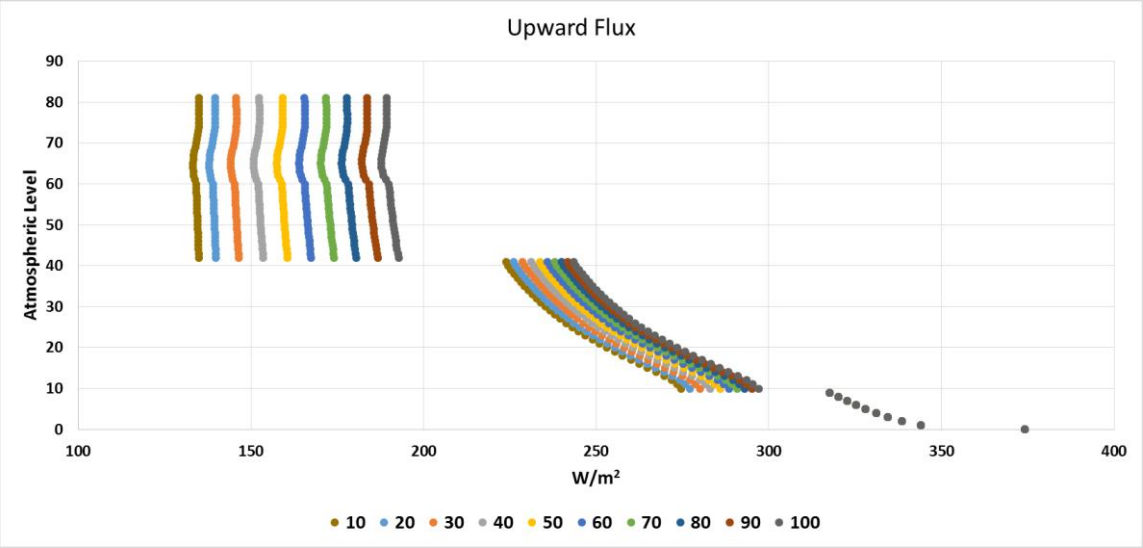

Figure 7: Upward Flux example for absorption only. This is when gas molecules and clouds are considered and is for the MLW atmospheric profile under a cloud water path of 45 g/m²

For upward and net fluxes, as particle size increased, the amount of flux through the cloud layer increased. However, for downward flux, the amount of flux through the cloud layer decreased when particle size increased. For a constant value of cloud water path, the optical depth increased when particle size decreased. Thus, 10 and 20 μm particles permitted the least amount of radiation to be transmitted (across all wavelengths).This matches with conclusions for optical depth derived by Yang (Yang et al. 2001) when defining properties of cirrus clouds. RRTM calculates optical depth similarly to Yang et al. (2001) but in terms of CWP instead of IWC.

As CWP increased, the amount of flux through the cloud layer decreased. This makes sense, as the more water present in the cloud, the more radiation it can absorb, thus transferring less through it. For a constant value of particle size, the optical depth increased when cloud water path increased. This is independent of the atmospheric profile as optical depth is a property of the cloud and not the surrounding atmosphere. In cloud layers with smaller cloud water path values, heating rates just below the cloud decks increased as particle size increased. In clouds with large cloud water paths, heating rates were generally unchanged across particle sizes.

Figure 8 shows an example of upward flux calculations when scattering by the clouds was included. Similar to when absorption was the only process considered, the flux values changed more with particle size and cloud water path rather than atmospheric profile and/or particle shape. For a fixed cloud water path, as particle size increased, the amount of radiation transmitted increased. Consequently, for a fixed particle size, as cloud water path increased, the amount of radiation transmitted decreased.

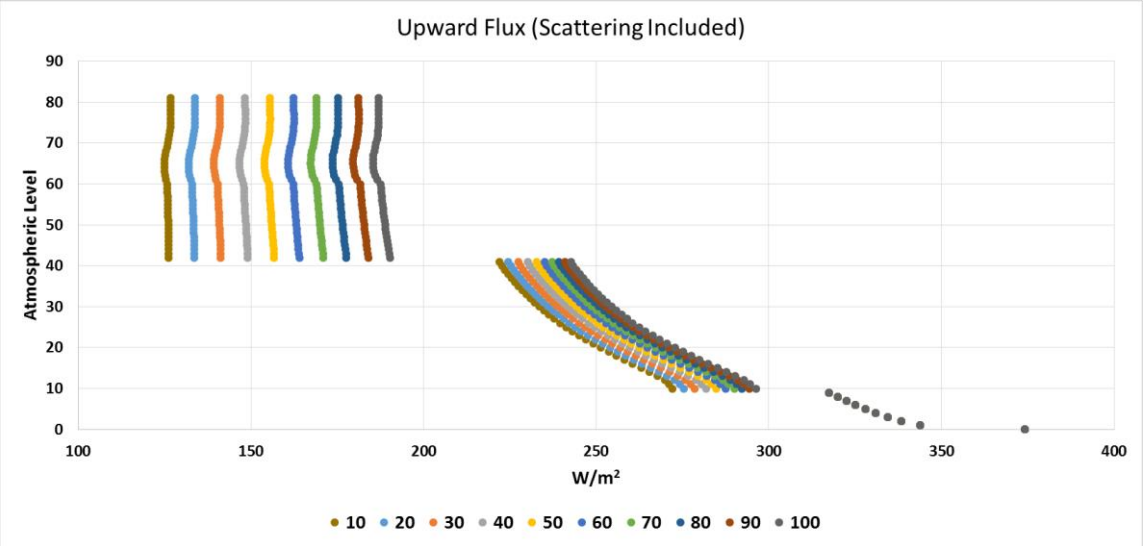

Figure 8: Upward Flux example for absorption + scattering. This is for the MLW profile with a cloud water path of 45 g/m²

Figure 9 shows an example of the difference between the upward fluxes of the two calculations mentioned above. For this analysis, positive values indicate that the absorption only method was higher.

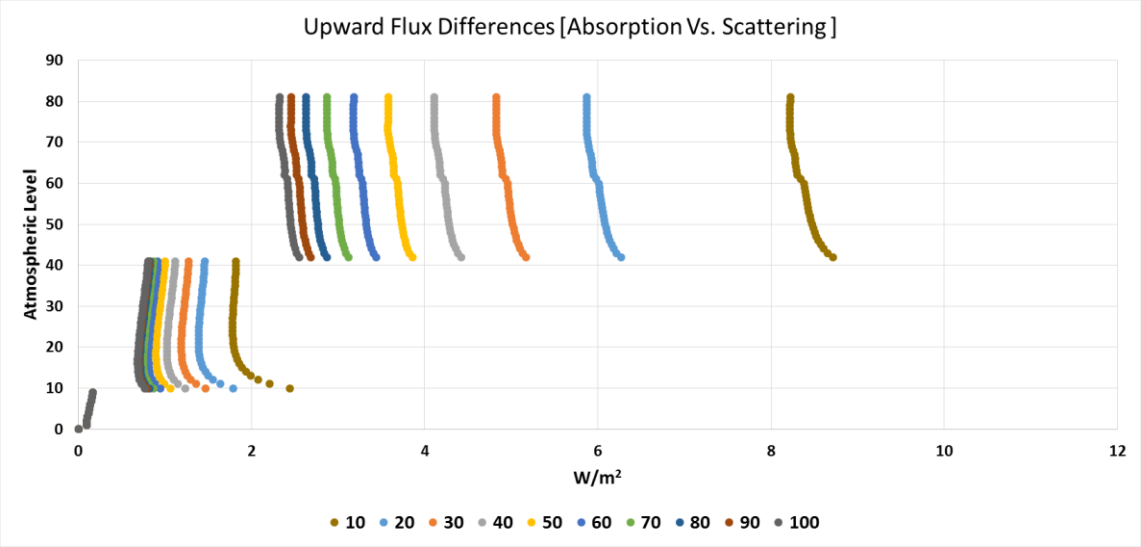

Figure 9: Upward Flux difference. This is for the MLW profile and a cloud water path of 45 g/m2

Analysis of the calculations performed by RRTM will be broken into three parts: absorption only (RRTM) vs absorption + scattering (DISORT); absorption only (RRTM) vs absorption only (DISORT); and absorption only (DISORT) vs absorption + scattering (DISORT). The first method examines how the magnitude of flux is changed when scattering of longwave IR is done by cloud. The second method compares fluxes in the CKD method versus the discrete ordinates method. The third method is the same as the first, but neglects the absorption of atmospheric gases outside of the clouds and uses only the discrete ordinates method.

4.1 Absorption Only (RRTM) vs Absorption + Scattering (DISORT)

Calculations of upward and downward flux were first performed with the RRTM algorithm across the various particle sizes, atmospheric profiles, cloud water paths, and cloud particle shapes. Calculations with the DISORT model were performed second. The

values when scattering was included were then subtracted from when scattering was not considered, creating a difference between the two methods as briefly shown in Figure 8.

We will first look at the results from when both low clouds and high clouds were considered. The overall pattern from optically thin clouds (1 g/m^2 cloud water path) to extremely optically thick clouds (375 g/m^2 cloud water path) was roughly the same for both spheres and hexagons as particle shapes (regardless of atmospheric profile) with hexagons producing slightly larger differences, especially in larger particles. Figures shown here are all for the MLW case. Appendix A-G show calculations for the other five atmospheric profiles which generally vary little from the MLW case.

For differences in upward TOA flux, values were between 0.5 (100 μm particles) to 4 (10 μm particles) W/m^2 when cloud water path was 1 g/m^2. These differences then increased exponentially when cloud water path increased to 10 g/m^2. Smaller sized particles saw the largest increase, but by 10 g/m^2, values ranged from generally 1.5 W/m^2 (100 μm particles) to 11 W/m^2 (10 μm particles) for spheres and 2.5 W/m^2 (100 μm particles) to 11.5 W/m^2 (10 μm particles) for hexagons.

After cloud water path values reached 125 g/m^2, all flux difference values began to show signs of an asymptote, leaving roughly the same difference for each particle size at cloud water path values of 125 as at 375 g/m^2. This is because at this point there is so much water present in the cloud that absorption becomes the dominant process, regardless of particle size. With the large amount of water present, the cloud is acting almost as a perfect blackbody. Although the patterns were roughly the same, hexagonal particles produced upward flux differences at TOA higher than spherical particles, especially for larger particles. Larger particles produced differences that reached upwards of 3.5 W/m^2 for hexagonal particles, but only 2.25 W/m^2 for spherical particles. The largest

difference (11.71 W/m^2) in upward TOA flux occurred in the tropical atmospheric profile with hexagon particles, a particle size of 10 µm and a cloud water path of 10 g/m^2. All upward TOA flux differences were positive, meaning when absorption was the only consideration, outgoing upward flux values were higher than when scattering was included. Figure 10 shows the MLW case, while the other profiles are shown in Appendix A.

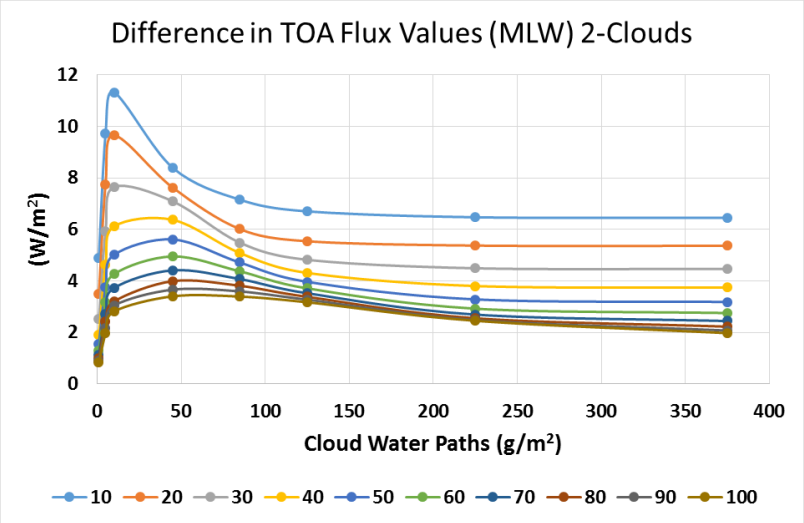

Figure 10: Method 1: Difference in upward TOA flux for 2-clouds. Positive values indicate flux was higher when scattering was neglected:

Downward SFC flux values for increasing cloud optical thickness showed a different pattern. For optically thin clouds, difference in flux values ranged from near -0.5 (100 µm particles) to -1.5 W/m^2 (10 µm particles). As with upward flux differences, magnitudes rose (negatively) significantly when cloud water path increased to 10 g/m^2 ranging from about -0.75 (100 µm particles) to -3 W/m^2 (10 µm particles). As more water was added into the cloud, smaller particles began to have smaller differences than larger

particles. Between 45 and 125 g/m^2, 10 and 20 µm particles produced flux differences that were about a 1 W/m^2 less than those of 90 and 100 µm particles. As cloud water path values were increased to 125 g/m^2, flux differences began to show signs of an asymptote and revert to the original orientation: smaller particle sizes producing the larger (negative) differences. However, unlike upward TOA flux differences, the spread in flux difference values across the various particle sizes at cloud water path of 375 g/m^2 were within 1 W/m^2 of each other. The largest difference produced (-3.68 W/m^2) occurred in MLW, for 10 µm particles, hexagon particle shape, and a cloud water path of 10. Almost all values for downward SFC flux were negative except in the tropical case, where some values in optically thin clouds were actually positive. But the overwhelming trend across all atmospheric profiles indicates that when scattering is included, downward SFC flux values are higher than when scattering is neglected. Figure 11 shows this analysis for the MLW case and the other profiles are in Appendix A.

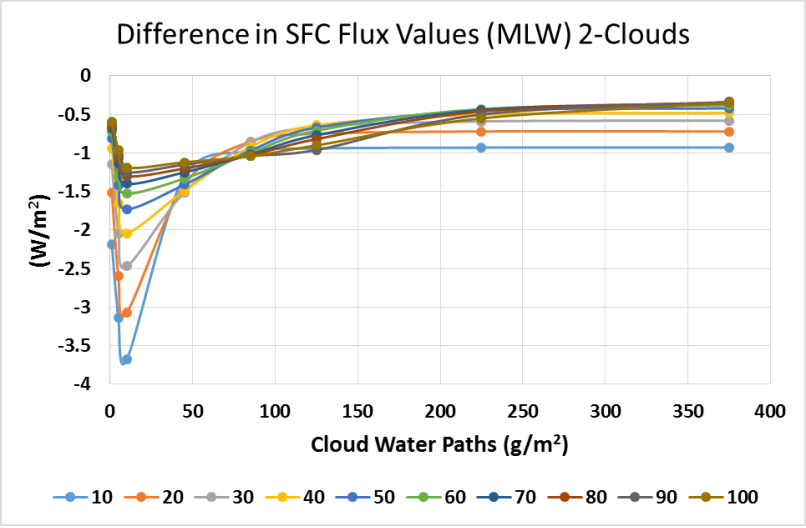

Figure 11: Method 1: Difference in downward SFC flux for 2-clouds. Negative values represent that flux was greater when scattering was included

Next, we will look at the case when only low clouds were considered. These cloud particle shapes are only spherical. For upward TOA flux differences, all values were reduced significantly when compared to the two-cloud case, but the same pattern was produced: very low numbers for a cloud water path of 1 g/m^2, exponentially increasing when cloud water path was raised to 10 g/m^2 (especially for smaller particle sizes), and leveling off after cloud water paths of 125 and 225 g/m^2. The reduction in flux differences makes sense as the low clouds have much more water vapor in them, providing an opportunity for more absorption to take place and less scattering. All values were positive, regardless of particle size and atmospheric condition. The largest difference (3.0 W/m^2) occurred under the MLW atmosphere with a particle size of 10 µm and a cloud water path of 10. Figure 12 shows this analysis for the MLW case and the other profiles are in Appendix B.

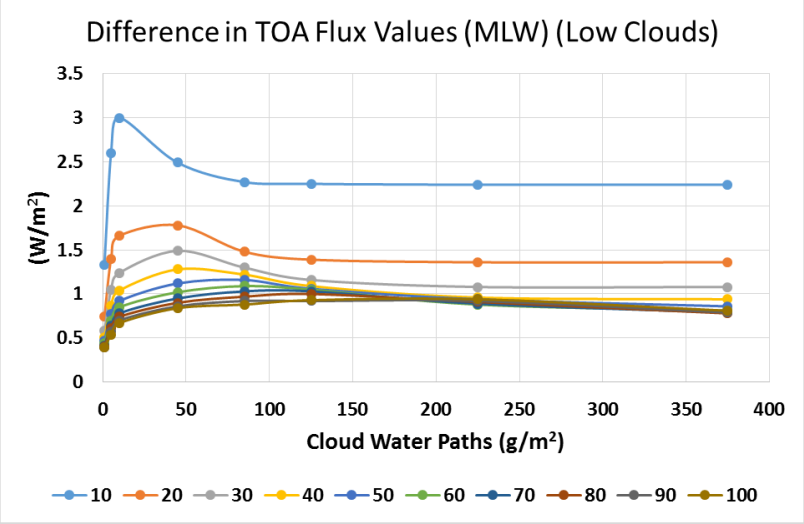

Figure 12: Method 1: Difference in upward TOA flux for low-clouds. Difference in upward TOA flux for MLW for 10 particle sizes when only low clouds were considered. Positive values indicate flux was higher when scattering was neglected

For downward SFC flux differences, the pattern remained the same as the two-cloud case. Very low differences were present for a cloud water path of 1 g/m^2 and increased significantly when cloud water path increased to 10 g/m^2. A small window of smaller particles producing smaller differences occurred when cloud water path was between 45 and 85 g/m^2. All differences eventually converge towards similar values for all particle sizes for cloud water paths greater than 225 g/m^2. The differences in this scenario were smaller than when two cloud layers were considered, but not as much change as upward TOA flux. As with the two-cloud consideration, almost all values were negative except in the tropical case where cloud water paths of 10 g/m^2 or less were positive. The largest difference (-2.74 W/m^2) occurred in the MLW atmosphere with a particle size of 10 μm and a cloud water path of 10. This pattern indicates that scattering of radiation in upper level clouds has a smaller effect on the SFC than scattering of radiation in the lower level clouds. Figure 13 shows this analysis for the MLW case and the other profiles are in Appendix B.

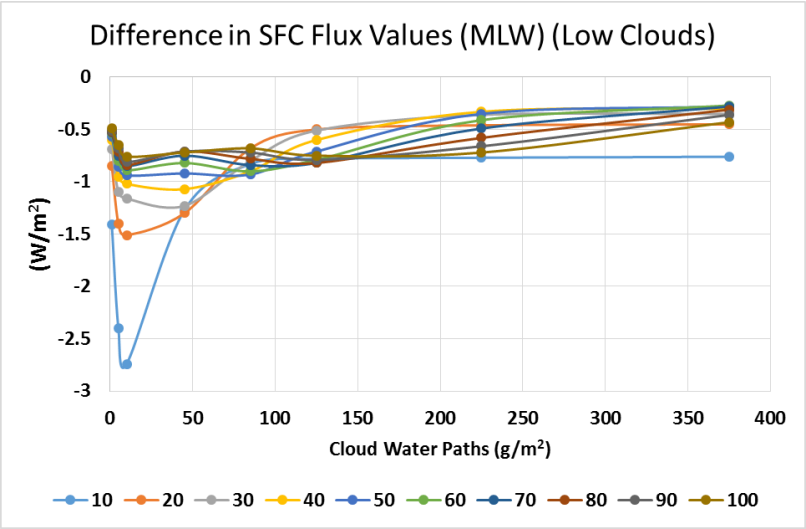

Figure 13: Method 1: Difference in downward SFC flux for low-clouds. Difference in downward SFC flux for MLW for 10 particle sizes when only low clouds were considered. Negative values indicate flux was lower when scattering was neglected

Third, we will look at the scenario when only high clouds are considered. These particles are only hexagons and are all ice. Upward TOA flux differences produced the same pattern as the low-cloud case and two-cloud scenario, but magnitudes were closer (if not higher in some instances) to that of the two-cloud scenario. Once again low differences in flux were produced when cloud water path was 1 g/m^2, exponentially increased when CWP was increased to 10 g/m^2, and leveled off after 125-225 g/m^2. In all atmospheric profiles, 90 and 100 µm particles actually had higher difference values when cloud water path was 85 g/m^2 or higher, sometimes approaching 3.5 W/m^2 higher than the 2-cloud case. The largest difference (11.54 W/m^2) occurred again in the tropical case, with a particle size of 10 µm and a cloud water path of 10. This pattern indicates that cirrus clouds have a greater impact on upward TOA flux when scattering is included than lower clouds do. Figure 14 shows this analysis for the MLW case and the other profiles are in Appendix C.

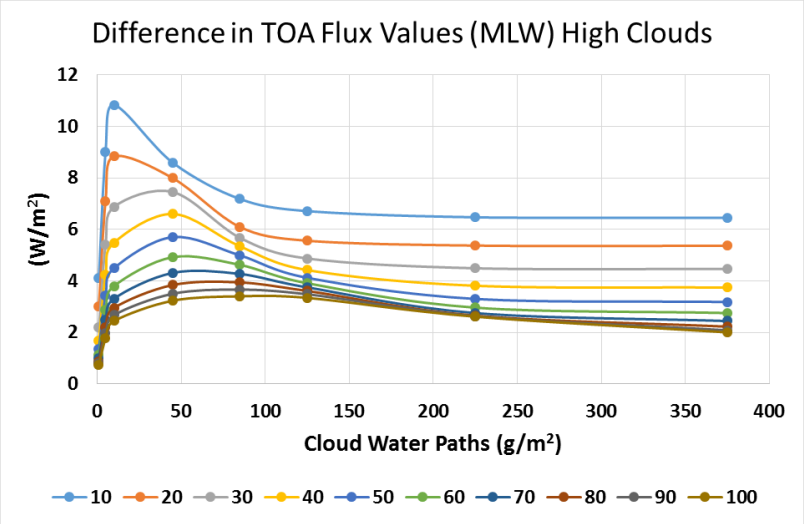

Figure 14: Method 1: Difference in upward TOA flux for high-clouds. Difference in upward TOA flux for MLW for 10 particle sizes when only high clouds were considered. Positive values indicate flux was higher when scattering was neglected

For downward SFC flux differences, values were roughly the same for all cloud particle sizes in all atmospheric profiles as the two-cloud case, but only for cloud water paths of 10 g/m^2 or less. Unlike the two-layer and the low-cloud only cases, smaller particles produced larger flux differences for all cloud water paths. The pattern here is more of a mirror image (in shape, not in magnitude) of the upward TOA flux difference in the high-cloud only scenario. After cloud water paths of 85 g/m^2, differences for all particle sizes begin to level off and have a large spread amongst them. Larger particles sizes produced larger differences compared to when the low-cloud or two-cloud cases were performed. For almost all atmospheric profiles, differences in SFC flux were negative, and we infer that flux values at the SFC are higher when scattering is included. This is shown in figure 15.

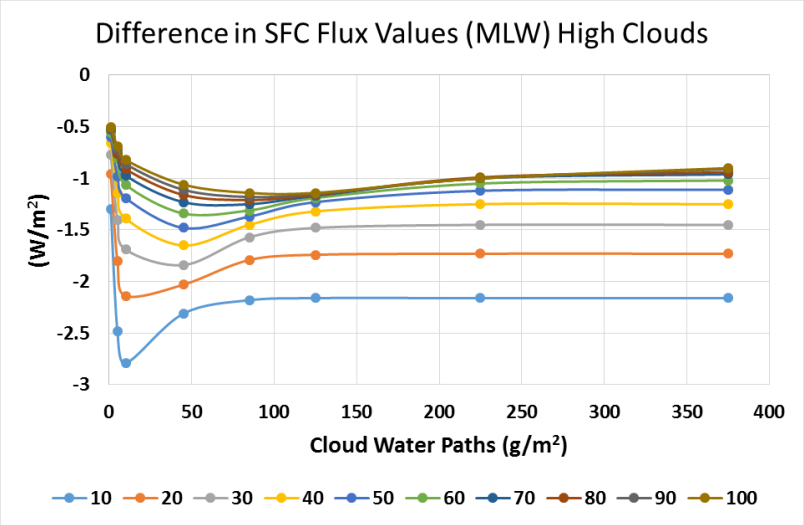

Figure 15: Method 1: Difference in downward SFC flux for high-clouds. Difference in downward SFC flux for 10 particle sizes when only high clouds were considered. Negative values indicate flux was lower when scattering was neglected

Under the tropical profile, when cloud water path was 10 g/m^2 or less, difference values were positive and were actually higher than the two-cloud case, and smaller particles were higher than the low-cloud only case. Overall, especially for smaller particles, difference in downward SFC flux was smaller in magnitude for this case compared to when the two-cloud or low-cloud only cases were considered. The largest difference (-2.79 W/m^2) occurred under the MLW profile with a particle size of 10 μm and a cloud water path of 10. From this analysis we can infer that scattering of IR by cirrus clouds has a greater impact on SFC flux for smaller particles than larger particles. When two clouds are present, the scattering by lower clouds has a greater impact on SFC flux, especially for smaller particles.

4.2 Absorption Only (RRTM) vs Absorption Only (DISORT)

In the second set of testing, calculations of upward and downward flux were first performed with the RRTM algorithm across the same conditions as before. Then,

calculations with absorption only from DISORT were calculated. The values when DISORT was used were then subtracted from when absorption only with RRTM was considered, creating a similar set of differences as section 4.1. Positive values indicate that absorption only in RRTM had a higher flux, while negative values indicate that absorption only using DISORT had a higher flux.

This method will be an indication of how well DISORT can calculate fluxes compared to RRTM when only absorption of the cloud is concerned, and not any of the absorption from the gas molecules. If the values are relatively close (+/- 1 W/m^2), we can infer that gas absorption (other than water vapor) plays little role in flux when compared to cloud cover. With this, we can assume that using DISORT not just for cloud absorption, but for cloud scattering (as tested earlier) will be an accurate depiction of the way radiation is transferred in a cloudy sky atmosphere. This method of tests will also compare the quadrature method that RRTM uses versus the discrete ordinates method that DISORT uses.

As previously analyzed, we will first look at the two-cloud condition, then low clouds, and then high clouds. The overall pattern of upward TOA flux differences between RRTM and DISORT show a couple of different traits. As cloud water path increases from 1 to 10 g/m^2, an inflection point occurs, and 10 μm particles change from having the largest positive difference to the largest negative difference, and the 100 μm particles do the opposite. Then another inversion occurs between 10 and 45 g/m^2 in cloud water path, where larger particles produced the largest negative difference. Between 85 and 125 g/m^2, another reversal in magnitude occurs, but the spread becomes increasingly smaller between 10 and 100 μm particle sizes. As cloud water path is increased to 375, nearly all particle sizes have the same difference value. Despite the many reversals, differences

across both particle shapes and atmospheric profiles are between -0.6 and +0.6 W/m^2. The largest positive difference (+0.62 W/m^2) occurred under the MLW profile with a particle size of 20 µm and a cloud water path of 1 g/m^2. The largest negative difference (-0.54 W/m^2) occurred under the tropical profile with a particle size of 90 µm and a cloud water path of 45 g/m^2. Because these differences are extremely small, it can be deduced that running DISORT in the absorption only method may be just as effective as running RRTM. The only down-side to this method is the increase in computation time. Figure 16 shows this analysis for the MLW case. Similar trends appeared for all other atmospheric profiles.

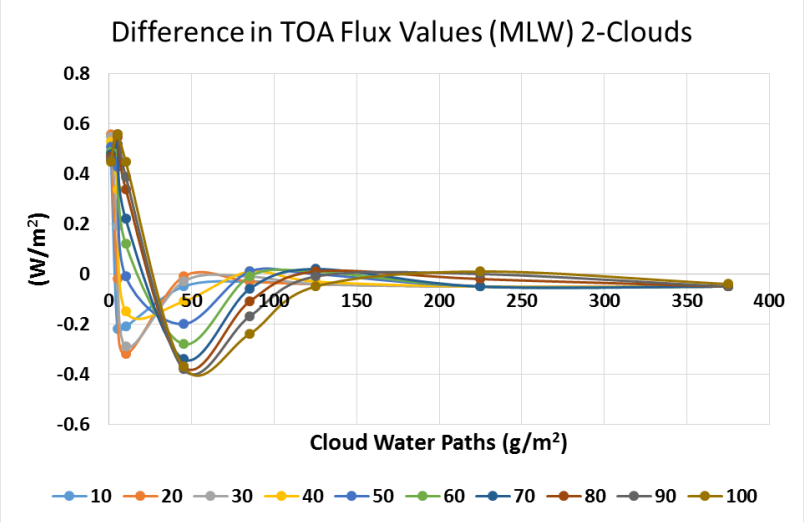

Figure 16: Method 2: Difference in upward TOA flux for 2-clouds. Difference in upward TOA flux for MLW for Absorption in RRTM vs Absorption in DISORT. Positive values indicate RRTM had a higher solution while negative values are where DISORT had a higher solution

Downward SFC flux differences followed a similar pattern to upward TOA flux, with many inversions. However, the particle sizes are reversed. At a cloud water path of 5 g/m^2, the 100 µm particle size had the most negative difference, and at cloud water path of 85 g/m^2, it had the most positive. The magnitudes are along the same lines as

well, with values ranging between roughly -0.5 and +0.2 W/m^2. As cloud water path increases towards 375 g/m^2, all difference values converge to around -0.05 W/m^2 for all the atmospheric profiles and particle sizes, and around -0.45 W/m^2 for the Garand profile. As with the TOA upward flux, using DISORT in the absorption only mode is just as effective as RRTM, but increases in computational time. Figure 17 shows this analysis for the MLW case and similar trends appeared in all other atmospheric profiles.

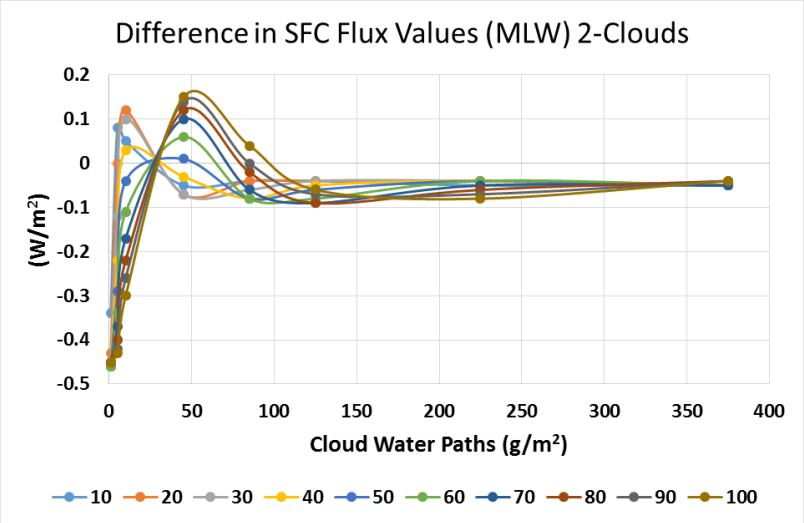

Figure 17: Method 2: Difference in downward SFC flux for 2-clouds. Difference in downward SFC flux for MLW for Absorption in RRTM vs Absorption in DISORT. Positive values indicate RRTM had a higher solution while negative values are where DISORT had a higher solution

For the low-cloud only case, the patterns for both upward TOA flux and downward SFC flux differences are almost mirror images in shape, but vary slightly in magnitude. For the upward TOA flux differences, all values are positive regardless of atmospheric profiles. The widest spread between particle sizes occurs in the optically thin clouds, and nearly all particle sizes converge at 375 g/m^2 to around 0.15 to 0.20 W/m^2. The largest difference (0.35 W/m^2) occurs at a cloud water path of 1 g/m^2 with a particle of 20 μm.

Figures 18 and 19 shows these analysis for the MLW case. Similar trends appeared in all other atmospheric profiles.

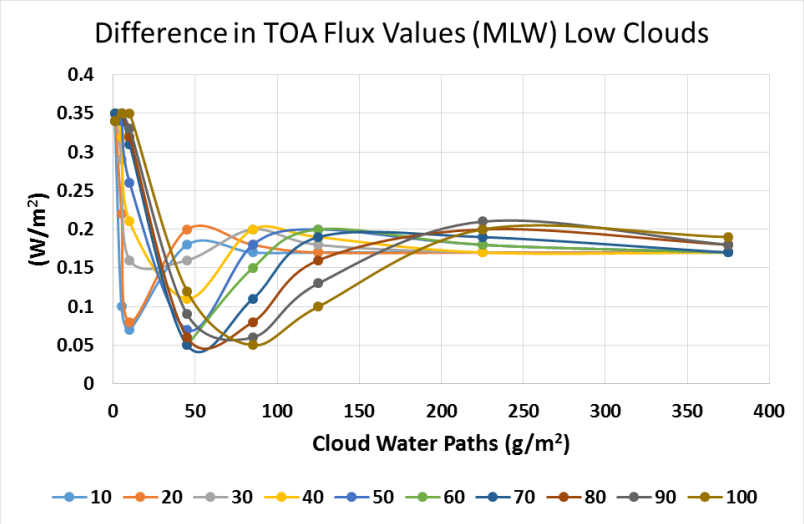

Figure 18: Method 2: Difference in upward TOA flux for low-clouds. Difference in upward TOA flux for MLW and low clouds only for Absorption in RRTM vs Absorption in DISORT. Positive values indicate RRTM had a higher solution while negative values are where DISORT

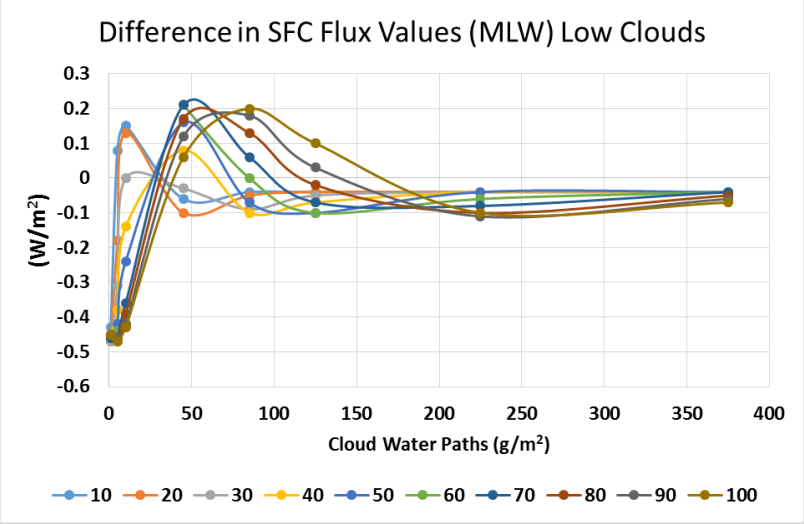

Figure 19: Method 2: Difference in downward SFC flux for low-clouds. Difference in downward SFC flux for MLW for Absorption in RRTM vs Absorption in DISORT. Positive values indicate RRTM had a higher solution while negative values are where DISORT had a higher solution

For the high-cloud only case, a similar pattern in both shape and magnitude as the two-cloud case for almost all atmospheric profiles occurred for both upward TOA and SFC flux differences. For upward TOA flux differences, in some instances, the values were higher for the high-cloud case only than with the two-cloud case. Figures 18 and 19 shows this analysis for the MLW case.

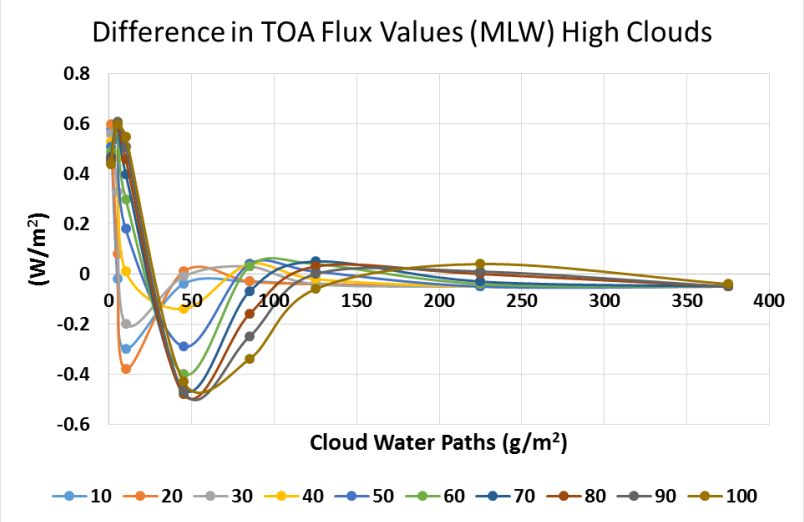

Figure 20: Method 2: Difference in upward TOA flux for high-clouds. Positive values indicate RRTM had a higher solution while negative values are where DISORT had a higher solution

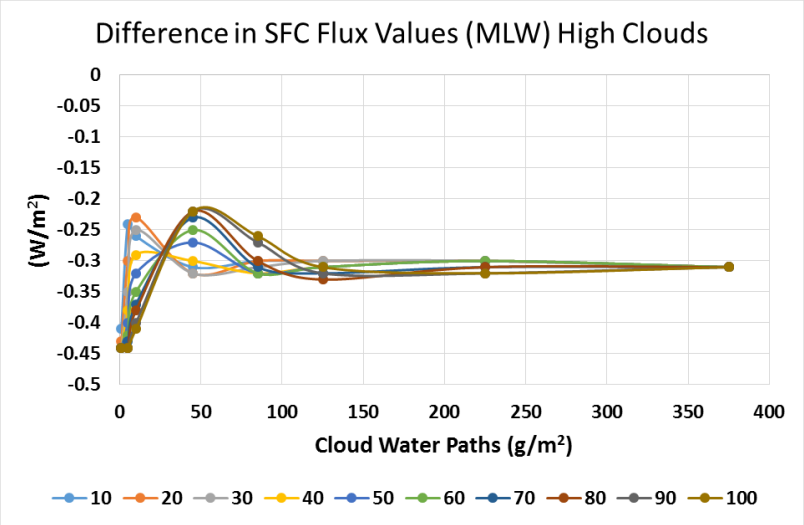

Figure 21: Method 2: Difference in downward SFC flux for high-clouds. Difference in downward SFC flux for MLW and high clouds only for Absorption in RRTM vs Absorption in DISORT. Positive values indicate RRTM had a higher solution while negative values are where DISORT had a higher solution

4.3 Absorption Only (DISORT) vs Absorption + Scattering (DISORT)

In the third method of testing, calculations of upward and downward flux were first performed with the absorption only algorithm using DISORT. Then, values with scattering included from DISORT were calculated. The values when scattering was included were then subtracted from when scattering was neglected in DISORT, creating a similar set of differences as the above two methods. Positive values indicate that absorption only in DISORT had a higher flux, while negative values indicate that including scattering using DISORT had a higher flux. This testing is done to see if DISORT can produce similar differences in flux as RRTM when gas absorption is neglected. This method will compare both absorption and scattering using discrete ordinates, rather than one method using the quadrature method as in RRTM.

Once again we will analyze the two-cloud case first for both upward TOA and downward SFC flux differences. Increasing the cloud water path produced similar results for both hexagon and spherical particles for both upward TOA and downward SFC flux

differences, although hexagon values were slightly higher especially for larger particles. This was similar to the two-cloud case when comparing absorption only in RRTM and scattering with DISORT. Upward TOA values were between roughly 0.2 (100 µm particles) and 3.75 W/m^2 (10 µm particles) at a cloud water path of 1 g/m^2 across all atmospheric profiles for spheres and 0.5 (100 µm particles) to 4.3 W/m^2 (10 µm particles) for hexagons. They then increased to a range of 1.75 (100 µm particles) to 12.4 W/m^2 (10 µm particles) as cloud water path increased to 10 g/m^2. Larger particles had higher magnitudes in differences through cloud water path of 85 g/m^2 after which values decreased and leveled off through cloud water paths of 225 and 375 g/m^2. For smaller particles (10, 20, and 30 µm in hexagons; and 10 & 20 µm in spheres) the largest difference occurred when the cloud water path was 10 g/m^2. For all other particles, the largest difference occurred when cloud water path was 45 g/m^2. In this method, the largest difference (12.11 W/m^2) occurred in the tropical profile with a hexagon particle of 10 µm and a cloud water path of 10. All values were positive, indicating that even when gas absorption in the atmosphere is ignored, scattering of IR radiation by clouds still produces less upward outgoing flux. Figure 22 shows this analysis for the MLW case. Similar trends appeared in all other atmospheric profiles.

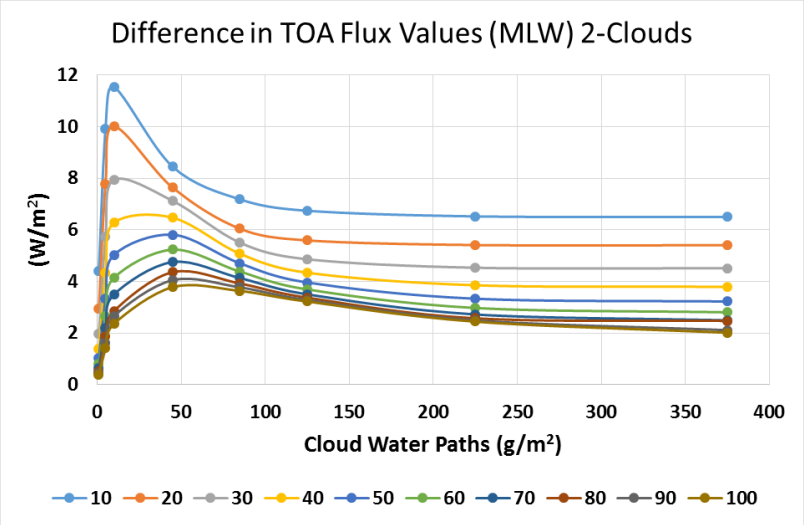

Figure 22: Method 3: Difference in upward TOA flux for 2-clouds. Difference in upward TOA flux for MLW for 10 particle sizes between absorption only with DISORT and scattering with DISORT. Positive values indicate that flux was higher when scattering was neglected

Downward SFC flux difference values were also in the same magnitude as in the first method for both spheres and hexagons and for all atmospheric profiles. Values were small for a cloud water path of 1 g/m^2 and increased negatively through cloud water paths of 10 g/m^2. Around 45 g/m^2, larger particles began to have a bigger difference than smaller particles. After a cloud water path of 125 g/m^2, values began to taper off and resume their original relationship of smaller particles producing larger differences. The largest difference (-3.73 W/m^2) was for a 10 µm hexagon particle in the MLW atmosphere at a cloud water path of 10. All difference values were negative for both spheres and hexagons across all atmospheric profiles (which did not occur in the first method of tests in the tropical case), indicating once again that when scattering is neglected the downward SFC fluxes are lower than when scattering is included. Figure 23 shows this analysis for the MLW case. Similar trends appeared in all other atmospheric profiles.

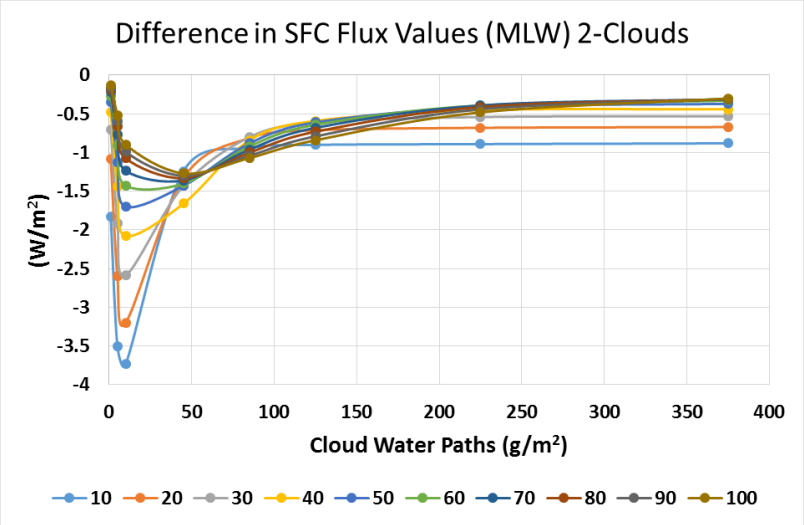

Figure 23: Method 3: Difference in downward SFC flux for 2-clouds. Negative values indicate that flux was lower when scattering was neglected

Looking next at the low-cloud only case, upward TOA flux differences continued to follow the same pattern as with the two-cloud case as well as the first method of testing. Magnitudes of the difference values were about 80% smaller, ranging from 0.8 (100 µm particles) to roughly 3 W/m^2 (10 µm particles). Figure 24 shows this analysis for the MLW case. Similar trends appeared in all other atmospheric profiles.

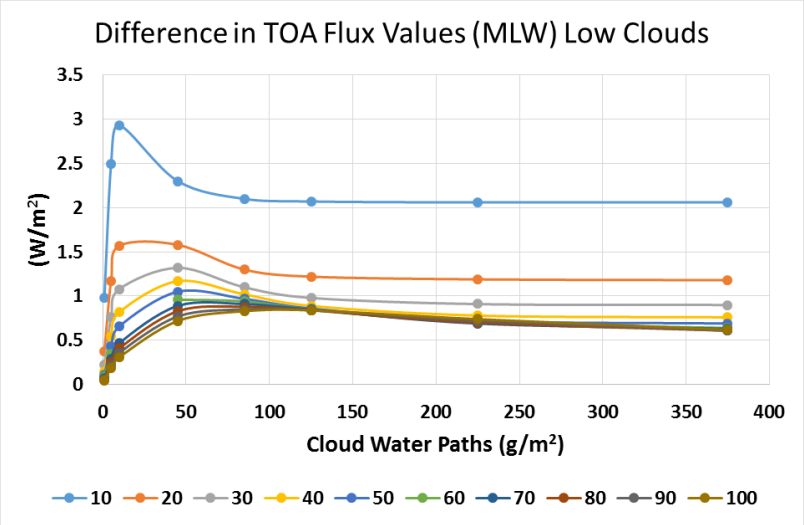

Figure 24: Method 3: Difference in upward TOA flux for low-clouds. Positive values indicate absorption had a higher flux than when scattering was included

Downward flux differences also behaved similarly to the first method. At cloud water path of near 45 g/m^2 smaller particles began to show a smaller difference than larger particles. As cloud water path increased through the 100-300 g/m^2 range, larger particles began to have smaller differences once again, and converged to nearly the same number by 375 g/m^2 for all particle sizes. All values were negative, regardless of atmospheric profile (including tropical, which had some positive values in low cloud water paths in the first method). Thus, surface downward flux is always higher when scattering is taken into effect. The largest difference (-2.9 W/m^2) was at a 10 µm particle in the MLW atmosphere at a cloud water path of 10. Figure 25 shows this analysis for the MLW case.

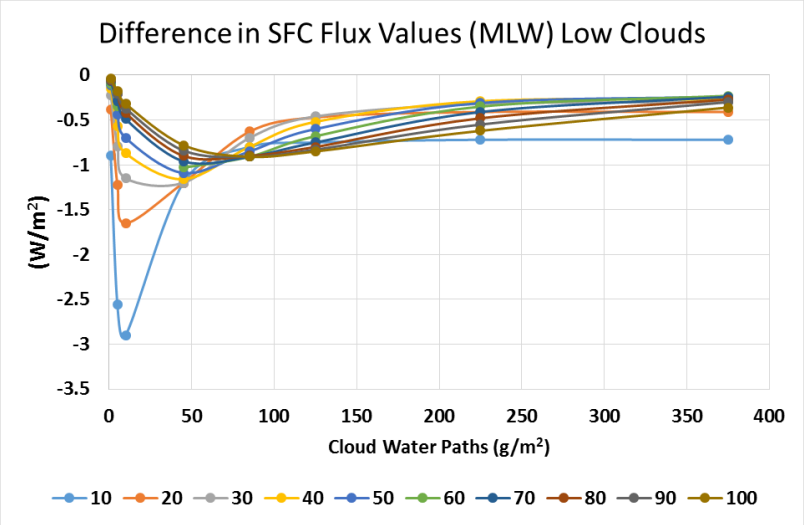

Figure 25: Method 3: Difference in downward SFC flux for low-clouds. Difference in downward SFC flux for MLW between absorption only with DISORT and including scattering with DISORT for low clouds only. Negative values indicate that flux was lower when scattering was neglected

In the high-cloud only case, upward flux differences also followed closely those of the first method, but varied slightly in magnitude. For all particle sizes in all atmospheric profiles, difference values were lower than those of the first method in the cloud water path of 1 g/m^2, but were larger in all the remaining cloud water paths. The largest difference (+11.97 W/m^2) was found in the tropical atmospheric profile for a cloud water path of 10 g/m^2 and a 10 µm particle. When compared to the two-cloud layer case, differences from a cloud water path of 45 g/m^2 and less are lower and those from cloud water paths of 85 g/m^2 and greater are higher. This happens for all atmospheric profiles and this pattern existed in the first method as well. Figure 26 shows this analysis for the MLW case.

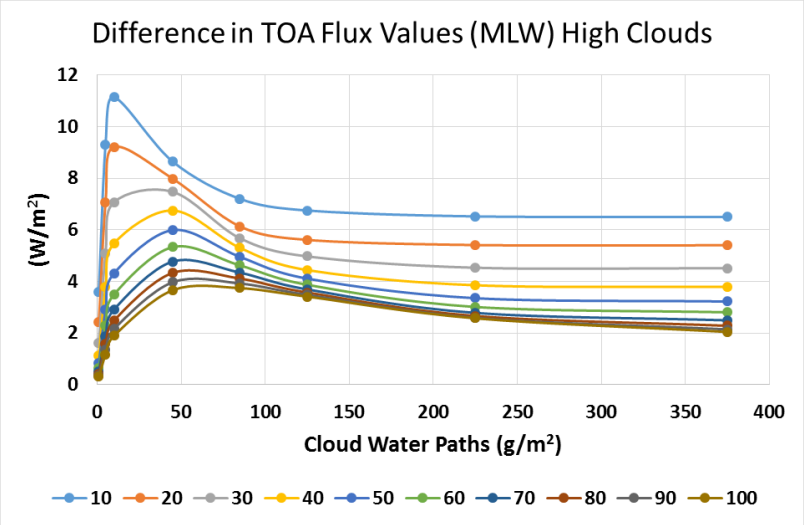

Figure 26: Method 3: Difference in upward TOA flux for high-clouds. Difference in upward TOA flux for MLW between absorption only with DISORT and including scattering with DISORT for high clouds only. Positive values indicate that flux was higher when scattering was neglected

Downward SFC flux differences also followed closely to those of the first method. When only a high cloud is present, the resulting difference in downward SFC fluxes is more of a mirror image of the upward TOA flux differences, but smaller in magnitude. All values are smaller than those of the first method, regardless of atmospheric profile or particle size. The largest difference (-2.52 W/m^2) was found once again in the MLW atmosphere with a cloud water path of 10 g/m^2 and a 10 µm particle. All values were negative across all atmospheric profiles. In some particle sizes, for cloud water paths of 1 to 10 g/m^2, the sum of the SFC downward flux differences in the high-cloud and low-cloud only cases is nearly equal the two-cloud case. This typically occurs in particles greater than 40 µm. For cloud water paths greater than 10 g/m^2 this property is not valid because of the inflection of particle size differences present in the two-cloud and low-cloud cases, but not present in the high-cloud case. Figure 27 shows this analysis for the MLW case.

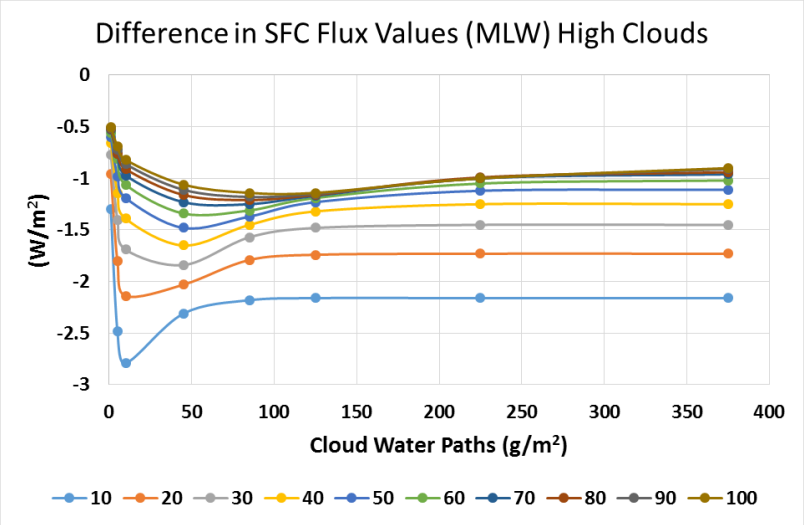

Figure 27: Method 3: Difference in downward SFC flux for high-clouds. Difference in downward SFC flux for MLW between absorption only with DISORT and including scattering with DISORT for high clouds only. Negative values indicate that flux was lower when scattering was neglected

4.4 Net Flux

Net flux is defined as the following equation:

$$F_{net} = F_{up} - F_{down} \quad (7)$$

Where F_{up} is upward flux and F_{down} is downward flux. RRTM calculates downward flux first, and as a boundary condition, always has a zero value at the top of the atmosphere. Thus, the net flux at the top of the atmosphere is always equal to the upward flux at the top of the atmosphere. Consequently, a difference in net flux between absorption only and when scattering is included will also be equal to just the difference in upward flux. Because of this relationship, it is redundant to compare differences in net flux at the top of the atmosphere.

At the surface, net flux will have a value different from upward or downward, because both directions have a non-zero magnitude. When comparing absorption only in RRTM to scattering with DISORT, a difference in net flux at the surface will be almost zero because the amount of gas absorption at the surface is negligible. When comparing

absorption only in DISORT to scattering with DISORT, a difference in net flux at the surface will be exactly zero because upward flux is not affected by a cloud deck and gas absorption is ignored. Thus, comparing net fluxes at the surface will be just as redundant as at the top of the atmosphere because the value will be either exactly or near-zero.

Therefore, net flux (and net flux difference) should be compared at the cloud layers or just below them, where upward minus downward flux has a significant non-zero answer. In the low-cloud only case, the net flux difference will be examined at level 9 (just below the cloud deck) and level 10 (at the cloud deck). In the high-cloud only case, the net flux difference will be examined at level 41 (just below the cloud deck) and level 42 (at the cloud deck). These layers will also be significant for looking at heating rate as well later on.

4.4.1 Absorption only (RRTM) vs. Absorption + Scattering (DISORT)

In the level 9 case, magnitude of net flux difference ranges from 0.5 to 5 W/m^2 depending on particle size and cloud water path. All values are positive, meaning that absorption only has a higher magnitude than when scattering is included and that upward flux is higher than downward flux. These magnitudes are evident at both level 9 and level 10. However at level 9, when CWP ranges from 85-125 g/m^2, net flux differences are increasing in magnitude with a decrease in particle size. This inverse proportionality is similar to what occurred at the SFC in previous methods. Below 85 g/m^2 cloud water path and shortly afterwards, the opposite pattern occurs. Once cloud water path begins to get above 125-225 g/m^2, maximum net flux differences begin to occur at smaller particles again. In level 10, the magnitude of net flux difference always increases with decreasing particle size across all cloud water paths and atmospheric profiles. The largest net flux difference (4.98 W/m^2) was seen at level 9 in the MLW case with particle size of 10 µm

and a cloud water path of 10. Figures 28 and 29 shows this analysis for the MLW case while other profiles are shown in Appendix D.

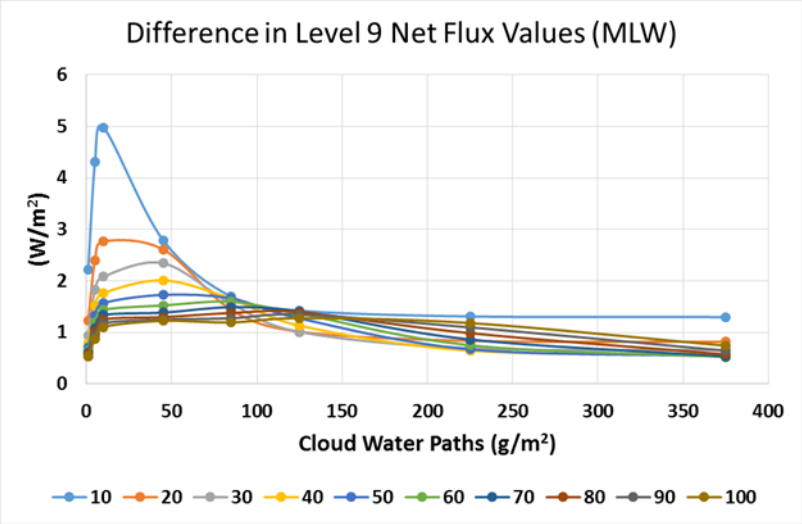

Figure 28: Method 1: Difference in net flux for level 9. Difference in level 9 net flux for MLW for 10 particle sizes. Positive values indicate that net flux was higher when scattering was neglected

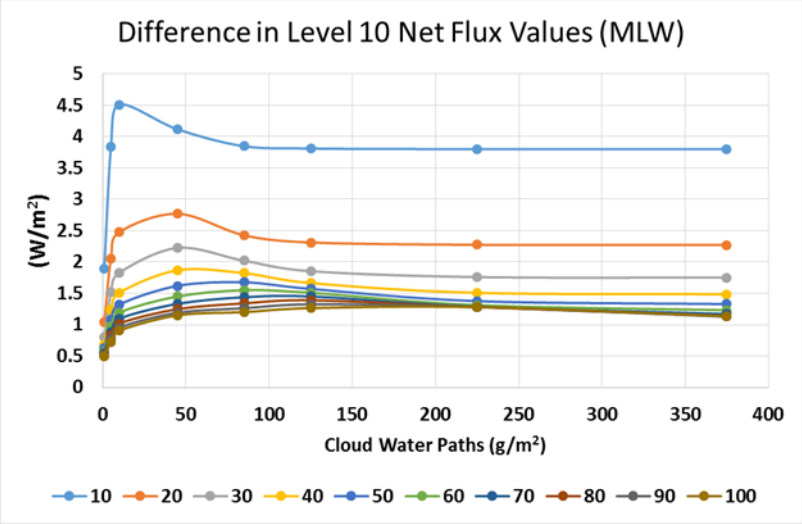

Figure 29: Method 1: Difference in net flux for level 10. Difference in level 10 net flux for MLW. Positive values indicate that net flux was higher when scattering was neglected

In the high-cloud only case, the difference in net flux follows a similar pattern to that of the upward flux at the TOA but slightly higher due to the larger values of downward flux than those observed at the top of the atmosphere. Magnitudes of net flux differences increase sharply when cloud water path increases from 1 to 10 g/m^2. After a cloud water path of roughly 85 g/m^2, difference in net flux begins to asymptote. This pattern is the same for level 41 as it is for level 42. For both levels, regardless of atmospheric profile and cloud water path, net flux difference increases when particle size decreases. There is no reversal like the low-cloud case. Net flux difference is always positive, meaning that the values calculated when scattering was included were less than when values were calculated with absorption only. The maximum net flux difference (12.94 W/m^2) was seen in the tropical case on level 42 for a cloud water path of 10 and 10 µm particles. Figures 30 and 31 shows this analysis for the MLW case while other profiles are shown in Appendix E.

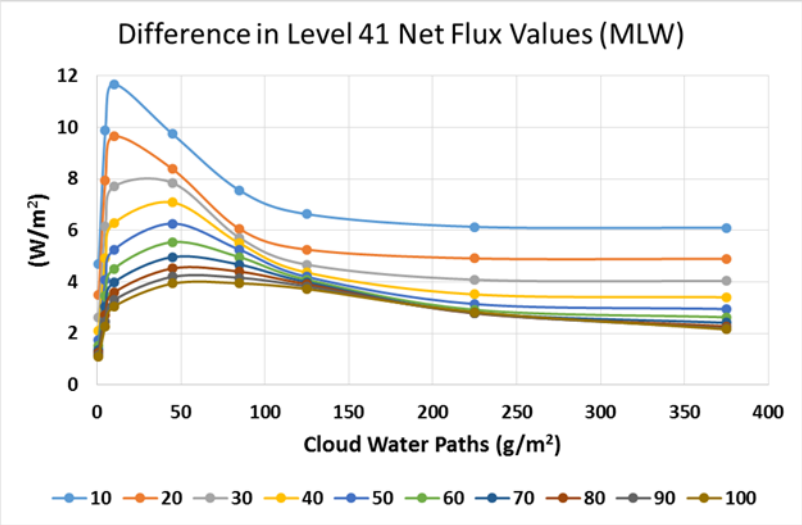

Figure 30: Method 1: Difference in net flux for level 41. Difference in net flux in level 41 for MLW. Positive values indicate that net flux was higher when scattering was neglected

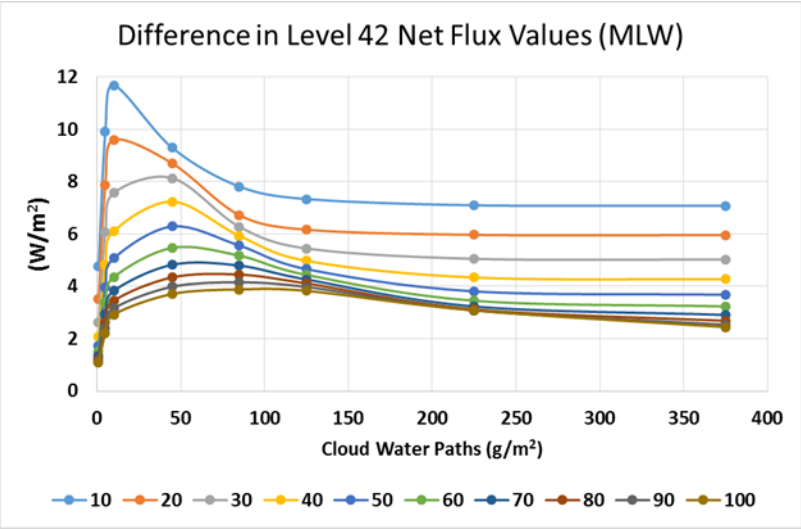

Figure 31: Method 1: Difference in net flux for level 42. Difference in net flux in level 42 for MLW. Positive values indicate that net flux was higher when scattering was neglected

4.4.2 Absorption Only (RRTM) vs. Absorption Only (DISORT)

In the low-cloud case, net flux difference ranges from -0.4 to +0.9 W/m^2 for level 9 depending on particle size, and cloud water path. Net flux difference for level 10 has a much smaller range, typically between 0.1 and 0.6 W/m^2, depending on particle size and cloud water path. For both levels, as cloud water path increases, the spread in net flux difference amongst particle sizes becomes increasingly smaller. For all atmospheric profiles (except MLW), the range in net flux difference for level 10 is within 0.1 or 0.2 W/m^2 regardless of cloud water path amongst all the cloud particle sizes. Typically, the average net flux difference is about 0.5 W/m^2, which is extremely low. Small magnitudes when comparing the net flux in this method gives reason to believe that gas molecular absorption plays such a small roll compared to absorption by the cloud. Figures 32 and 33 show this analysis for the MLW case. Similar results were present in the other atmospheric profiles.

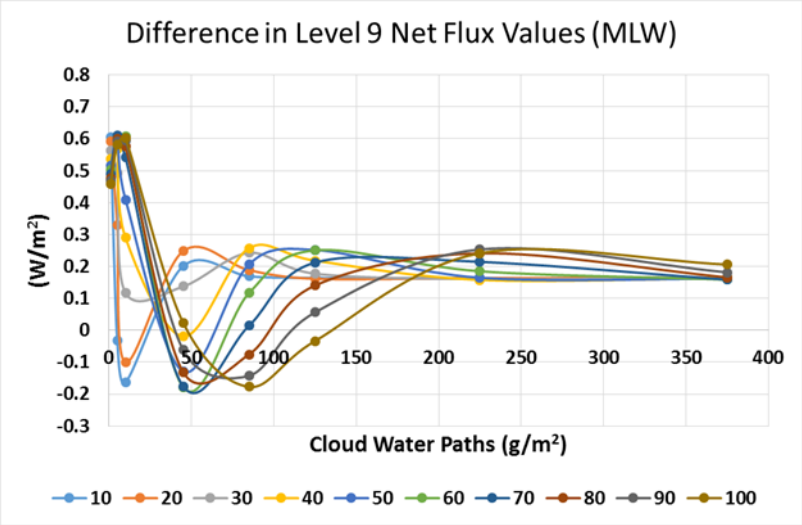

Figure 32: Method 2: Difference in net flux for level 9. Difference in level 9 net flux for absorption in RRTM vs absorption in DISORT. Positive values indicate RRTM had a higher solution while negative values mean DISORT had a higher solution

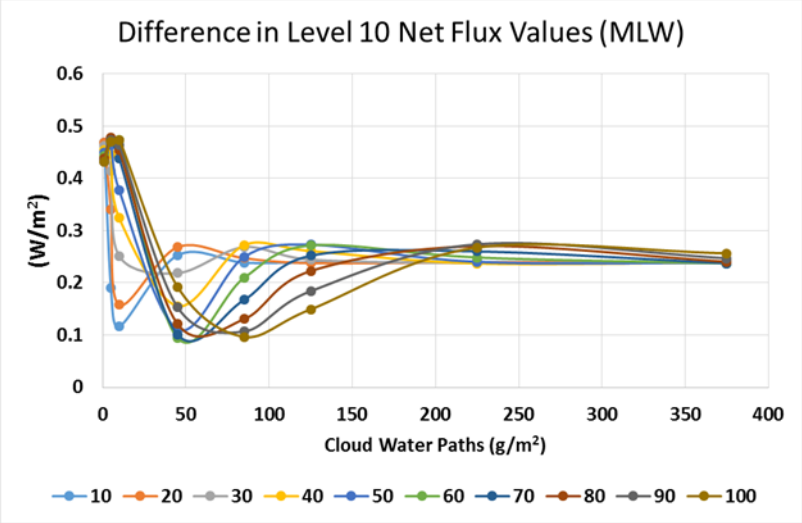

Figure 33: Method 2: Difference in net flux for level 41. Difference in level 41 net flux for absorption in RRTM vs absorption in DISORT. Positive values indicate RRTM had a higher solution

In the high-cloud case, the difference in net flux generally ranges between -0.2 and +1 W/m^2 depending on particle size and cloud water path. The spread amongst particle sizes is slightly larger. This is due to the hexagonal ice particles being used vice the spherical liquid particles in the low-cloud only case. Regardless, the magnitudes are

small enough that the difference between them is negligible, even in optically thin clouds. This continues to give credence to the DISORT algorithm in calculations being close to that of RRTM. Figures 34 and 35 show this analysis for the MLW case. Similar results were present in the other atmospheric profiles.

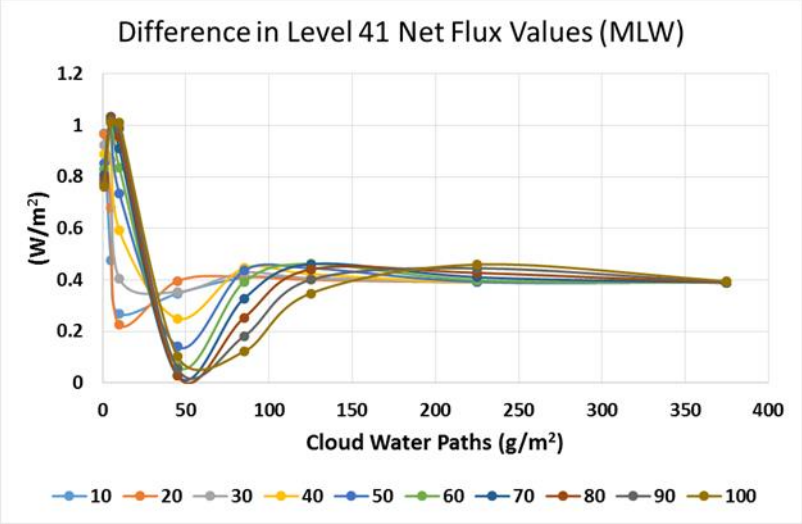

Figure 34: Method 2: Difference in net flux for level 20. Difference in level 10 net flux for absorption in RRTM vs absorption in DISORT. Positive values indicate RRTM had a higher solution

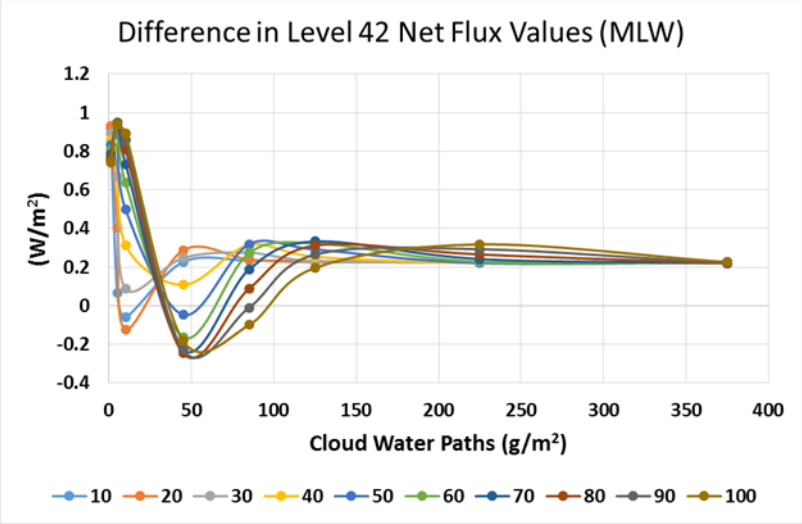

Figure 35: Method 2: Difference in net flux for level 42. Positive values indicate RRTM had a higher solution while negative values indicate that DISORT had a higher solution

4.4.3 Absorption Only (DISORT) vs. Absorption + Scattering (DISORT)

In the low-cloud only case, a similar pattern exists as in the first method of testing for both level 9 and 10. Magnitudes of net flux difference are all positive in both levels and can get as high as 5.14 W/m^2 in level 9. Unlike the first method, all particle sizes (except for 10 and 20 μm) see an increase in difference between cloud water path of 10 and 45 g/m^2 for both levels. The drop in magnitude for 10 μm particle sizes is large, but not as much as the first method. Figure 36 shows this analysis for the MLW case. Similar results were present in the other atmospheric profiles.

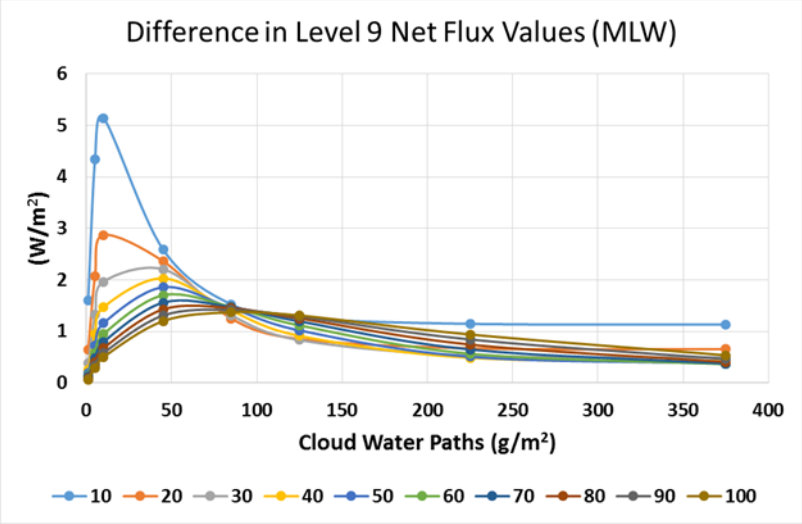

Figure 36: Method 3: Difference in net flux for level 9. Difference in level 9 net flux for MLW for 10 particle sizes for absorption in DISORT vs scattering in DISORT. Positive values indicate that net flux was higher when scattering was neglected

In the high-cloud only case, a similar pattern also exists to that of the first method for both levels. Figures 37 shows this analysis for the MLW case. Similar results were present in the other atmospheric profiles.

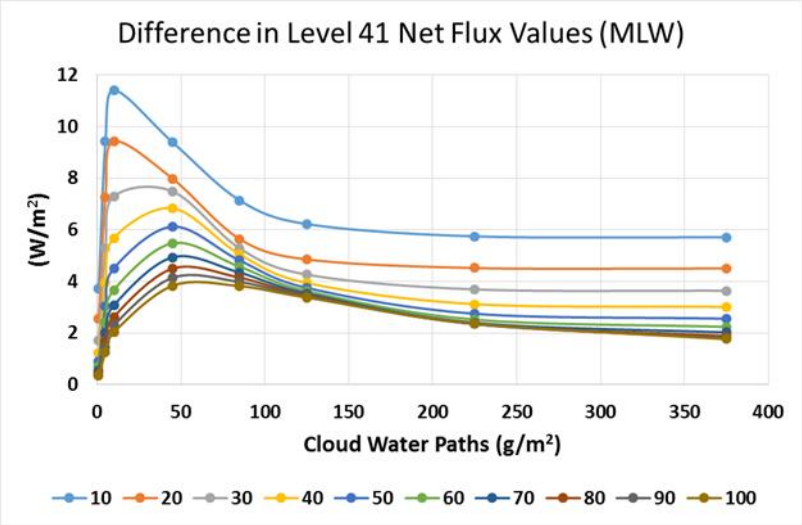

Figure 37: Method 3: Difference in net flux for level 41. Difference in level 41 net flux for absorption in DISORT vs scattering in DISORT. Positive values indicate a higher net flux occurred when scattering was neglected

4.5 Heating Rates

Heating rate is defined as the following equation

$$H = \frac{\Delta F_{net}}{\Delta P} \quad (8)$$

Where F_{net} is described in Equation 7 and P is pressure. A positive heating rate indicates a warming state, and a negative heating rate indicates a cooling state. Within the atmosphere, many things can cause a change in heating rate, including gas molecules and cloud cover. Molecular heating can be seen most easily in the stratosphere during the production of ozone. Heating in the lower atmosphere can be seen at nighttime where clouds act to inhibit cooling at the levels below them.

Because heating rate is a change in net flux, the heating rate at the top of the atmosphere will always be zero, as there is no layer above it to have a change with. But, level 81 will have the largest negative heating rate because the change in pressure between level 81 and level 82 is the smallest compared to any other level (an increasing smaller value in the denominator will increase the overall value). It is negative because

at the very top layers of the atmosphere, net flux is increasing with levels, thus making the numerator negative while keeping the denominator positive. Heating rate at the surface will also be large. The change in pressure is larger at the surface, but the change in net flux is more significant, thus leaving a higher number in the numerator instead of the opposite occurring at the top of the atmosphere. It is positive, because in the lower portion of the atmosphere net flux is decreasing with height, creating a positive number in the numerator and a positive number in the denominator.

We will examine two sections of the atmosphere when comparing heating rates between RRTM and DISORT: the stratosphere and the cloud decks and levels just below them. In order to express heating rate in Kelvin per day, a conversion factor of $0.0035 \frac{g\ K\ m}{day\ s^2\ W}$ is multiplied by the heating rate equation.

4.5.1 Absorption Only (RRTM) vs. Absorption + Scattering (DISORT)

First, we examined the stratosphere when comparing absorption only in RRTM to absorption + scattering in DISORT. The stratosphere is defined as levels 60 through 82. In the stratosphere, there are no clouds present, only gas molecules. Thus, using DISORT in this region will render significantly different results, regardless of particle sizes because there is effectively nothing to scatter the radiation, and no clouds to absorb it. Here we can see the full extent of molecular gas absorption and its effect on the atmosphere as shown in figure 38.

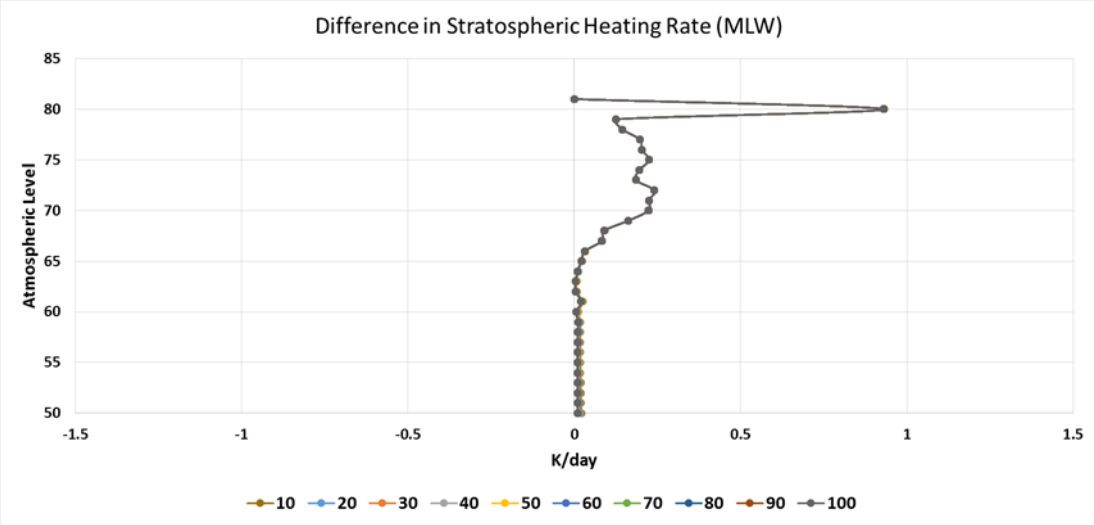

Figure 38: Method 1: Difference in stratospheric heating rate. Difference in heating rate in the stratosphere for MLW comparing absorption only in RRTM to scattering with DISORT

In all atmospheric profile cases, the difference in values for all particle sizes and all cloud water paths between absorption only and including scattering are upwards of 0.2 to 0.3 K/day and are all positive. When compared to the rest of the atmosphere (except the cloud decks) this is the largest difference in magnitudes of heating rate. Particle size and cloud water path rendered little to no difference in calculations because no clouds are present. This is effectively a “clear sky” atmosphere. The Garand profiles have some negative values in this region because of the inconsistent amount of ozone present pre-loaded into its profile. But the overall trend is still a positive one.

Next, we will examine the two cloud decks. In level 9, for cloud water paths of 1-10 g/m^2, all values are positive regardless of particle size and atmospheric profile. But, after cloud water path increases, values become negative and begin to asymptote for optically thick clouds. Ten micron particles produce the largest negative values, approaching -1 K/day in all atmospheres. SAS and MLW have the lowest magnitudes, but are still upwards of -.8 K/day. As particle size increases, magnitudes decrease in the

optically thick clouds, but still remain negative. Thus, when scattering is included, the level just below the cloud deck has as much of a difference in smaller particles as the stratosphere does with all particles. Figure 39 shows this analysis for the MLW case while other profiles are shown in Appendix F.

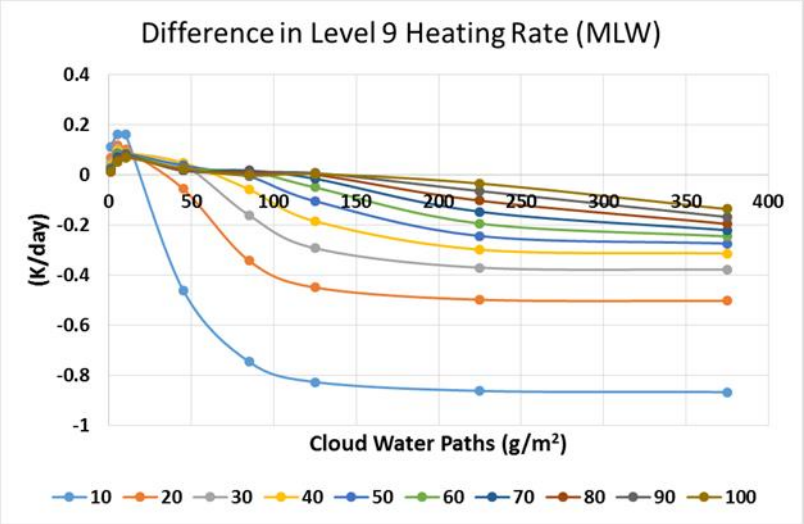

Figure 39: Method 1: Difference in heating rate for level 9. Positive numbers indicate higher heating rates when scattering was neglected, while negative numbers indicate higher heating rate when scattering was included

In level 10, however, the trend is the complete opposite and is greatly reduced in magnitude. All values are positive, but only reach upwards of 0.16 K/day in all atmospheric profiles. All differences increase when cloud water path increases from 1 to 10 g/m^2, but begin to asymptote by the time cloud water path is 45 to 85 g/m^2. 30 μm particles and above do not even reach 0.1 K/day, which is much smaller than the magnitudes observed in the stratosphere. Thus, heating rate of the cloud deck itself is left nearly unaffected when scattering is neglected. Figure 40 shows this analysis for the MLW case while other profiles are also in Appendix F.

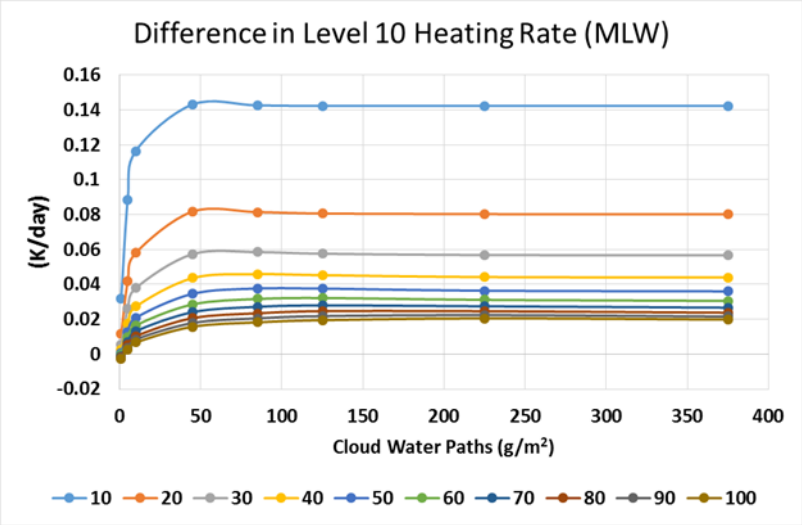

Figure 40: Method 1: Difference in heating rate for level 10. Positive numbers indicate higher heating rates when scattering was neglected, while negative numbers indicate higher heating rate when scattering was included

In level 41, a similar pattern exists as did for level 9, but magnitudes are larger. 10 and 20 µm particles can approach -2.5 K/day in the MLS and tropical cases. In the MLW, and SAS cases, they approach -1 K/day and in the Garand profiles, they reach -2 K/day. In cloud water paths between 45 and 85 g/m^2, the difference in heating rates are significantly different for particle sizes less than 20 µm. They are much more positive and in the MLW case, are upwards of +0.4 K/day. Because heating rate is a change in net flux, and the largest changes in net fluxes occurred between 10 and 45 g/m^2 for small particles this might explain the anomalous behavior. It is possible that if 5 µm particles were plotted, an even steeper rise would occur here, but this feature needs more research. Figure 41 shows this analysis for the MLW case, while other profiles are shown in Appendix G.

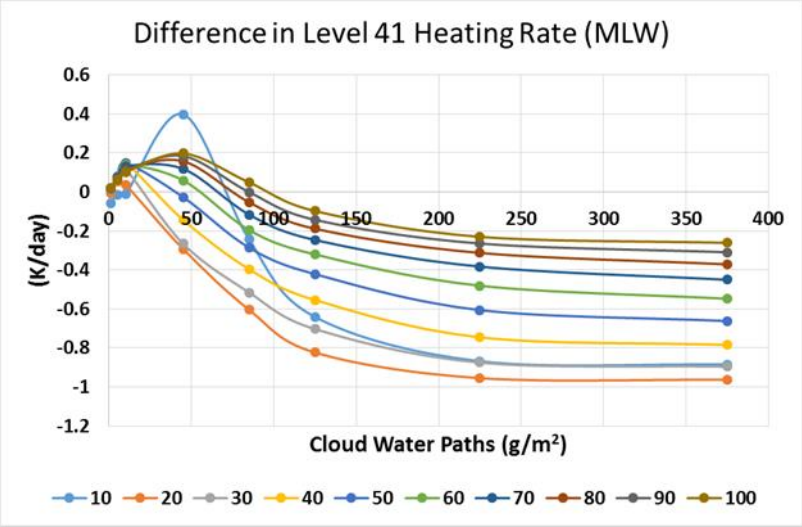

Figure 41: Method 1: Difference in heating rate for level 41. A large anomaly can be seen at a CWP of 45 g/m² where small particles show a much different case than larger ones

In level 42, on the cloud deck, the pattern is similar to that of level 10, however magnitudes are even smaller. These values are still much smaller than those seen in the stratosphere, especially in larger particle sizes. Figure 42 shows this analysis for the MLW case. Appendix G show the other atmospheric profiles.

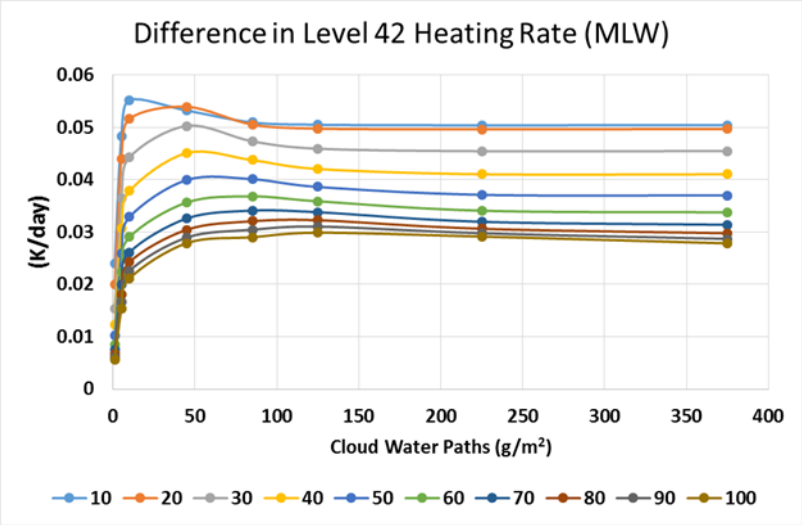

Figure 42: Method 1: Difference in heating rate for level 42. Values are much smaller than what was seen at level 10 or in the stratosphere. Positive values indicate heating rate was higher when scattering was neglected

4.5.2 Absorption Only (RRTM) vs. Absorption Only (DISORT)

When looking at the stratosphere, this method of comparison produces the same results as the first method. Regardless of atmospheric profile, particle size, and cloud water path, difference in heating rates approach 0.2 and 0.3 K/day in the stratosphere.

For level 9, the greatest amount of change occurs between the different particle sizes more so than in upward, downward, and even net flux differences. In the tropical case, heating rate differences approach -0.3 K/day for 10 and 20 µm particles when cloud water path is 10 g/m^2, and also approach -0.3 K/day for 90 and 100 µm particles when cloud water path is 45 and 85 g/m^2. SAS, MLS, MLW, and the Garand profiles produce similar patterns as well, but magnitudes only reach -0.2, -0.25, -0.1, and -0.25 K/day respectively. When cloud water path is increased to 375 g/m^2, values range between -0.1 and -0.2 K/day regardless of particle size across most atmospheric profiles. Figure 43 shows the case for the MLW profile.

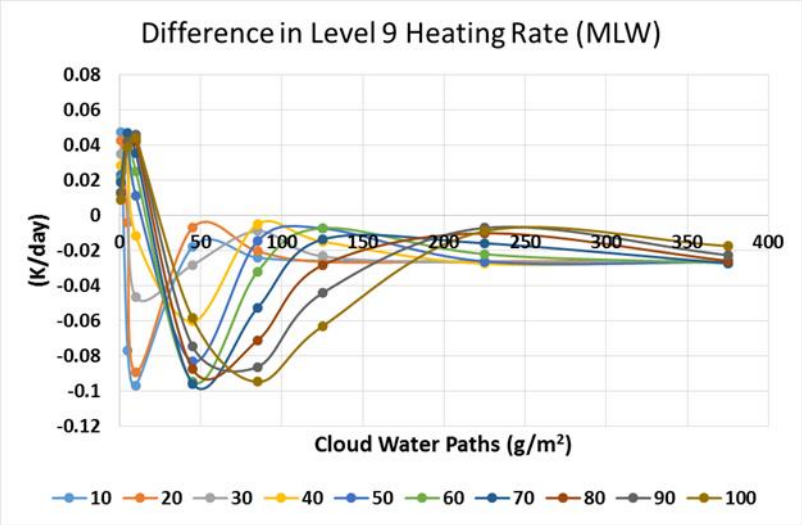

Figure 43: Method 2: Difference in heating rate for level 9. Difference when comparing absorption only in RRTM to absorption only in DISORT. Positive values indicate RRTM had a higher solution, whereas negative values indicate DISORT had a higher solution

For level 10, the range in differences and the magnitudes are much smaller. In the MLW case, magnitudes do not even reach 0.01 K/day, and in all other profiles magnitudes do not reach 0.02 K/day, regardless of particle size. Figure 44 shows this analysis for the MLW case.

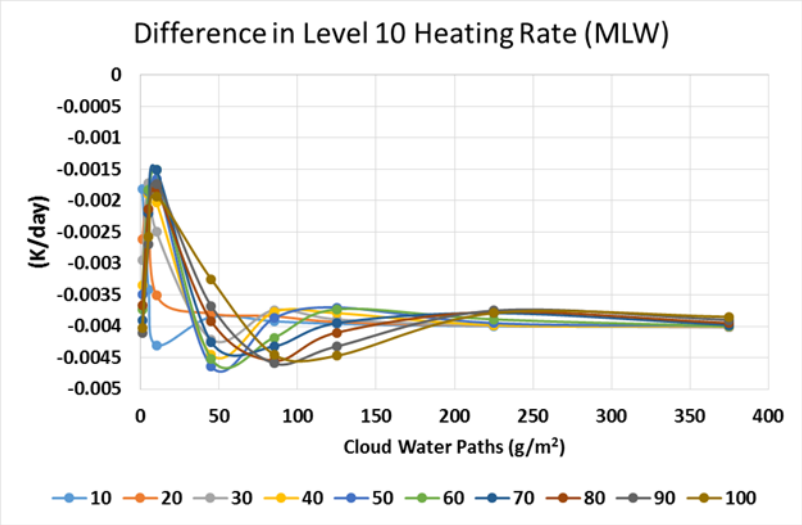

Figure 44: Method 2: Difference in heating rate for level 10. Difference in heating rate for level 10 when comparing absorption only in RRTM to absorption only in DISORT. Negative values indicate DISORT had a higher solution

In the high-cloud only case, Level 41 produces similar extreme values, approaching 0.3 and even 0.4 K/day when cloud water path was 5 g/m^2. An inversion is present between cloud water paths of 10 and 45, where increasing particle sizes begins to increase the magnitude of the difference in heating rate. As cloud water path is increased to 125 g/m^2 and above, all values regardless of particle size begin to converge and settle near 0.05 to 0.15 K/day. Figure 45 shows this analysis for the MLW case.

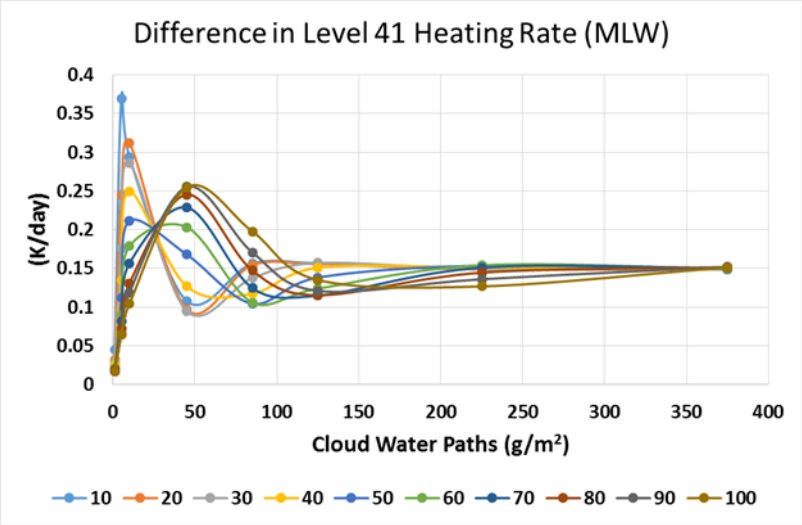

Figure 45: Method 2: Difference in heating rate for level 41. Difference in heating rate for level 41 when comparing absorption only in RRTM to absorption only in DISORT. Positive values indicate RRTM had a higher solution, whereas negative values indicate DISORT

In level 42, the spread in heating rate difference amongst the particle sizes is much lower, similar to level 10. Only the MLS and the Garand profiles reached a max near 0.01 K/day. All values converge and asymptote for thicker clouds as well, regardless of particle size. Figure 46 shows this analysis for the MLW case.

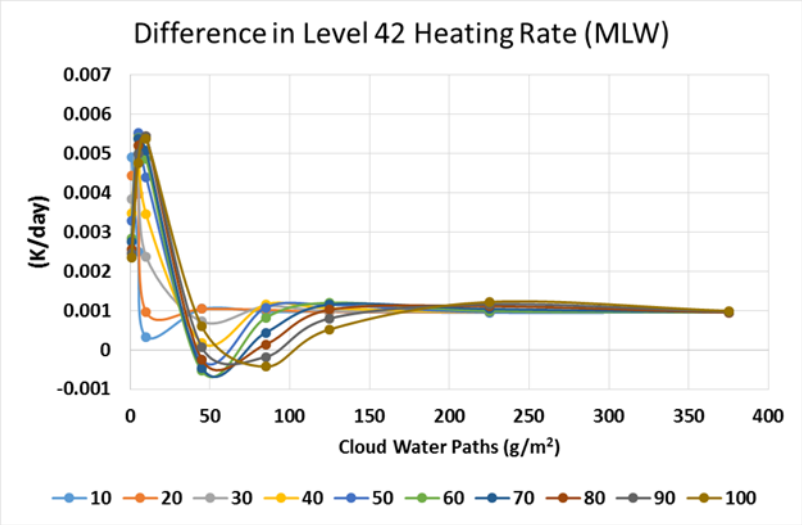

Figure 46: Method 2: Difference in heating rate for level 42. Positive values indicate RRTM had a higher solution, whereas negative values indicate DISORT had a higher solution

4.5.3 Absorption Only (DISORT) vs. Absorption + Scattering (DISORT)

In the stratosphere, because there is no gas absorption to consider in DISORT, almost all differences in heating rates are near zero, or are at least significantly less than anywhere else in the profile regardless of particle size or cloud water path. At the top of the atmosphere, unlike the first and second method of testing, the magnitudes of all particle sizes converge to zero. This is especially evident when only low clouds are present. Figure 47 shows this analysis for the MLW case.

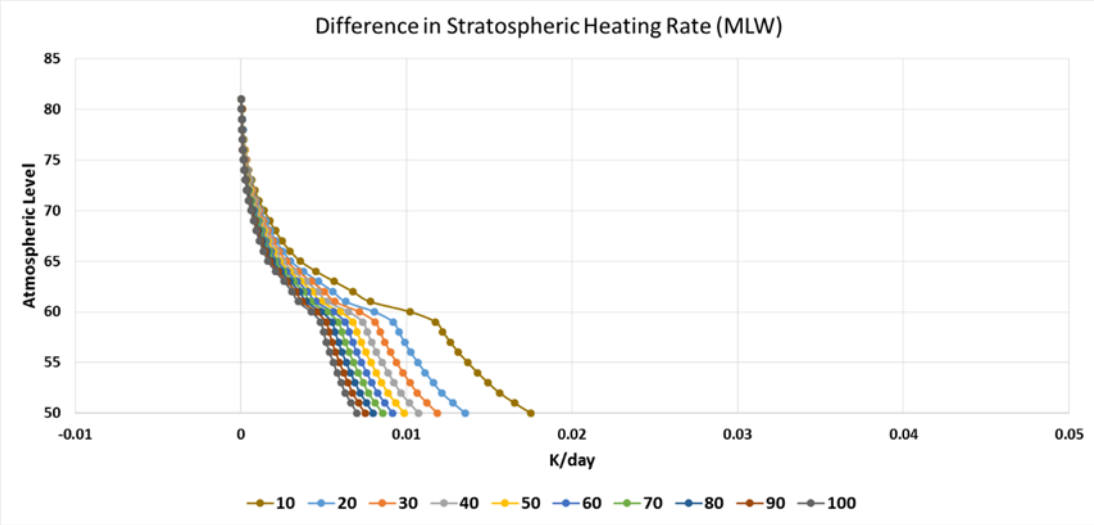

Figure 47: Method 3: Difference in stratospheric heating rate. Difference in heating rate in the stratosphere for 10 particle sizes in MLW between absorption only in DISORT and scattering in DISORT. Because there is no cloud layer present and gas absorption is neglected, differences are nearly zero

The low-cloud only level 9 case reveals a similar pattern to that of the first method of testing, with the exception of higher magnitudes in cloud water paths of less than 10 g/m^2. Magnitudes when cloud water paths are 45 g/m^2 or greater show smaller differences than that of the first method of testing, but only by a small fraction. For all cloud water paths, as particle size increases, the difference becomes greater. In the optically thinner clouds, that difference is positive, and in the thicker clouds that difference is negative. For level 10, all differences are positive and are on the same order of magnitude for all atmospheric profiles. Figures 48 and 49 shows this analysis for the MLW case which had similar results in the other atmospheric profiles.

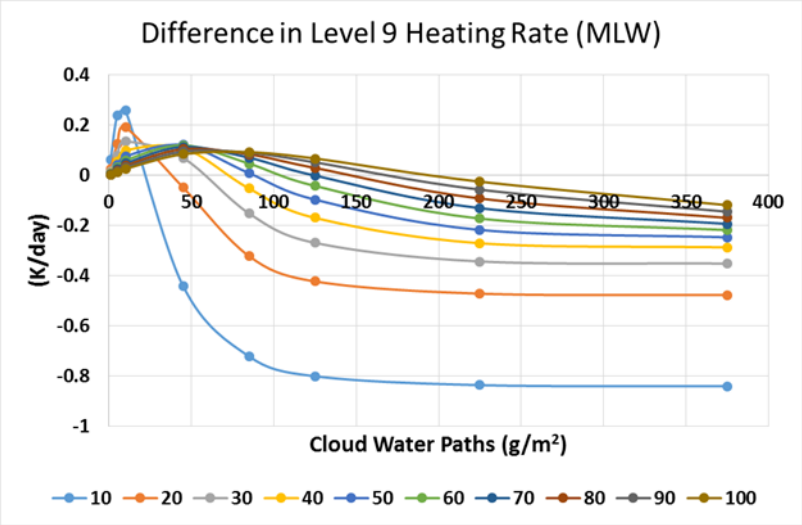

Figure 48: Method 3: Difference in heating rate for level 9. Difference in level 9 heating rate for the MLW case when comparing absorption with DISORT vs scattering with DISORT. Positive numbers indicate higher heating rates when scattering was neglected, while negative numbers indicate higher heating rate when scattering was included

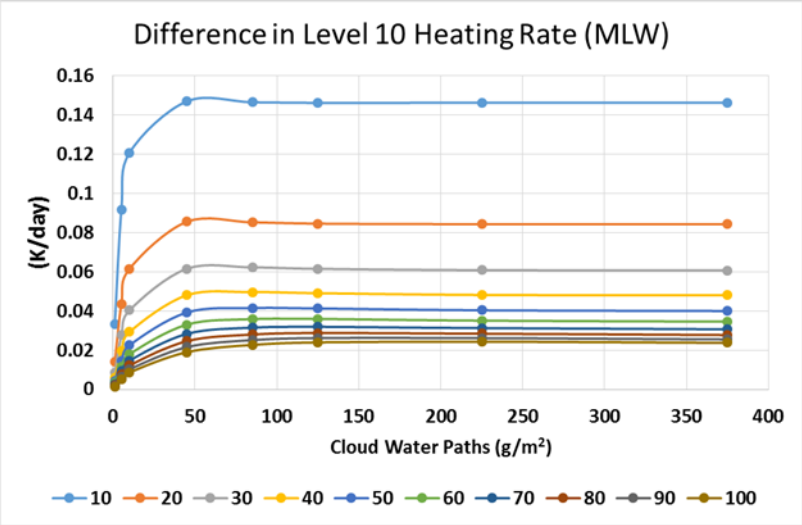

Figure 49: Method 3: Difference in heating rate for level 10. Positive numbers indicate higher heating rates when scattering was neglected

In the high-cloud only case, similar patterns to the first method of testing exist once again for both level 41 and level 42. In all atmospheric profiles, the 10 µm particles produce differences that are extensively different than the 20 µm particles when cloud water path is 45 g/m^2, and in some cases even 85 g/m^2. In the MLW case, 10 µm particles

produce a difference in heating rate of +0.3 K/day when cloud water path is 45 g/m^2 in level 41. It is estimated that particle sizes even smaller than 10 µm would produce an even larger extreme in the positive. This trend is only evident on the cloud water paths of 45 and 85 g/m^2. Figure 50 shows this analysis for the MLW case.

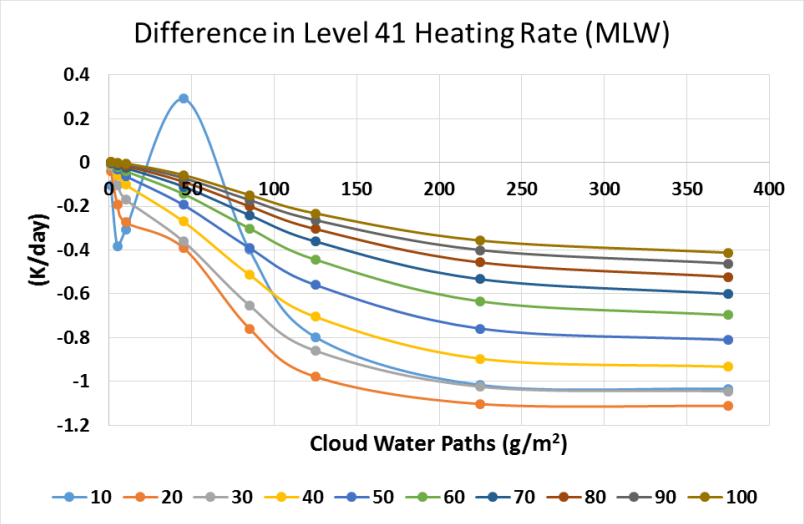

Figure 50: Method 3: Difference in heating rate for level 41. A large anomaly is present again for small particles when CWP is 45 g/m^2

For level 42, similar patterns and magnitudes exist when compared to the first method of testing as well, with the MLW and SAS magnitudes almost 1/3 of what the rest of the profiles have.

4.6 Other Analysis

It was also an objective to determine which part of the IR spectrum produced the largest difference between absorption only and when scattering was included. All values shown up to this point are for the entire IR spectrum, ranging from 3.08 µm to 1000 µm. RRTM has the capability to break down these composite values into the 16 bands as

described in Appendix H. Here we will take a brief look at how these 16 bands contribute to the difference between absorption and scattering at the TOA and SFC.

When we look at upward TOA flux differences, the bands that contribute the most in the high-cloud only and the two-cloud cases are bands 2 and 3 in small particles. They provide up to 39% of the total difference in optically thin clouds and upwards of 61% in optically thick clouds. Bands 5-8 provide a smaller amount (3-14% based on cloud water path), and bands 10-16 provide little or no contribution to the total difference. Band 1 provides about 1-3%. As particle size increases, bands 2 and 3 contribute less, and bands 1 and 5-9 contribute more. Bands 10-16 contribute little or nothing.

Upward TOA flux differences for the low-cloud only case however depends much more heavily on bands 5-9 and much less on bands 2 and 3. As particle size increases, band 6 becomes the dominant contributor reaching over 40%.

When looking at downward SFC flux differences, the bands that contribute the most in all three cloud combinations are bands 6-8. For small particles, band 8 contributes upwards of 75% of the total difference, while for larger particles, band 6 provides the most amount, especially in optically thin clouds. Bands 10-16 provided little or no contribution.

Bands 4 and 14 have some potential errors in them. For all upward flux differences (which are positive in all cloud combinations), band 4 shows differences that are negative (working against the total flux difference). For all downward flux differences (which are mostly negative), band 14 is exactly zero for every particle in every cloud water path. While the lack of contribution from band 14 is not significant (all near IR bands provided hardly any difference), the opposing contribution from band 4 may be speculative. Band 4 lies on the edge of the atmospheric window and it is possible that this band may have much higher values, which would increase the total flux difference as well. These two

bands need to be researched further. These trends (both good and bad) are the same across all atmospheric profiles.

4.7 Doubling Carbon Dioxide

Another test that was performed was taking one of the atmospheric profiles and doubling the carbon dioxide concentration to 800 ppm and re-running all the same conditions as before. This was done to see what consequences (if any) adding in more carbon dioxide to the atmosphere would have on fluxes and heating rates when scattering of cloud particles was considered. The Garand profile was the one selected to have carbon dioxide doubled.

Under the two-cloud case, when carbon dioxide was doubled the difference between absorption only and cloud scattering changed both at the surface and at the top of the atmosphere. For both spherical and hexagonal cloud particle shapes, the reduction in TOA upward fluxes ranged from roughly 0.03 - 0.25 W/m^2. The lowest reductions occurred for high particle sizes and low cloud water paths; while the highest reductions were seen at lower particle sizes and cloud water paths of 5-10 g/m^2. The highest fractional reduction occurred when cloud water paths were low and particle sizes were high. The conditions where the smallest fractional reduction occurred was low particle sizes and cloud water paths of 45-85 g/m^2. At the surface, unlike the top of the atmosphere, there was an increase in the difference of downward flux. The amount of increase ranged from roughly 0.02 to 0.08 W/m^2. Similarly to the TOA, however, the largest change at the SFC occurred with low particle sizes and cloud water paths of 5-10 g/m^2. The smallest change occurred with medium sized particles and cloud water paths of 125-225 g/m^2. When viewed as fractional changes, the most susceptible conditions to an increase occurred again with larger particle sizes and low cloud water paths. The

region least susceptible to change was that of low particle sizes and cloud water paths of 45-85 g/m^2.

For the low-cloud only case, a small reduction in upward TOA flux differences occurred ranging from 0.01 to 0.09 W/m^2. The largest decrease occurred for small particle sizes and cloud water paths above 5 g/m^2. The smallest decrease occurred with large particle sizes and small cloud water paths. At the surface an increase in downward flux difference occurred ranging from 0.01 to 0.06 W/m^2. The largest occurring once again at small particle sizes and cloud water paths of 5-10 g/m^2, and the smallest occurring at medium sized particles in optically thick clouds. As a fraction, the larger changes (over 6%) at the TOA were for large particle sizes and cloud water paths of 5-45 g/m^2 and at the SFC (5%), large particles and low cloud water paths. Conditions where the least amount of change as a fraction occurred where the actual change was the highest.

For the high-cloud only case, a similar trend occurred as in the two-cloud case. At the top of the atmosphere the amount decreased from roughly 0.03 to 0.24 W/m^2. The largest decrease occurred with small particle sizes and cloud water paths of 5-10 g/m^2. The lowest decrease occurred for large particle sizes and optically thin clouds. At the surface, the amount increased ranged from 0.03 to 0.07 W/m^2. The largest increase was observed for small particle sizes and cloud water paths of 5-10 g/m^2, and the smallest increase occurred for large particle sizes and optically thin clouds. As a percent of reduction at the TOA or increase at the SFC, the regions that were most susceptible to change (4.3% and 4.8% for TOA and SFC respectively) were for those of large particle sizes and low cloud water paths. Areas with the least susceptibility (1.5 and 3.4% for TOA and SFC respectively) to change occurred for low particle sizes and cloud water paths of 45-85 g/m^2.

Change in net flux differences for the low-cloud only case at and just below the cloud decks also occurred when carbon dioxide was doubled. For low clouds, just below the cloud deck saw a decrease in net flux ranging from 0.004 to 0.13 W/m^2. On the cloud deck changes ranged from a small increase of 0.001 W/m^2 to a decrease in 0.1 W/m^2. The largest decreases in net flux occurred for both levels for small particles and cloud water paths of 5-10 g/m^2 and the smallest changes occurred for large particles and low cloud water paths.

Net flux difference changes for the high-cloud only case just below and on the cloud deck were all decreases in values, ranging from 0.02 to 0.24 W/m^2. The largest changes occurred for both level 41 and level 42 when particle sizes were small and cloud water paths were 5-10 g/m^2. Smallest changes occurred when cloud water path was 1 g/m^2 and particles were large. As a percent, this reflects roughly 1.2 to 2.6% decrease with larger particles once again being more susceptible to change.

Heating rates for the low clouds were relatively unchanged, with the majority of cases increasing or decreasing by less than 0.001 K/day. However, a small section of level 9 saw an increase of 0.01 to 0.02 K/day when particle sizes were low and cloud water path was high. This was roughly a 3% increase. For high clouds, this trend continued. Most cases on the cloud saw less than 0.001 K/day change, but a small section of level 41 when particle sizes were small and cloud water paths were large saw a decrease of roughly 0.015 K/day (roughly 1%).

5. CONSIDERATIONS

While the results of these tests have been quality controlled and checked for errors, there are some nuances within RRTM that may be providing either incorrect or misleading data. While these conditions may not generally effect the overall outcome, they may need to be researched further.

One of the biggest limitation of RRTM is the lack of partial skies. RRTM forces a cloud fraction of 1.0, meaning the skies are completely overcast (no break in cloud cover). We know from recorded surface observations and satellite imagery that overcast conditions are not always the case in day to day meteorology. Thus, the values calculated here are for a 100% sky cover case, which does not occur all the time. It is unknown whether if cloud fraction were able to be reduced to 50%, if the difference in flux values would be reduced to 50% as well. However, having a broken- or scattered-sky case may introduce limb darkening/brightening effects which may in-turn produce larger values. As noted in the Joseph and Min 2003 paper when they used real-time cloud conditions, difference in absorption vs scattering reached upwards of 35 W/m^2 because of the edges of the clouds. With the two-cloud case, with cloud fraction forced to be 1, it provided another even unlikelier situation where overcast cirrus was above overcast cumulus.

Another factor that may play a role in calculating more accurate differences in fluxes would be to include a mid-level stratus deck. While three cloud layers at the same time is not a highly observed phenomena in meteorology, it does exist on occasion. It would also be imperative to allow for scattered and broken sky conditions with three cloud layers as well, as the chances for 3 overcast decks are slim. But a middle deck may increase the difference in both upward TOA flux and downward SFC flux. Introducing a

third middle deck would also allow for more cloud combinations (middle- and upper-deck only, low- and middle-deck only, middle-deck only) to be tested.

Changing the cloud resolution may have an impact on flux differences as well. In these tests both the low and high cloud decks were given a resolution of 0.25 km (roughly 820 ft). Increasing the physical thickness of the cloud may induce higher differences, while reducing the physical thickness may induce lower differences. In certain meteorological situations, lower-deck clouds are often thicker than upper-deck clouds. Thus, increasing the low-deck or decreasing the upper-deck might render more accurate results. Li and Fu (2000) did a similar study where increasing the resolution from 0.25km to 1km (what a typical GCM would use) increased the amount of flux error both at the TOA and SFC.

Cloud water paths in the two-cloud cases were set to the same amount for both cloud layers. But we know that cloud water paths for cirrus and cumulus clouds are often different across the latitudes. While the atmospheric profiles were accurate to their respective part of the globe, it is possible that using more realistic combinations of cloud water path for the two-cloud case would be more appropriate.

As noted in section 4.6, bands 4 and 14 may be not calculating the correct flux values (and therefore flux differences) which may contribute to inaccuracies in total flux differences for the entire IR spectrum RRTM uses.

6. SUMMARY AND CONCLUSIONS

GCMs and climate models use radiative transfer models when computing atmospheric conditions for the future. However, when calculating IR radiative flux, only absorption of clouds, aerosols, and gas molecules are used and any scattering effects that clouds may induce are neglected. Previous studies have been done in the past that suggest that the negligence of incorporating scattering of IR radiation by clouds has led to incorrect flux and heating rates.

Testing of the RRTM was performed here to attempt to validate or dismiss the negligence of scattering IR radiation in cloudy skies. This was performed in three methods: one to test the difference between absorption only and absorption plus scattering using DISORT; a second method to test the difference between absorption only in RRTM and absorption only in DISORT; and a third method to test the difference in absorption only of DISORT and absorption plus scattering using DISORT. The first method is to test the validity of clouds on scattering of infrared radiation. The second method is to test the significance of gas absorption when compared to cloud absorption. The third method is to test the significance of just cloud absorption and scattering, while neglecting the gas molecule absorption.

Through an 82 layer atmosphere across six atmospheric profiles, it was shown that under certain cloud properties, neglecting the scattering effects increases the upward flux on the top of the atmosphere by at most 12 W/m^2 and decreases the downward surface flux on the surface by at most 4 W/m^2. These values are on the same order of magnitude as from the Fu et al. (1997), Chou et al. (1999), and Joseph and Min (2003) studies mentioned in Section two. What differs greatly here is the amount of different particle sizes tested. Rather than just one or two radii being tested, 10 different radii

spanning from 10 to 100 μm were tested. Hexagonal particle shapes proved to increase not only the magnitude of the difference, but also the spread between the lowest and highest particle size when compared to spherical particles.

When compared to the values calculated by Trenberth, Fasullo, and Kiehl (2009), the highest values are roughly 5% of the outgoing infrared radiative budget and 2-3% of the back radiation towards the surface.

Net flux and heating rate differences were also analyzed near cloud decks for all three methods. Difference in net flux just below the cloud level for both low clouds and high clouds was always positive, meaning when scattering is included, the net flux values are lower. Net flux peaked near 5 W/m^2 in the MLW case for low clouds and 13 W/m^2 in the tropical case for high clouds. Difference in the heating rates for low clouds with small particles and high cloud water paths were on the order of -1 K/day just below the cloud deck and 0.08 to 0.18 K/day on the cloud deck. For high clouds with small particles and high cloud water paths, heating rates just below the cloud deck reached up to almost -2 K/day and 0.08 to 0.18 K/day on the cloud deck. Similar responses occurred across the six atmospheric profiles. These values are also similar to the ones from the Chou and Joseph studies, although a little bit higher in magnitude.

When comparing the effects of gas molecules to those of clouds, absorption by gas molecules was significantly less than that of the clouds. Even when doubling carbon dioxide in the atmosphere to 800 ppm, the effects were still minimal, as the scattering of clouds is much more dominant than scattering of gas molecules. Upward, downward and net flux differences were all less than 1 W/m^2 and heating rates for just below the cloud decks reached a maximum of almost 0.4 K/day, while on the cloud decks the maximum

was barely above 0.01 K/day. Heating rates in the stratosphere peaked near 0.3 K/day regardless of cloud properties due to the abundance of ozone.

When comparing the absorption and scattering of the clouds and not including any gas absorption outside of the clouds, similar values were produced compared to when gas absorption was included. This implies that using discrete ordinates for cloud scattering is just as effective as using the RRTM algorithm. Since the chemistry (outside of water vapor) of the atmosphere provides such small variances in flux and heating rates, it is understood why some of it was removed in the earlier studies.

When broken down into the 16 bands, bands 2 and 3 provided much of the difference in comparing absorption versus scattering in the top of the atmosphere, while bands 5 through 9 provided much of the difference at the surface. Far IR (band 1), although small in optically thin clouds was higher in optically thick clouds. Bands 10 – 16 (near IR) were almost completely insignificant in providing any contribution to the difference. Band 4 and 14 provided the same small values regardless of particle size and may be considered faulty or erroneous. More research may need to be done into these two bands to see if those values are representative or not. It is possible that the difference in composite values of fluxes and heating rates may be higher if band 4 values are incorrect. In an effort to save on computing time, bands 10 through 16 could be eliminated, while still providing a fairly accurate representation of fluxes.

Because gas molecular absorption plays such a small role compared to cloud absorption (and scattering), doubling carbon dioxide in the atmosphere changed the differences in fluxes minimally. In both the upward flux at TOA and downward flux at SFC, changes in the difference when scattering was included was roughly 1-5%. Heating rates just below the cloud decks ranged between +0.001 to -0.03 K/day.

REFERENCES

Briegleb, Bruce P., and David H. Bromwich. "Polar Radiation Budgets of the NCAR CCM3." *Journal of Climate* 11, no. 6 (1998): 1246-1269.

Chou, Ming-Dah, Kyu-Tae Lee, Si-Chee Tsay, and Qiang Fu. "Parameterization for Cloud Longwave Scattering for Use in Atmospheric Models." *Journal of Climate* 12, no. 1 (1999): 159-169.

Coakley, James A., and Ping Yang. *Atmospheric Radiation: A Primer with Illustrative Solutions*. 2014

Drake, Frances. "Global Cloud Cover and Cloud Water Path from ISCCP C2 Data." *International Journal of Climatology* 13, no. 6 (1993): 581-605.

Ebert, Elizabeth E., and Judith A. Curry. "A Parameterization of Ice Cloud Optical Properties for Climate Models." *Journal of Geophysical Research* 97, no. D4 (1992): 3831.

Fu, Qiang, and K. N. Liou. "On the Correlated K -Distribution Method for Radiative Transfer in Nonhomogeneous Atmospheres." *Journal of the Atmospheric Sciences* 49, no. 22 (1992): 2139-2156.

Fu, Qiang, and K. N. Liou. "Parameterization of the Radiative Properties of Cirrus Clouds." *Journal of the Atmospheric Sciences* 50, no. 13 (1993): 2008-2025.

Fu, Qiang, K. N. Liou, M. C. Cribb, T. P. Charlock, and A. Grossman. "Multiple Scattering Parameterization in Thermal Infrared Radiative Transfer." *Journal of the Atmospheric Sciences* 54, no. 24 (1997): 2799-2812.

Fu, Qiang, Ping Yang, and W. B. Sun. "An Accurate Parameterization of the Infrared Radiative Properties of Cirrus Clouds for Climate Models." *Journal of Climate* 11, no. 9 (1998): 2223-2237.

Fu, Qiang. “Cloud-Radiative Processes.” In *Encyclopedia of Atmospheric Sciences,* edited by North, Gerald R., John Pyle, and Fuqing Zhang, 13-15. Elsevier / Acad. Press, 2015.

Garand, L., D. S. Turner, M. Larocque, J. Bates, S. Boukabara, P. Brunel, F. Chevallier, G. Deblonde, R. Engelen, M. Hollingshead, D. Jackson, G. Jedlovec, J. Joiner, T. Kleespies, D. S. Mckague, L. Mcmillin, J.-L. Moncet, J. R. Pardo, P. J. Rayer, E. Salathe, R. Saunders, N. A. Scott, P. Van Delst, and H. Woolf. "Radiance and Jacobian Intercomparison of Radiative Transfer Models Applied to HIRS and AMSU Channels." *Journal of Geophysical Research* 106, no. D20 (2001): 24017.

Hong, Gang, Ping Yang, Bryan A. Baum, Andrew J. Heymsfield, and Kuan-Man Xu. "Parameterization of Shortwave and Longwave Radiative Properties of Ice Clouds for Use in Climate Models." *Journal of Climate* 22, no. 23 (2009): 6287-6312.

Horváth, Ákos, and Roger Davies. "Comparison of Microwave and Optical Cloud Water Path Estimates from TMI, MODIS, and MISR." *Journal of Geophysical Research* 112, no. D1 (2007).

Hu, Y. X., and K. Stamnes. "An Accurate Parameterization of the Radiative Properties of Water Clouds Suitable for Use in Climate Models." *Journal of Climate* 6, no. 4 (1993): 728-742.

Iacono, Michael J., Eli J. Mlawer, Shepard A. Clough, and Jean-Jacques Morcrette. "Impact of an Improved Longwave Radiation Model, RRTM, on the Energy Budget and Thermodynamic Properties of the NCAR Community Climate Model, CCM3." *Journal of Geophysical Research* 105, no. D11 (2000): 14873.

King, Michael, Steven Platnick, W. Paul Menzel, Steven A. Ackerman, and Paul A. Hubands. "Spatial and Temporal Distribution of Tropospheric Clouds Observed by MODIS On-board the Terra and Aqua Satellites." *IEEE Transactions on Geoscience and Remote Sensing* 51, no. 7 (2013): 3826-3851

Joseph, Everette, and Qilong Min. "Assessment of Multiple Scattering and Horizontal Inhomogeneity in IR Radiative Transfer Calculations of Observed Thin Cirrus Clouds." *Journal of Geophysical Research* 108, no. D13 (2003).

Key, Jeffrey R., and Axel J. Schweiger. "Tools for Atmospheric Radiative Transfer: Streamer and FluxNet." *Computers & Geosciences* 24, no. 5 (1998): 443-451.

Lacis, Andrew A., and Valdar Oinas. "A Description of the Correlated K Distribution Method for Modeling Nongray Gaseous Absorption, Thermal Emission, and Multiple Scattering in Vertically Inhomogeneous Atmospheres." *Journal of Geophysical Research* 96, no. D5 (1991): 9027.

Li, J., and Qiang Fu. "Absorption Approximation with Scattering Effect for Infrared Radiation." *Journal of the Atmospheric Sciences* 57, no. 17 (2000): 2905-2914.

Li, J. "Accounting for Unresolved Clouds in a 1D Infrared Radiative Transfer Model. Part I: Solution for Radiative Transfer, Including Cloud Scattering and Overlap." *Journal of the Atmospheric Sciences* 59, no. 23 (2002): 3302-3320.

Liou, Kuo-Nan. "Influence of Cirrus Clouds on Weather and Climate Processes: A Global Perspective." *Monthly Weather Review* 114, no. 6 (1986): 1167-1199.

Liou, Kuo-Nan. *An Introduction to Atmospheric Radiation*. Amsterdam: Academic Press, 2002.

Mlawer, Eli J., Steven J. Taubman, Patrick D. Brown, Michael J. Iacono, and Shepard A. Clough. "Radiative Transfer for Inhomogeneous Atmospheres: RRTM, a Validated Correlated-k Model for the Longwave." *Journal of Geophysical Research* 102, no. D14 (1997): 16663.

Morcrette, J.-J., Impact of the radiation-transfer scheme RRTM in the ECMWF forecasting system, ECMWF Newsletter No. 91, 2001

O'Dell, Christopher W., Frank J. Wentz, and Ralf Bennartz. "Cloud Liquid Water Path from Satellite-Based Passive Microwave Observations: A New Climatology over the Global Oceans." *Journal of Climate* 21, no. 8 (2008): 1721-1739.

Petty, Grant W. *A First Course in Atmospheric Radiation*. Madison, WI: Sundog Pub., 2006.

Rhode, Robert A. "Atmospheric Transmission". Global Warming Art. http://www.globalwarmingart.com/wiki/File:Atmospheric_Transmission_png (accessed November 1, 2015).

Schuster, Arthur. "Radiation through a Foggy Atmosphere." *The Astrophysical Journal* 21 (1905).

Stamnes, Knut, S-Chee Tsay, Warren Wiscombe, and Kolf Jayaweera. "Numerically Stable Algorithm for Discrete-ordinate-method Radiative Transfer in Multiple Scattering and Emitting Layered Media." *Applied Optics* 27, no. 12 (1988): 2502.

Stephens, Graeme L., Philip M. Gabriel, and Philip T. Partain. "Parameterization of Atmospheric Radiative Transfer. Part II: Selection Rules." *Journal of the Atmospheric Sciences* 58, no. 22 (2001): 3411-423.

Stokes, Gerald M., and Stephen E. Schwartz. "The Atmospheric Radiation Measurement (ARM) Program: Programmatic Background and Design of the Cloud and Radiation Test Bed." *Bulletin of the American Meteorological Society* 75, no. 7 (1994): 1201-1221.

Trenberth, Kevin E., John T. Fasullo, and Jeffrey Kiehl. "Earth's Global Energy Budget." *Bulletin of the American Meteorological Society* 90, no. 3 (2009): 311-323.

Wallace, John M., and Peter V. Hobbs. *Atmospheric Science an Introductory Survey*. Amsterdam: Elsevier, 2006.

Wendisch, Manfred, and Ping Yang. *A Comprehensive Introduction to Atmospheric Radiative Transfer*. Weinheim: Wiley-VCH, 2012.

Wiscombe, W. J. "The Delta– M Method: Rapid Yet Accurate Radiative Flux Calculations for Strongly Asymmetric Phase Functions." *Journal of the Atmospheric Sciences* 34, no. 9 (1977): 1408-1422.

Yang, Ping, Bo-Cai Gao, Bryan A. Baum, Yong X. Hu, Warren J. Wiscombe, Si-Chee Tsay, Dave M. Winker, and Shaima L. Nasiri. "Radiative Properties of Cirrus Clouds in the Infrared (8–13μm) Spectral Region." *Journal of Quantitative Spectroscopy and Radiative Transfer* 70, no. 4-6 (2001): 473-504.

Yang, Ping, Martin G. Mlynczak, Heli Wei, David P. Kratz, Bryan A. Baum, Yong X. Hu, Warren J. Wiscombe, Andrew Heidinger, and Michael I. Mishchenko. "Spectral Signature of Ice Clouds in the Far-infrared Region: Single-scattering Calculations and Radiative Sensitivity Study." *Journal of Geophysical Research* 108, no. D18 (2003).

Yang, Ping, Heli Wei, Hung-Lung Huang, Bryan A. Baum, Yong X. Hu, George W. Kattawar, Michael I. Mishchenko, and Qiang Fu. "Scattering and Absorption Property Database for Nonspherical Ice Particles in the Near- through Far-infrared Spectral Region." *Applied Optics* 44, no. 26 (2005): 5512.

Zdunkowski, Wilford, Thomas Trautmann, and Andreas Bott. *Radiation in the Atmosphere: A Course in Theoretical Meteorology*. Cambridge, UK: Cambridge University Press, 2007.

APPENDIX A

UPWARD AND DOWNWARD FLUX DIFFERENCES FOR 2 CLOUDS

Difference in upward TOA flux for the 2-cloud case for MLS, SAS, Garand, Doubled CO_2, and Tropical profiles

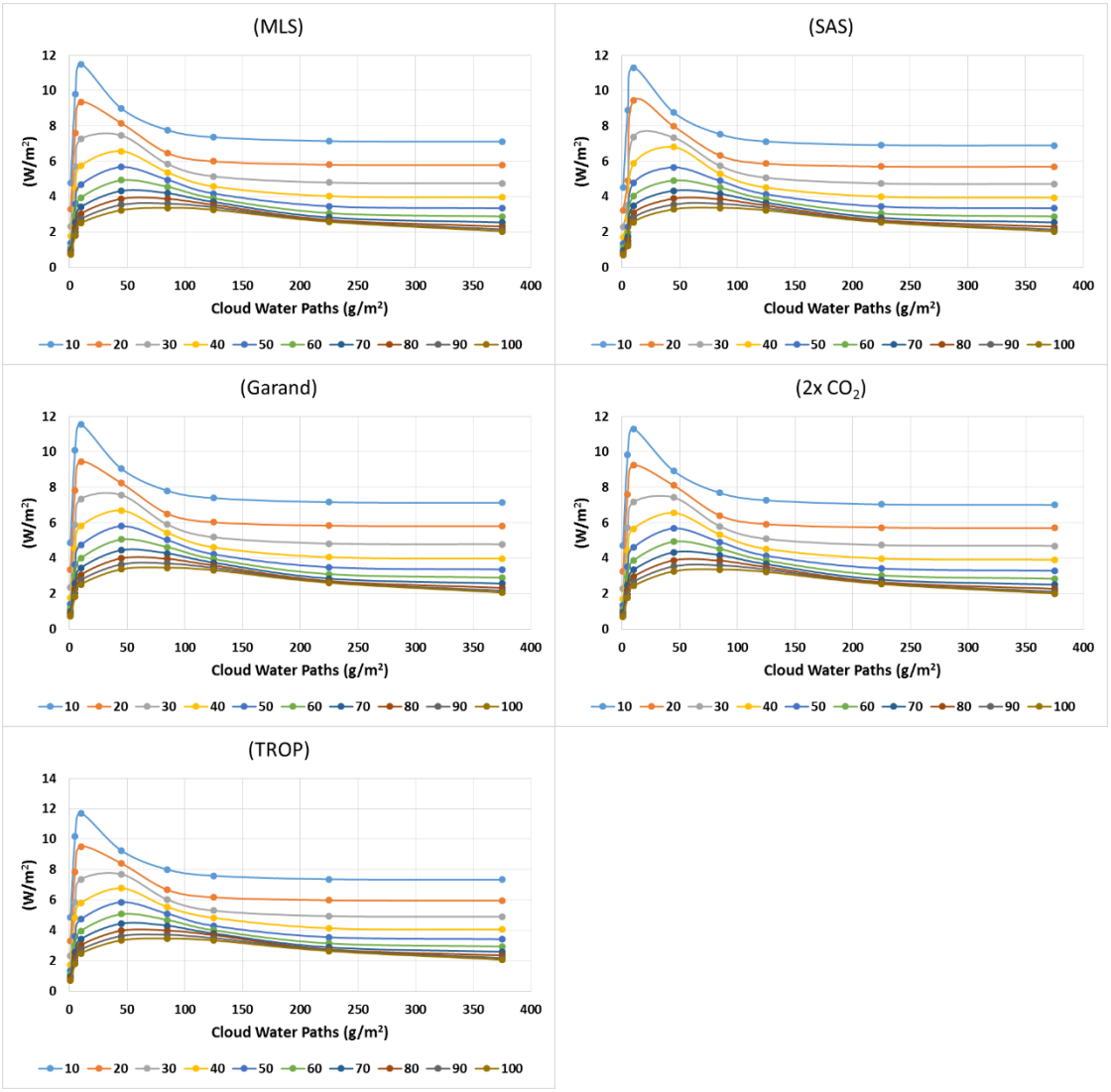

Difference in downward SFC flux for the 2-cloud case for MLS, SAS, Garand, Doubled CO_2, and Tropical profiles

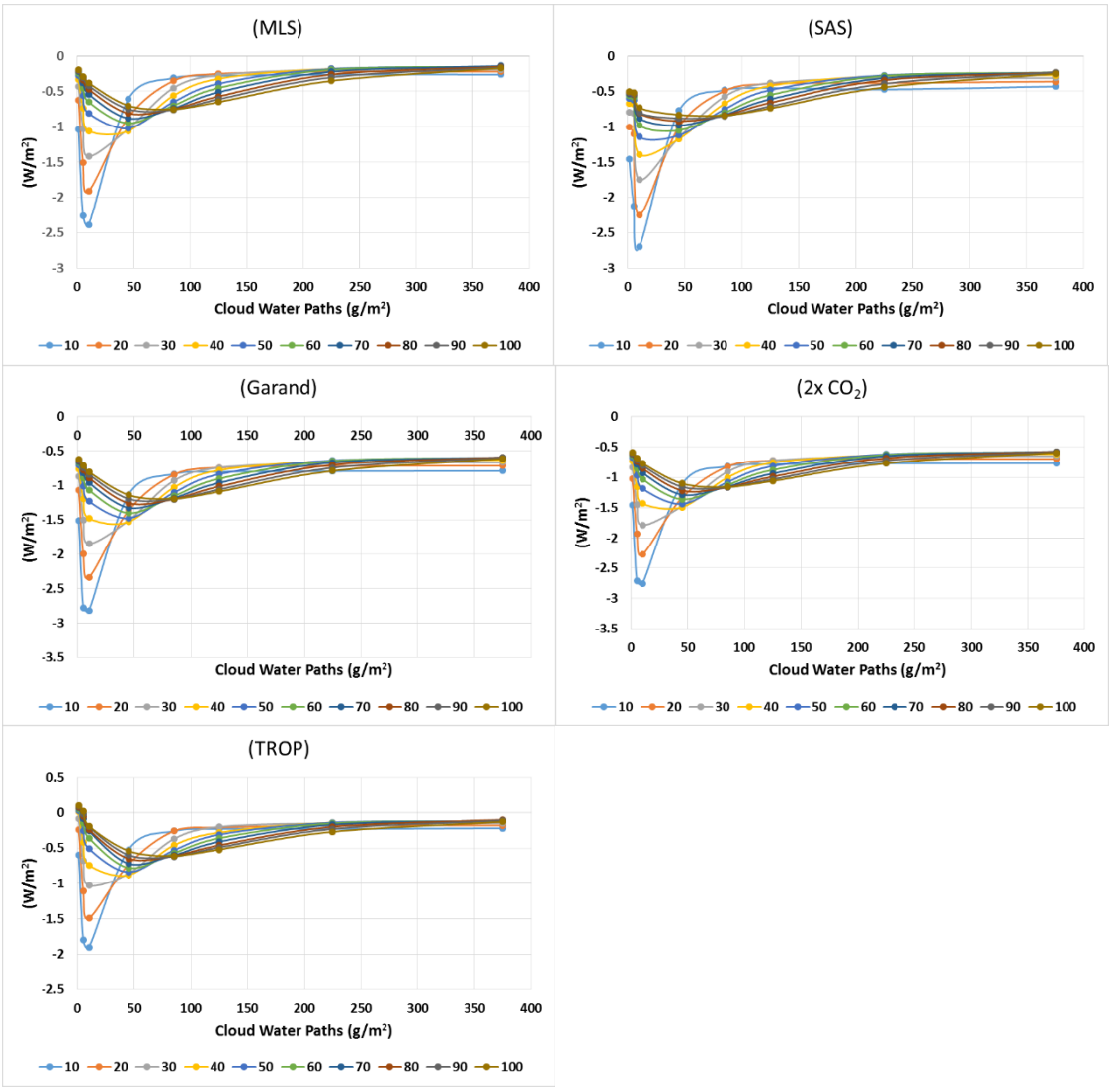

APPENDIX B

UPWARD AND DOWNWARD FLUX DIFFERENCES FOR LOW CLOUDS

Difference in upward TOA flux for the low cloud only case for MLS, SAS, Garand, Doubled CO_2, and Tropical profiles

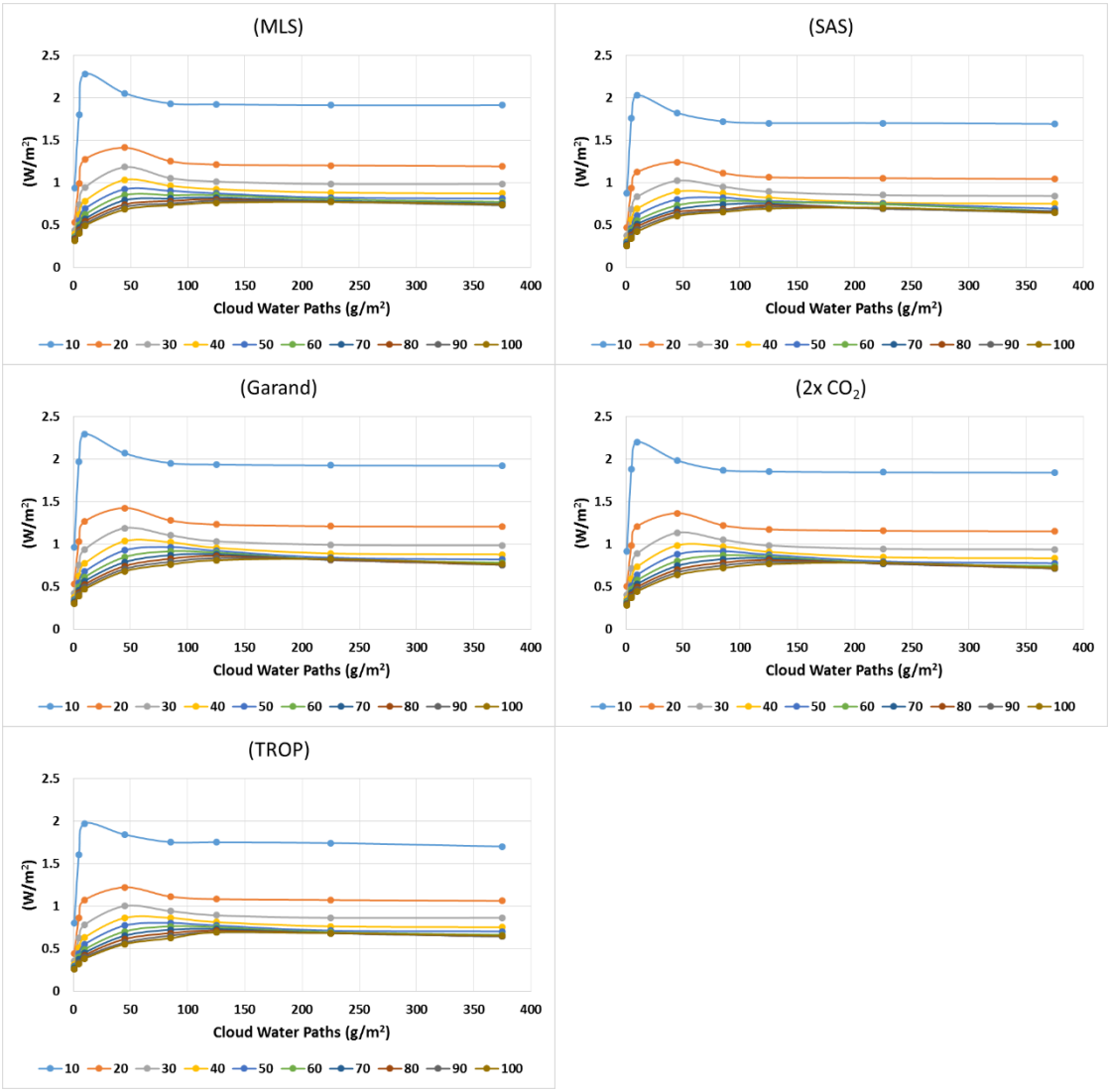

Difference in downward SFC flux for the low cloud only case for MLS, SAS, Garand, Doubled CO_2, and Tropical profiles

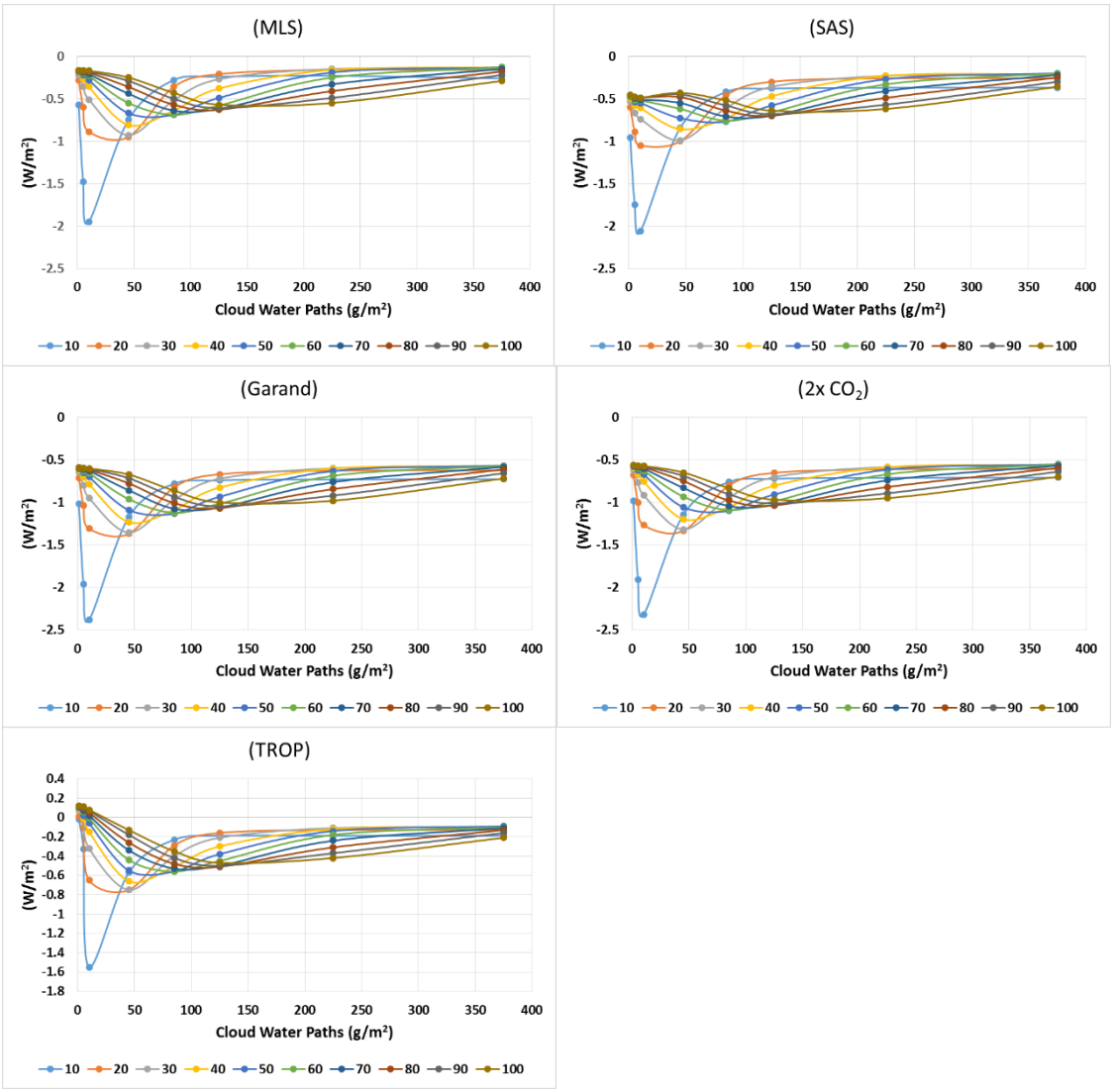

APPENDIX C

UPWARD AND DOWNWARD FLUX DIFFERENCES FOR HIGH CLOUDS

Difference in upward TOA flux for the high cloud only case for MLS, SAS, Garand, Doubled CO_2, and Tropical profiles

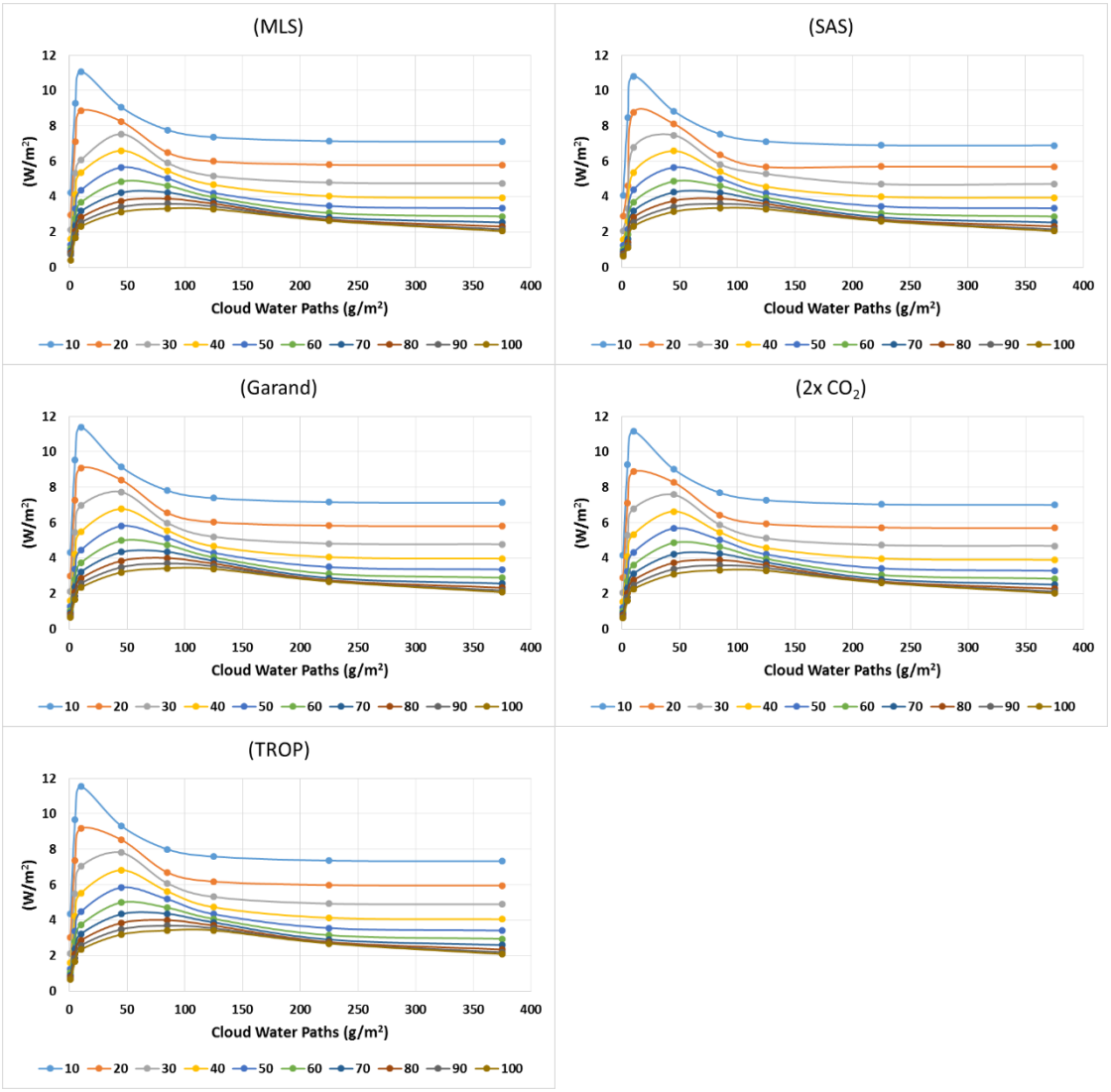

Difference in downward SFC flux for the high cloud only case for MLS, SAS, Garand, Doubled CO2, and Tropical profiles

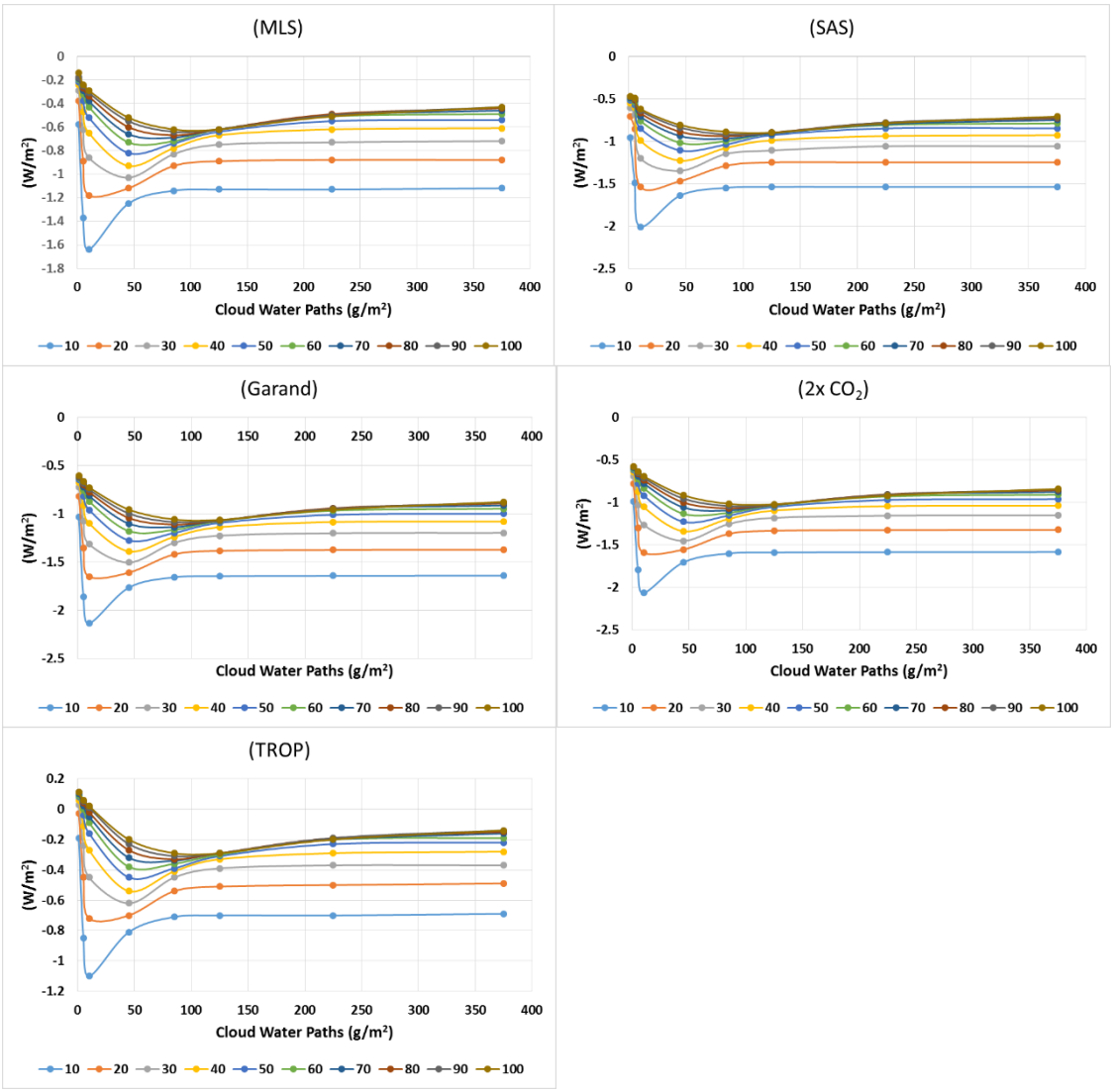

APPENEDIX D

NET FLUX DIFFERENCES FOR LEVEL 9 AND 10

Difference in net flux at level 9 for the MLS, SAS, Garand, Doubled CO_2, and Tropical profiles

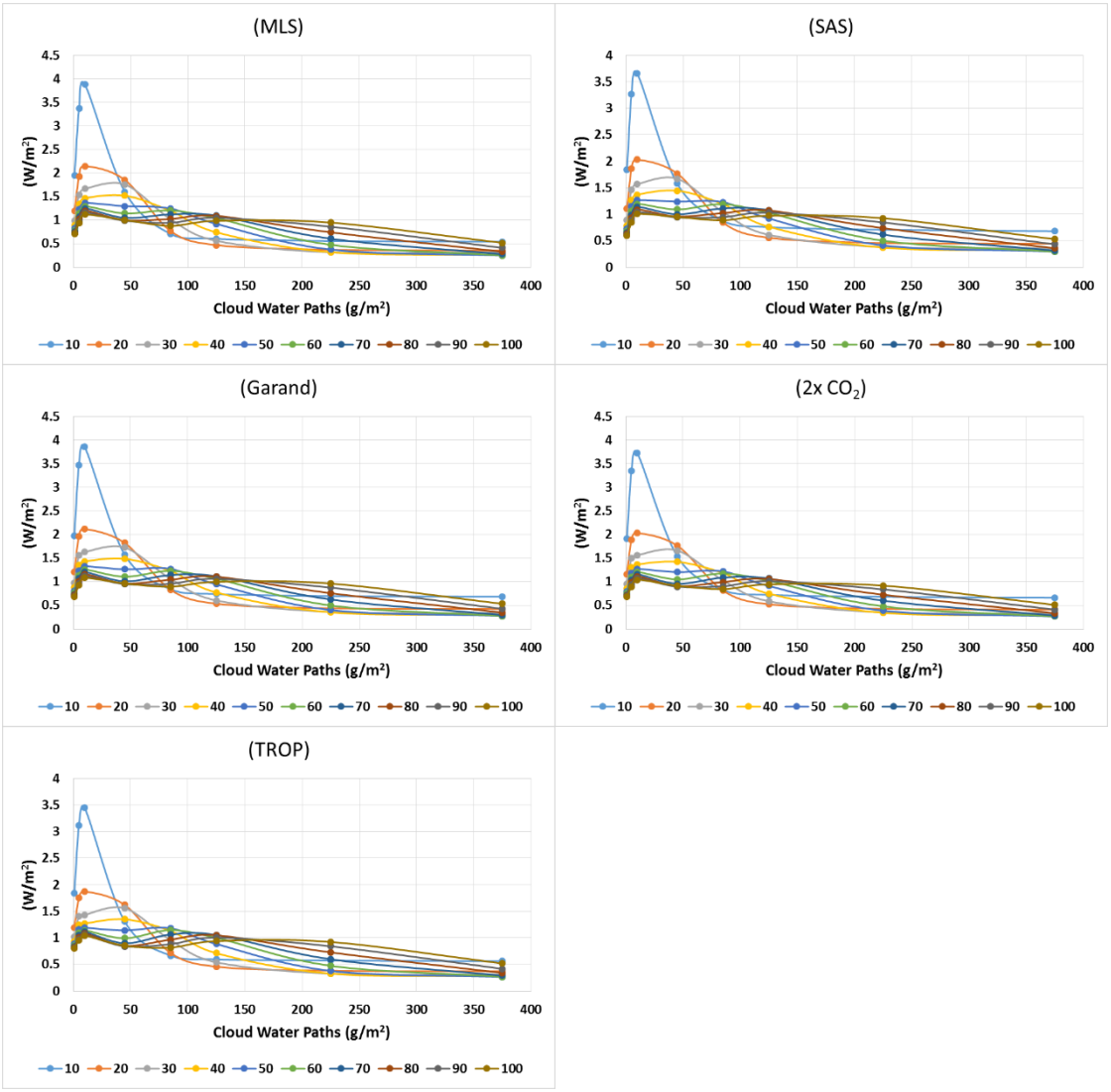

Difference in net flux at level 10 for the MLS, SAS, Garand, Doubled CO_2, and Tropical profiles

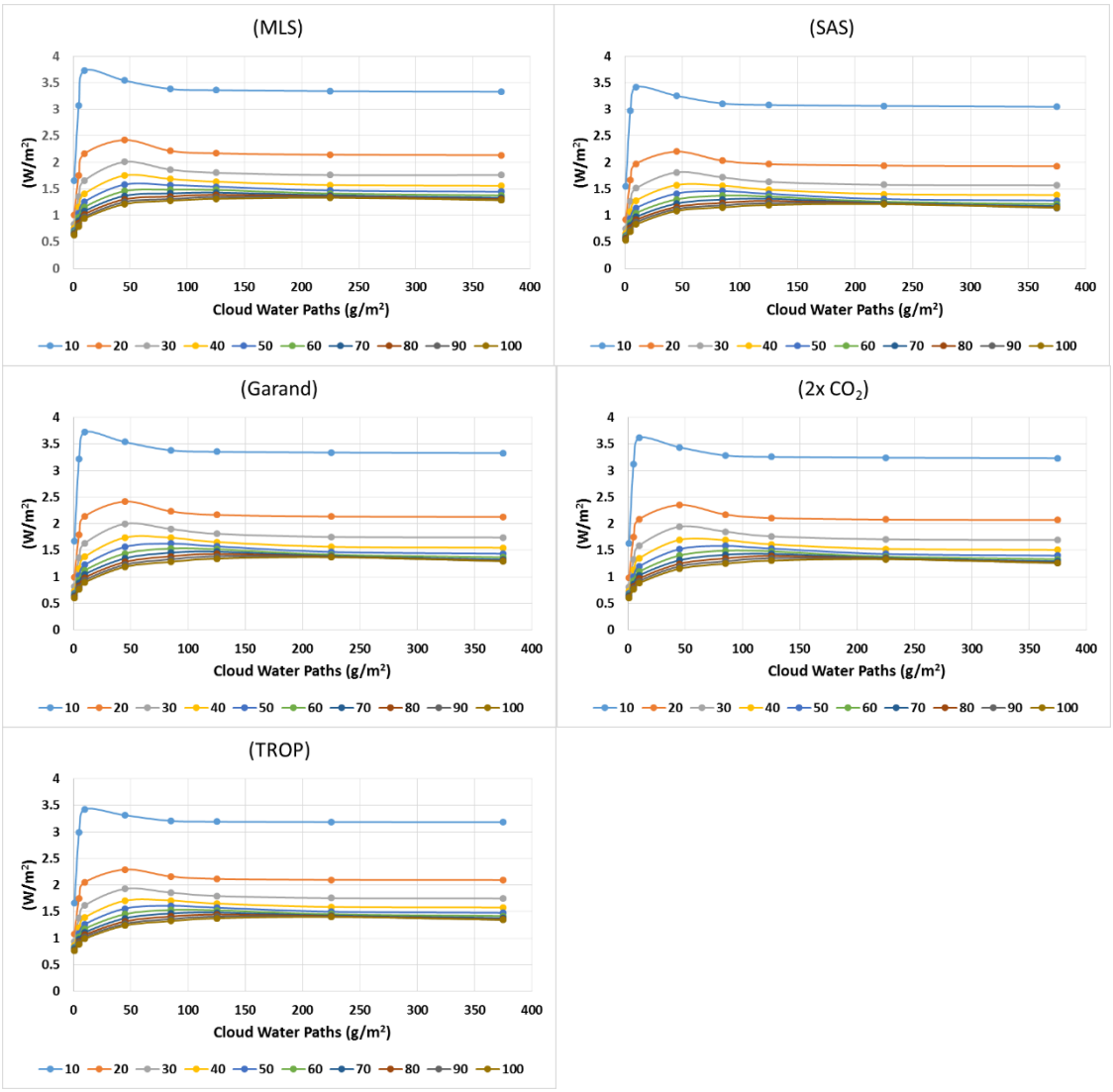

APPENDIX E

NET FLUX DIFFERENCES FOR LEVEL 41 AND 42

Difference in net flux at level 41 for the MLS, SAS, Garand, Doubled CO_2, and Tropical profiles

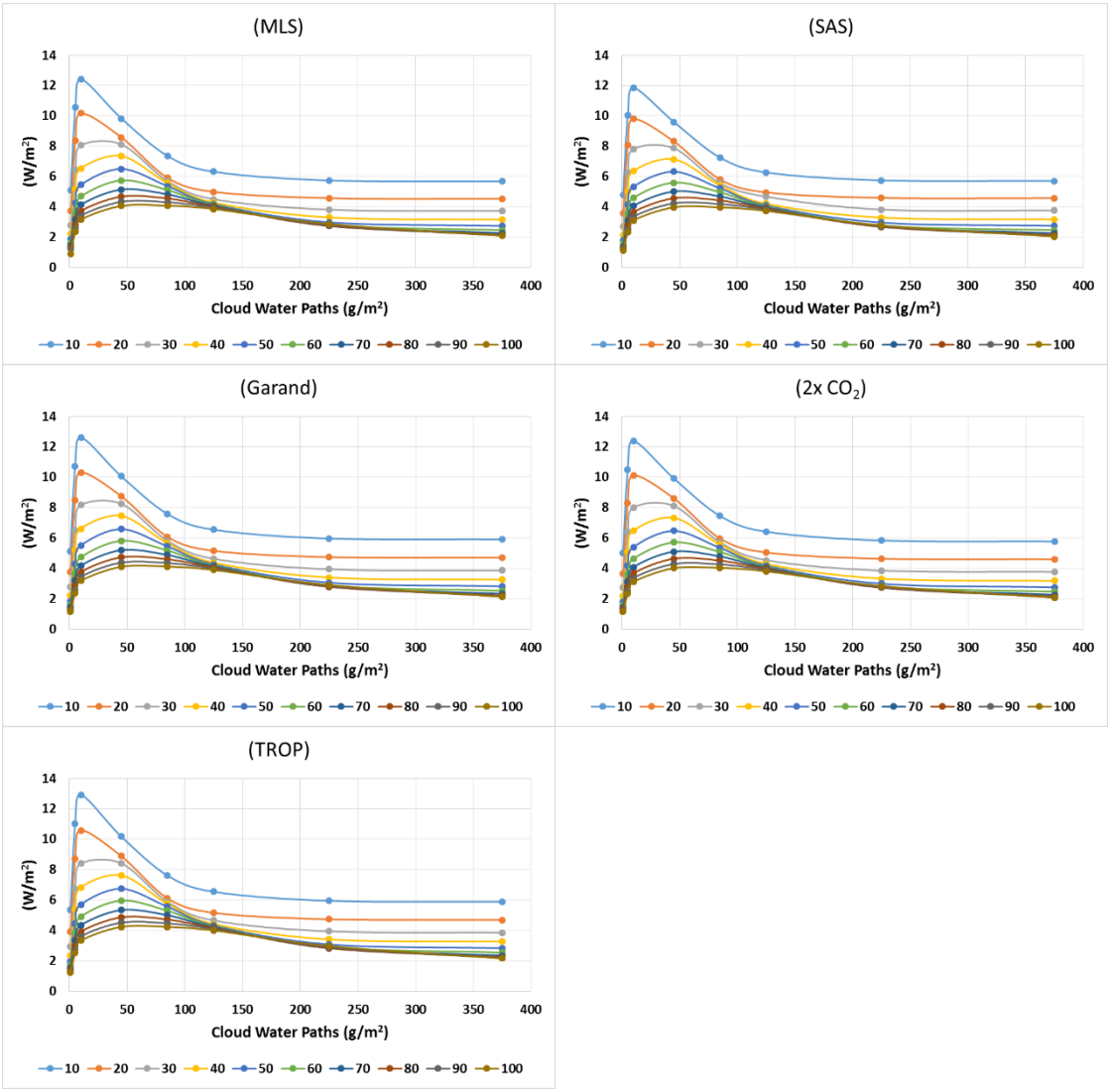

Difference in net flux at level 42 for the MLS, SAS, Garand, Doubled CO2, and Tropical profiles

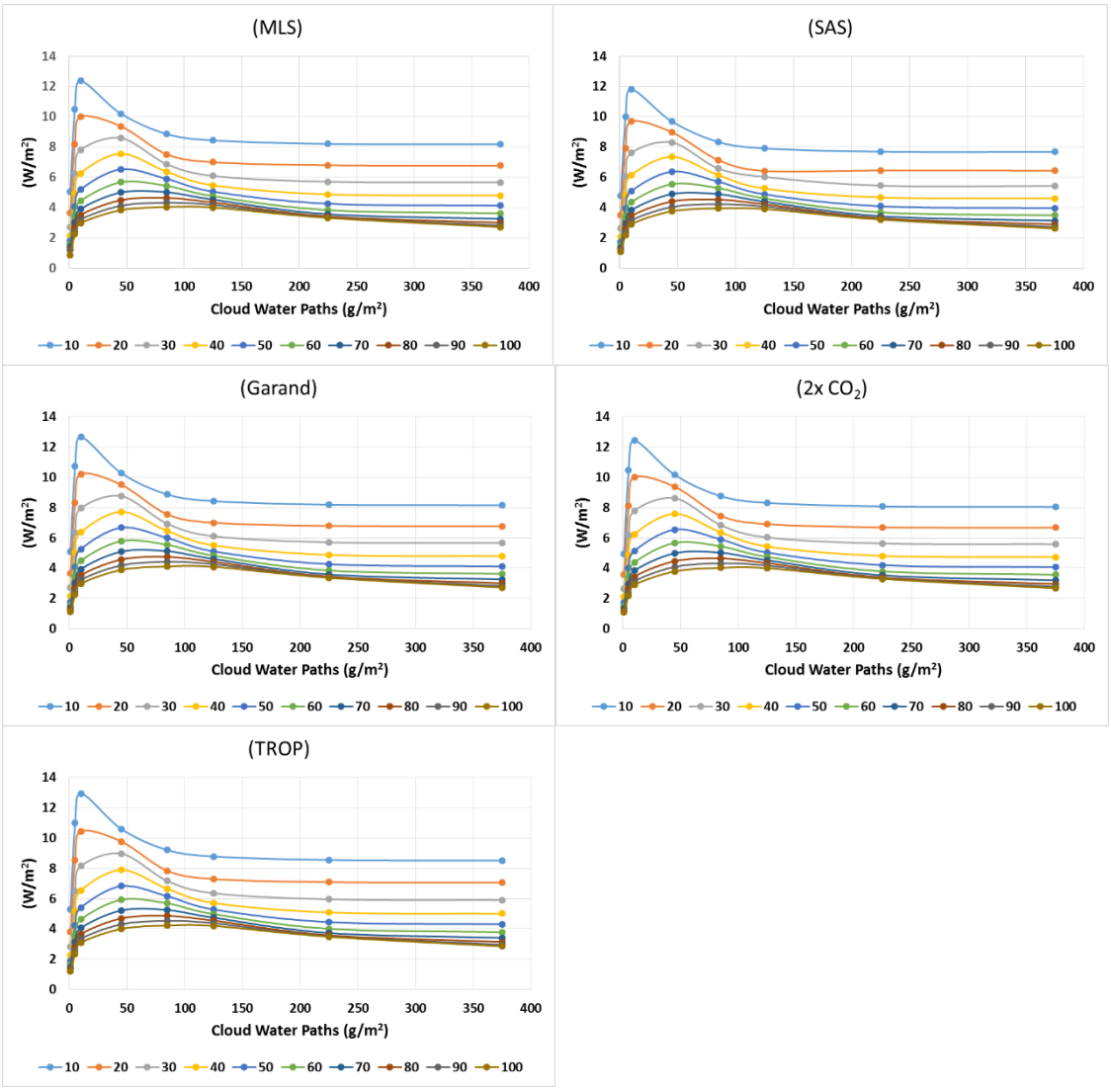

APPENDIX F

DIFFERENCE IN HEATING RATES FOR LEVEL 9 AND 10

Difference in heating rate at level 9 for the MLS, SAS, Garand, Doubled CO_2, and Tropical profiles

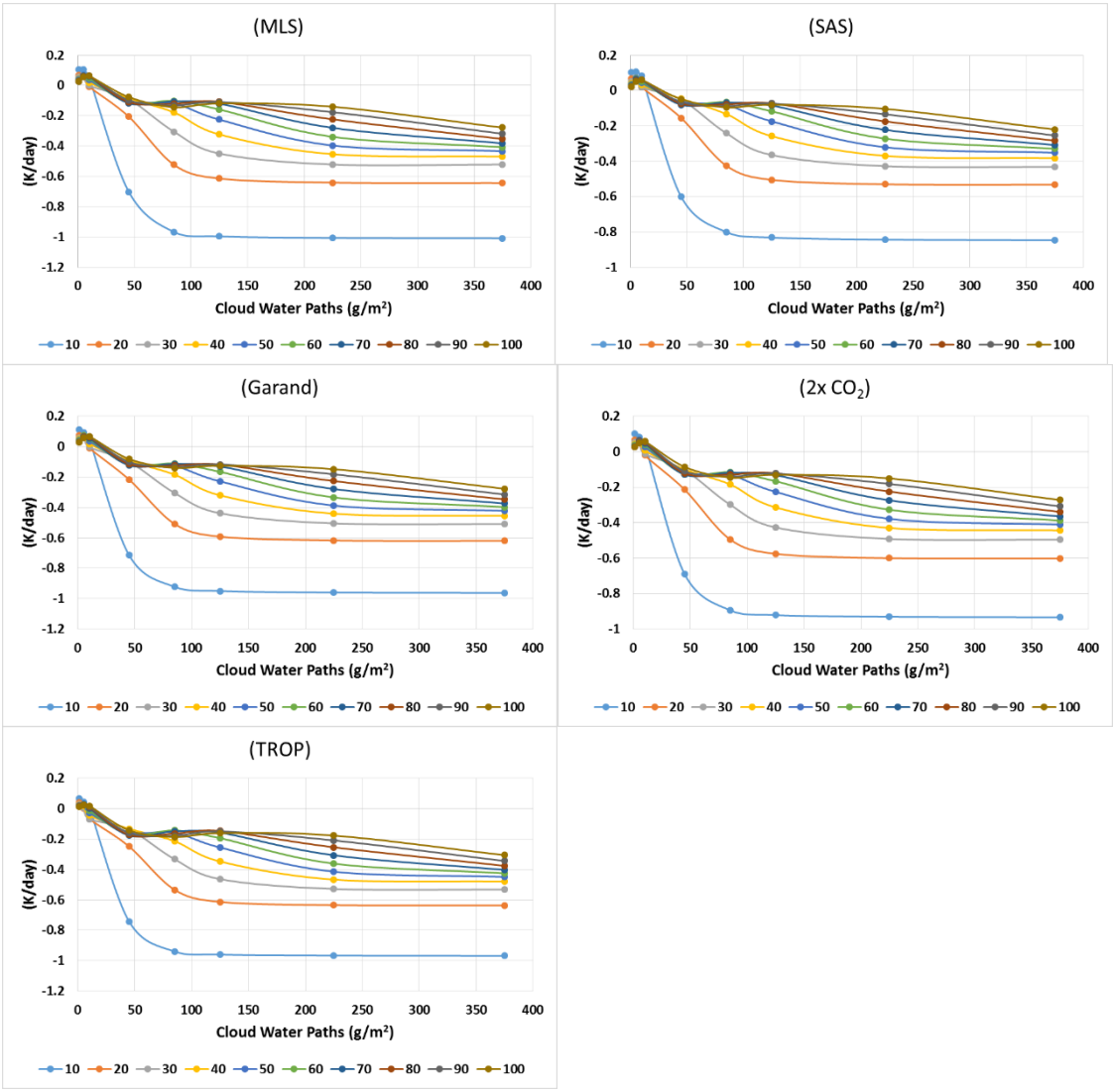

Difference in heating rate at level 10 for the MLS, SAS, Garand, Doubled CO_2, and Tropical profiles

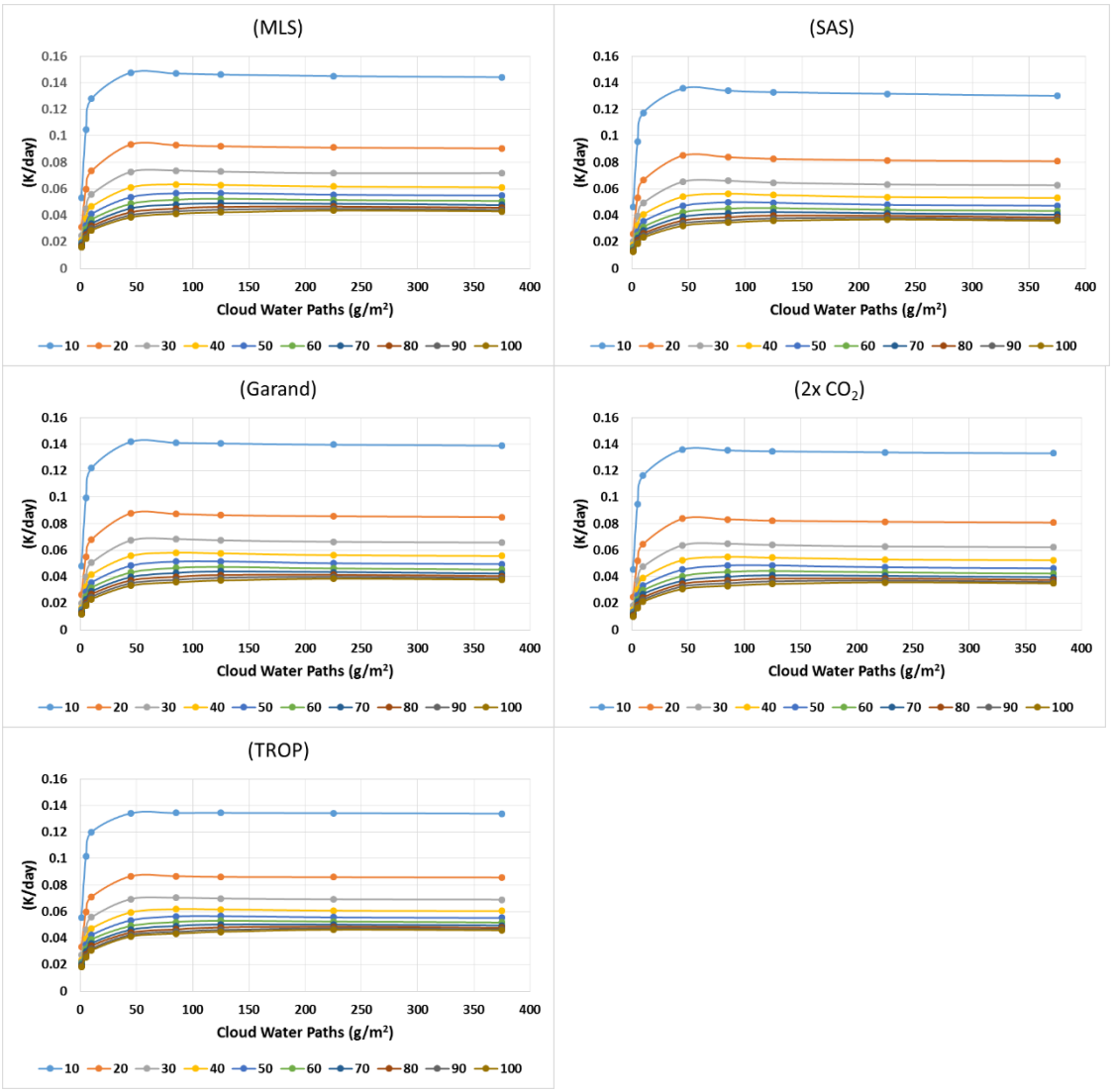

APPENDIX G

DIFFERENCE IN HEATING RATES FOR LEVEL 41 AND 42

Difference in heating rate at level 41 for the MLS, SAS, Garand, Doubled CO_2, and Tropical profiles

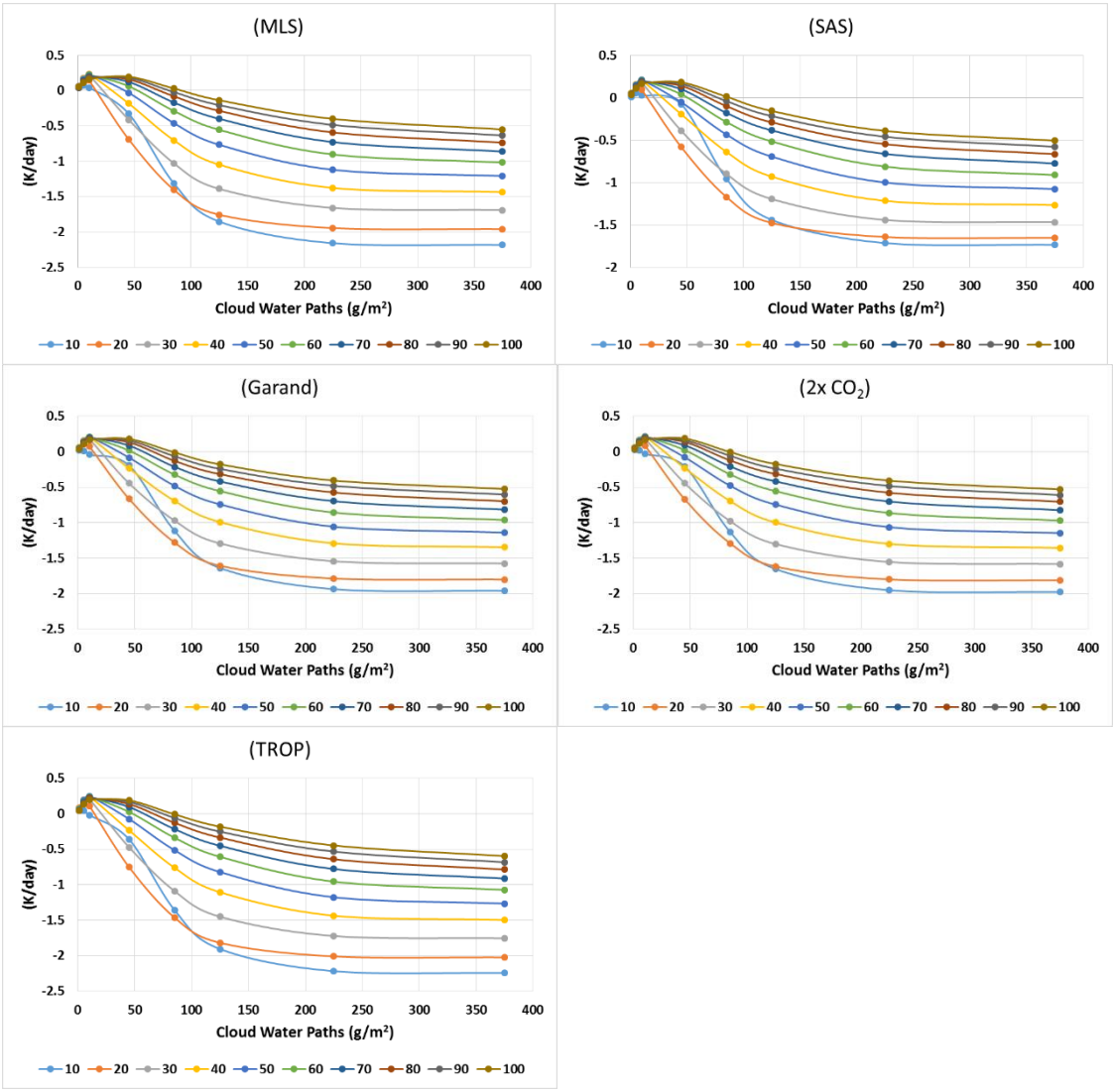

Difference in heating rate at level 42 for the MLS, SAS, Garand, Doubled CO_2, and Tropical profiles

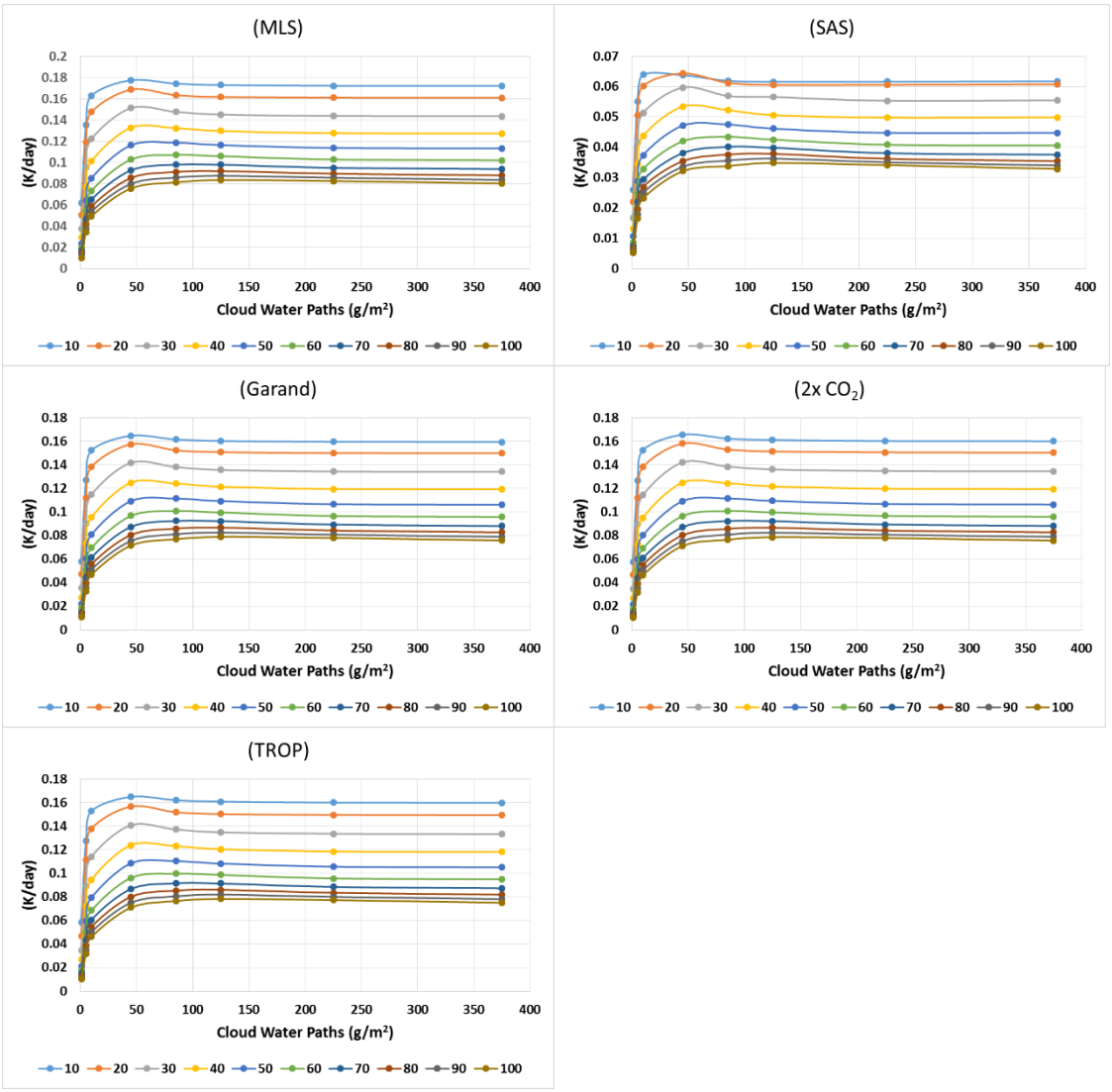

APPENDIX H

Band #	Wavenumber in cm^{-1}	Wavelength in µm	Tropospheric Chemistry	Stratospheric Chemistry	Halocarbons and CFCs
1	10-350	1000-28.57	H_2O N_2	H_2O N_2	
2	350-500	28.57-20	H_2O	H_2O	
3	500-630	20-15.873	H_2O CO_2 N_2O	H_2O CO_2 N_2O	
4	630-700	15.873-14.285	H_2O CO_2 N_2O	CO_2 O_3	
5	700-820	14.285-12.195	H_2O CO_2 O_3	CO_2 O_3	CCL_4
6	820-980	12.195-10.204	H_2O CO_2		CFC_{11} CFC_{12}
7	980-1080	10.204-9.259	H_2O O_3 CO_2	CO_2 O_3	
8	1080-1180	9.259-8.474	H_2O CO_2 O_3 N_2O	O_3 CO_2 N_2O O_2	CFC_{12} CFC_{22}
9	1180-1390	8.474-7.194	H_2O CH_4 N_2O	CH_4 N_2O	
10	1390-1480	7.194-6.756	H_2O	H_2O	
11	1480-1800	6.756-5.555	H_2O O_2	H_2O O_2	
12	1800-2080	5.555-4.807	H_2O CO_2		
13	2080-2250	4.807-4.444	H_2O N_2O CO_2 CO	O_3	
14	2250-2380	4.444-4.201	CO_2	CO_2	
15	2380-2600	4.201-3.846	N_2O CO_2 WV N_2		
16	2600-3250	3.846-3.076	H_2O CH_4	CH_4	

Table 1: Breakdown of chemistry and wavelength. This includes all 16 bands in RRTM